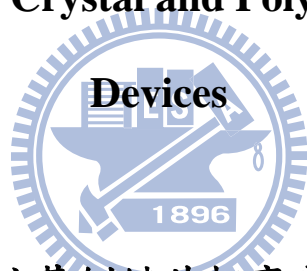# 國 立 交 通 大 學

材料科學與工程學系

博 士 論 文

Synthesis of Supramolecular Side-Chain Conjugated Polymers Containing Pyridyl Group: Applications in Chemosensor, Liquid Crystal and Polymeric Light-Emitting Devices

含超分子作用力之吡啶基側鏈共軛高分子在化學感測、液晶及高分子發光二極體元件之應用

研 究 生 ： 楊博仁

指導教授 ： 林宏洲　博士

中華民國九十八年十一月

含超分子作用力之吡啶基側鏈共軛高分子在化學感測、液晶及高分子

發光二極體元件之應用

Synthesis of Supramolecular Side-Chain Conjugated Polymers Containing Pyridyl Group: Applications in Chemosensor, Liquid Crystal and Polymeric Light-Emitting Devices

研究生：楊博仁　　　　　　　　　　　　Student: Po-Jen Yang

指導教授：林宏洲　博士　　　　　　　　Advisor: Dr. Hong-Cheu Lin

國立交通大學

材料科學與工程學系

1896

博士論文

中華民國九十八年十一月

I

ACKNOWLEDGEMENTS

含超分子作用力之吡啶基側鏈共軛高分子在化學感測、液晶及高分子發光二極體元件之應用

研究生：楊博仁　　　　　　　　　　指導教授：林宏洲 博士

國立交通大學材料科學與工程研究所

博士班

中 文 摘 要

　　本論文研究方向為探討一系列包含吡啶基側鏈共軛高分子，且利用超分子作用力作為自組裝之橋樑，並發展在化學感測、液晶及高分子發光二極體元件之應用。

　　第一個部份，一系列發光質子受體包含三各共軛環單體，包括一個末端吡啶基和二個側邊取代之甲氧基，是利用 Horner-Wadsworth-Emmons (HWE) 和 Sonogashira 偶合反應。然後，在以自由基聚合反應，依不同莫爾比和具有傳電洞能力的咔唑共聚。這些質子受體之共聚物和不同代數具有傳電子能力的噁二唑樹枝狀結構，利用氫鍵自組裝去形成超分子之側鏈共聚物。當引進咔唑基團在質子受體共聚物中，是有效的增加玻璃轉移溫度和有較小分子鏈的作用力，在這些發光質子受體之間，且相似的效應也發生在氫鍵樹枝狀錯合物中。另外，氫鍵樹枝狀錯合物螢光放光可以調控 61 nm 的紅位移，且激發咔唑基團可以獲得較強

的螢光強度比激發質子受體。電化學方面，引進噁二唑樹枝狀結構在氫鍵樹枝狀錯合物裡，可以獲得較低的最低未占分子軌道的能階和一個好的電子注入性質。質子受體高分子和它的氫鍵樹枝狀錯合物，在電致發光發光放光範圍為 464 到 519 nm，從藍光到綠光。元件方面，氫鍵樹枝狀錯合物顯示一個 519 nm 放光，驅動電壓為 6.5 V，一個最大發光 408 cd/m^2 在 18 V 和發光效率 0.39 cd/A 在 100 mA/cm^2。

第二部份，一系列側鏈型氫鍵液晶共聚高分子網路，包含不同共聚比之發光的質子受體和質子予體，是被成功的合成且利用自由基聚合方式。氫鍵共聚高分子網路擁有較高的玻璃轉移溫度比它們個別的均聚物。氫鍵共聚物和均聚物兩者都表現層列 A 液晶相。氫鍵共聚高分子網路隨著質子予體含量增加，澄清溫度也隨之增加且有利於穩定層列 A 液晶相。另外，氫鍵共聚高分子網路螢光放光可以調控 39 nm 的紅位移比照它的均聚物時，且在電致發光元件和螢光放光的光色可以被調控，從 496-500 nm 到 531-537 nm 為藍綠到綠光。

最後一部份，開發發光質子受體包含三各共軛環單體，包括一個末端吡啶基和二個側邊取代之甲氧基及二各雙鍵之共軛三環結構，是利用 Wittig and Pd-catalyzed Heck 偶合反應和聚合方式為自由基聚合。均聚物表現一個玻璃轉移溫度為 60 °C 和 融點為 150 °C。在醋酸溶液中，螢光放光最大紅位移可以從 460 到 605 nm。這均聚物具有高的感測和選擇性，對於鎳離子比其他過渡金屬離子，這是歸因於它具有較強的鍵結且焠熄常數為 5.65 × 10^6 M^{-1}。另外，當加入 PMDTA 到高分子和銅離子的錯合物，螢光的 ON-OFF-ON 切換行為可被發現，這未來利用在化學感測可以回收利用的價值。

Synthesis of Supramolecular Side-Chain Conjugated Polymers Containing Pyridyl Group: Applications in Chemosensor, Liquid Crystal and Polymeric Light-Emitting Devices

Student: Po-Jen Yang   Advisor: Dr. Hong-Cheu Lin

Department of Materials Science and Engineerong National Chiao Tung University

Abstract
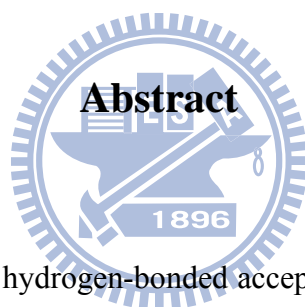
First, a novel light-emitting hydrogen-bonded acceptor containing three conjugated aromatic rings, including one pyridyl terminus and two lateral methoxyl groups, was successfully synthesized via Horner-Wadsworth-Emmons (HWE) olefination and Sonogashira coupling reaction. Moreover, different molar ratios of light-emitting H-acceptor monomer and hole-transporting monomer bearing a carbazole unit were copolymerized through free radical polymerization to obtain light emitting and hole-transporting H-acceptor copolymers. H-acceptor copolymers were complexed with different generations of dendritic H-donors bearing 1,3,4-oxadiazole (**OXD**) dendrons and terminal benzoic acids via H-bonded self-assembly to form supramolecular side-chain copolymers. In contrast to H-acceptor homopolymer, H-acceptor copolymers incorporated with carbazole moieties effectively enhance the glass transition temperatures (T_gs) and minimize the interchain interations of the

light-emitting H-acceptor units, and similar effects occur in their H-bonded dendritic complexes. In addition, red shifts of photoluminescence (PL) emissions in H-bonded dendritic complexes can be tuned up to 61 nm. Furthermore, H-bonded dendritic complexes excited **OXD** absorption can create a stronger fluorescence than that excited at acceptor absorption. The **OXD** dendritic wedges in H-bonded dendritic complexes can lower the LUMO energy levels and provide a better electron injection property. H-acceptor polymer and its H-bonded dendritic complexes showed electroluminescence (EL) emissions in the range of 464-519 nm from blue to green. In addition, a PLED device containing H-bonded dendritic complex showed an EL emission of 519 nm under a turn-on voltage of 6.5 V, with a maximum luminance of 408 cd/m^2 at 18 V and a luminance efficiency of 0.39 cd/A at 100 mA/cm^2, respectively.

Second, a series of H-bonded side-chain mesogenic copolymer networks containing different molar ratios of light-emitting proton acceptor and proton donor were synthesized via free radical polymerization. The H-bonded copolymer networks have higher glass transition temperatures (T_gs) than the individual hompolymers. Both H-bonded copolymer and homopolymer complex networks show mesomorphic behavior with the smectic A phase. The isotropization temperatures (T_is) and S$_A$ phase stabilities of the H-bonded copolymer networks increase as the molar ratios of H-donor unit increase. Furthermore, the red-shifts of PL emissions in H-bonded copolymer and homopolymer complex networks can be tuned up to 39 nm in contrast to H-acceptor homopolymer. The electroluminescence (EL) and photoluminescence (PL) results of H-acceptor homopolymer and its fully H-bonded cross-linking copolymer show emission colors varying from c.a. 496-500 nm (greenish-blue) to 531-537 nm (green), respectively.

Finally, a novel light-emitting receptor containing three conjugated aromatic

rings, including one pyridyl terminus and two lateral methoxyl groups (on the middle ring), was successfully synthesized via Wittig and Pd-catalyzed Heck coupling reactions. Homopolymer shows a T_g of 60 °C and T_i up to 150 °C. In CH$_3$COOH solution, homopolymer exhibits a pH-tunable photoluminescence with emission maximum varies from 460 to 605 nm. Homopolymer exhibits an extraordinary sensory selectivity for Ni^{2+} over other transition metal ions as a result of the stronger binding ability of the Ni^{2+} onto Homopolymer than other transition metals ions. Stern-Volmer constant for the Ni^{2+} ion sensing was determined through concentration dependent studies as 5.65 $\times$ 10^6 M^{-1}. In addition, the ON-OFF-ON fluorescent switch behavior upon the addition of **PMDTA** to the polymer-Cu^{2+} complexes demonstrates a superior reusability of this chemosensor which is important for the practical use.

Table of Contents

IX

Table Lists

XIII

Figure Lists

Chapter 1

Introduction

1.1 Introduction to Supramolecular chemistry

From before Linus Pauling's ground breaking work on the hydrogen bond in the 1930's[1] to Jean Marie Lehn's 'Chemistry beyond the molecule' that led to the term 'supramolecular chemistry', the nature of non-covalent bonds has fascinated chemists for over a century. In particular, the last thirty years have been exceptionally fruitful for scientists from a variety of disciplines who have made enormous advances in exploiting the non-covalent bond to construct sophisticated architectures.[2,3] As macromolecular structures and functional materials have continued to evolve with higher degrees of complexity and function, traditional covalent-based synthetic strategies have become increasingly difficult to employ. Accordingly, many scientists have begun to replace traditional polymer synthesis with self-assembly in order to overcome a variety of synthetic hurdles and to exploit the dynamic nature of the noncovalent bond. Tremendous growth and elegant advances in polymer science have taken place as supramolecular science, self-assembly, and polymer chemistry continue to converge.[3] This review explores the design principles and functionalization strategies inherent to one class of supramolecular polymers, side-chain functionalized polymers (SCFPs), and will high light the advances that

have given rise to the sophisticated non-covalent functionalization methods of today.

A large variety of recognition motifs and non-covalent forces have been reported for supramolecular polymers ranging from π–π interactions and hydrogen bonding to metal coordination and electrostatic interactions. Non-covalent interactions and forces can fall into three major classes: i) weak interactions (0–15 kcal mol^{-1} bond strength), ii) medium interactions (15–60 kcal mol^{-1} bond strength) and iii) strong interactions (above 60 kcal mol^{-1} bond strength).[4] Due to their high dependence on external influences such as pressure, solvent, and temperature, most non-covalent forces do not fall into a single category. Figure 1.1.1 describes the general division of noncovalent interactions based on bond strength. In general, π-π, cation-π, hydrophobic, or van der Waals interactions or hydrogen bonds are very weak. In contrast some metalcoordination complexes (strongly dependent on the ligand system and the metal used) and electrostatic interactions have very strong bond strength. Multiple hydrogen bonds and some metal-coordination complexes can be categorized as medium strength.

	Interaction Strength	
Weak (0-15 kcal/mol)	Medium (15-60 kcal/mol)	Strong (>60 kcal/mol)
Hydrogen Bonding Van-Der-Waals Interactions π–π Interactions	Multiple Hydrogen Bonds Metal Coordination	Metal Coordination Ionic Interactions

Figure 1.1.1 Organization of non-covalent interactions by bond strength.

1.2 Self-assembled liquid crystalline polymers

Non-covalent side-chain functionalization strategies were first reported for the synthesis of liquid crystalline materials.[5,6] Liquid crystals (LCs) possess orientational or weak positional ordering that give rise to materials with important characteristic of crystals but flow behaviour similar to liquids. Formation of this unique phase of matter is a direct consequence of the anisotropic alignment of small molecules or mesogens via non-covalent forces such as π-π stacking or hydrophobic interactions. Polymeric liquid crystals employ a variety of self-organizational processes to achieve long-range order. Conventional side-chain liquid crystalline polymers (SCLPs) are typically prepared via covalent tethering of mesogenic entities, structurally similar to low molecular weight LCs mesogens, with long, flexible aliphatic chains.[7] This spacer group, situated between the polymer backbone and the mesogen, decouples the motion of the polymer from the sidechain giving flexibility to the molecular orientation of the mesogenic components. In the field of self-assembled SCLPs, the principles described above for SCLPs are generally followed, yet covalent attachment of the mesogen is replaced with non-covalent bonds (Figure 1.2.1).

Kato and Fréchet were the first to explore the non-covalent attachment of traditional liquid crystalline components to a variety of polymer backbones.[8] In 1989 they disclosed their report describing binary mixtures of **2** and **3** to form thermotropic self-assembled SCLPs via simple single pyridine–benzoic acid hydrogen-bonded

3

complexes (**1**) (Figure 1.2.2). In this example, each component independently shows

liquid crystalline behaviour. However, when 1:1 mixtures of **2** and **3** or **4** and **3** are

prepared by slow evaporation from pyridine solutions, nematic mesophases with

higher transition temperatures than those of the individual components are observed.

This mesophase stabilization is attributed to the formation of extended mesogenic

units involving the hydrogen-bond bonded complex **1** shown in Figure **1.2.2**. While

Kato and Fréchet's novel class of liquid crystalline polymers was based on a single

weak non-covalent bond, this report held much significance not only for the field of

selfassembled SCLPs, but also established fundamental design strategies for the

preparation of supramolecular SCFPs in general. Following their original report,

much effort was directed toward examining self-assembled SCLPs engineered with a

variety of structural configurations.
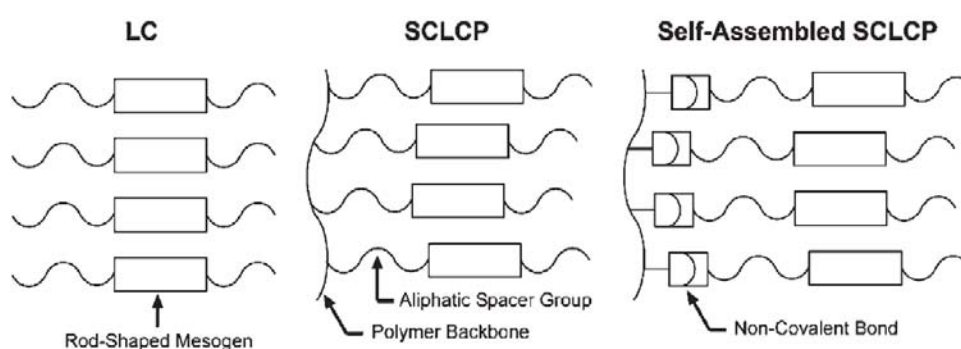
Figure 1.2.1   Schematic illustration of the structural components used to fabricate

simple LCs, SCLPs, to self-assembled SCLPs from rodshaped mesogens.
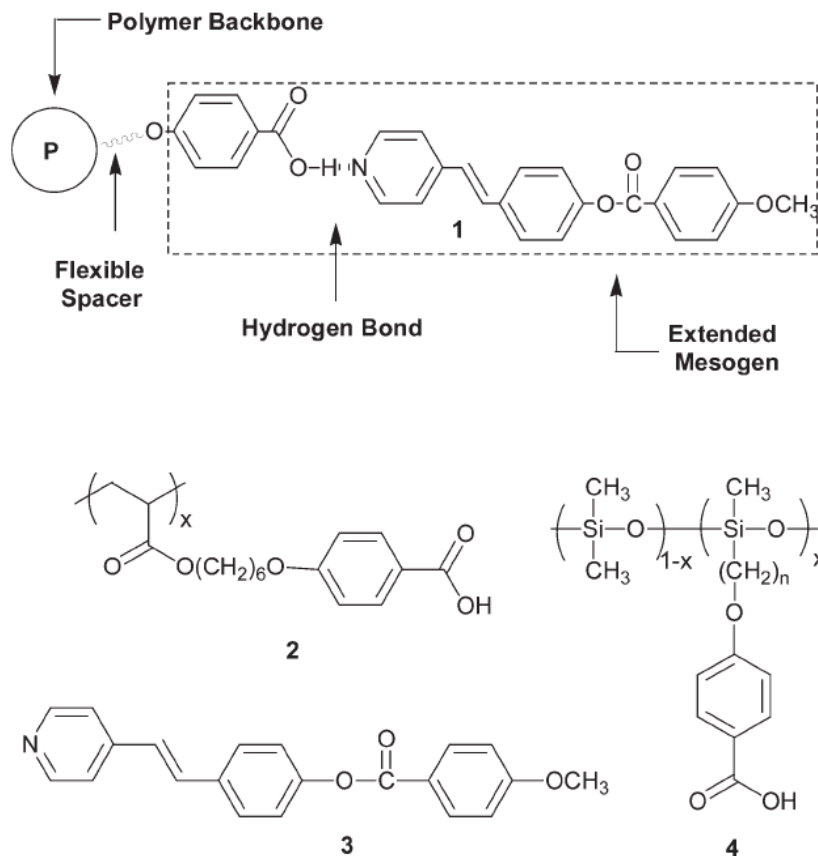
Figure 1.2.2 Molecular components used to prepare the first examples of self-assembled SCLPs.

Ikalla and co-workers have employed multiple interactions to fabricate supramolecular nanostructures with microsturctural control on two different length scales.[9] Here, more than one type of non-covalent bond is joined at a single anchoring site, thereby allowing for multi-functionalization at each repeat unit. The motivation for forming such complexes lies mainly in the ease of synthesis, allowing one to rapidly tailor the properties of the resultant materials. In one example, poly(4-vinylpyridine) was functionalized via proton transfer using methane sulfonic acid (see Figure 1.2.3).
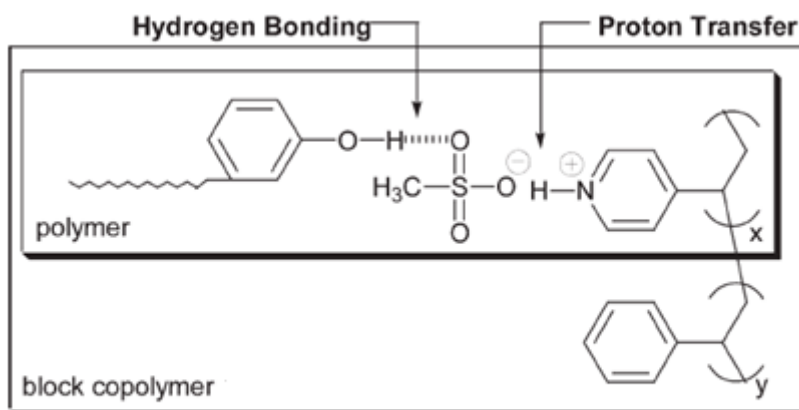
Figure 1.2.3 Complexes formed as a result of hydrogen bonding and proton transfer, which are joined at each repeat unit of poly(4-vinylpyridine).

1.3 Self-assembled π-conjugated systems polymers

π-Conjugated (semiconducting) polymers are by far the most promising functional polymers in view of applications in less expensive and flexible electronic devices. Prototype field-effect transistors (FET)s,[10] light-emitting diodes (LED)s,[11] photovoltaic cells, and related devices have already been fabricated, and Philips introduced the first commercial LED based on polymer technology in 2002. Nowadays a plethora of conjugated polymers exists having a base structure of alternating single and double/triple bonds of which some parent structures are shown.

In in oligo(p-phenylenevinylene)s was studied as a function of the conjugation length (**5-7**). It was found that only strong π-π interactions in the longest oligomer could phase separate from the tridodecyl chains. Columnar order in OPV derivatives was also reached using hydrogen-bonded dimers between carboxylic acids aided by

strong phase separation of the tridodecyloxyphenyl groups (**8**, **10**). Also, dimerization

of **OPVs** by coordination (**9**), ionic, and fluorophilic interactions have led to discrete

liquid-crystalline supramolecular structures that further organize into columnar

mesophases (see Figure 1.3.1).[12]
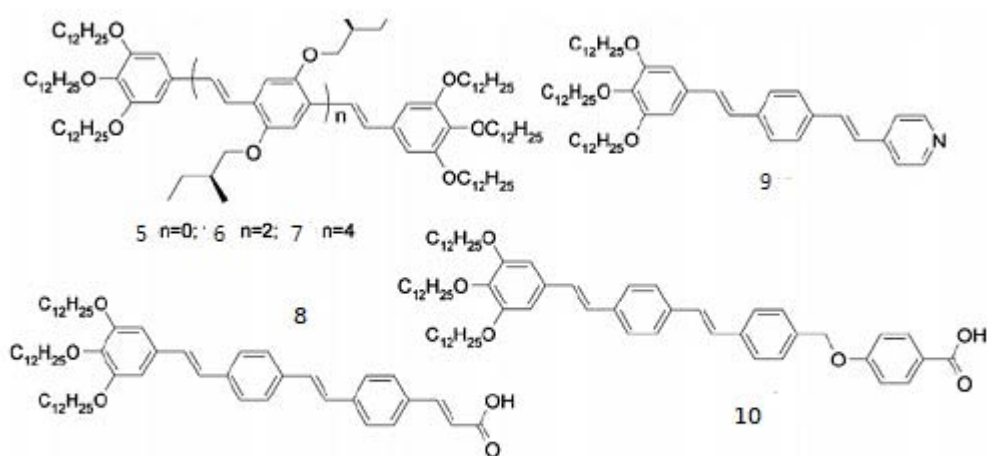
Figure 1.3.1   Rod like π-conjugated oligomers **5-10**.

Ajayaghosh et al. serendipitously extended this concept to **OPV** derivatives (**11-13**)

and reported a completely thermoreversible self-assembly process in a series of

hydrocarbon solvents from single **OPV** molecules to fibers and ultimately to an

entangled network structure. The absorption and emission properties showed dramatic

changes during gelation, which is an indication of strong intermolecular π electronic

coupling of the ordered **OPV** segments. In a comparative study it was shown that

gelation was cooperative and strongly dependent on the choice of hydrogen-bonding

motif, alkoxy side-chain length, and conjugation length. An alcohol **OPV** trimer (**11**) equipped with six lateral dodecyl chains easily forms a gel at moderate concentrations in hexane, whereas the aldehyde analogue (**13**) could not gelate the solvent or a methyl ester analogue (**12**) under extreme conditions. SEM, X-ray diffraction, and IR on the gel from **11** revealed an entangled network of fibers up to micrometer lengths and 100-150 nm in width consisting of well-ordered lamellae of stacked molecules positioned by hydrogen bonds (Figure 1.3.2).[13]
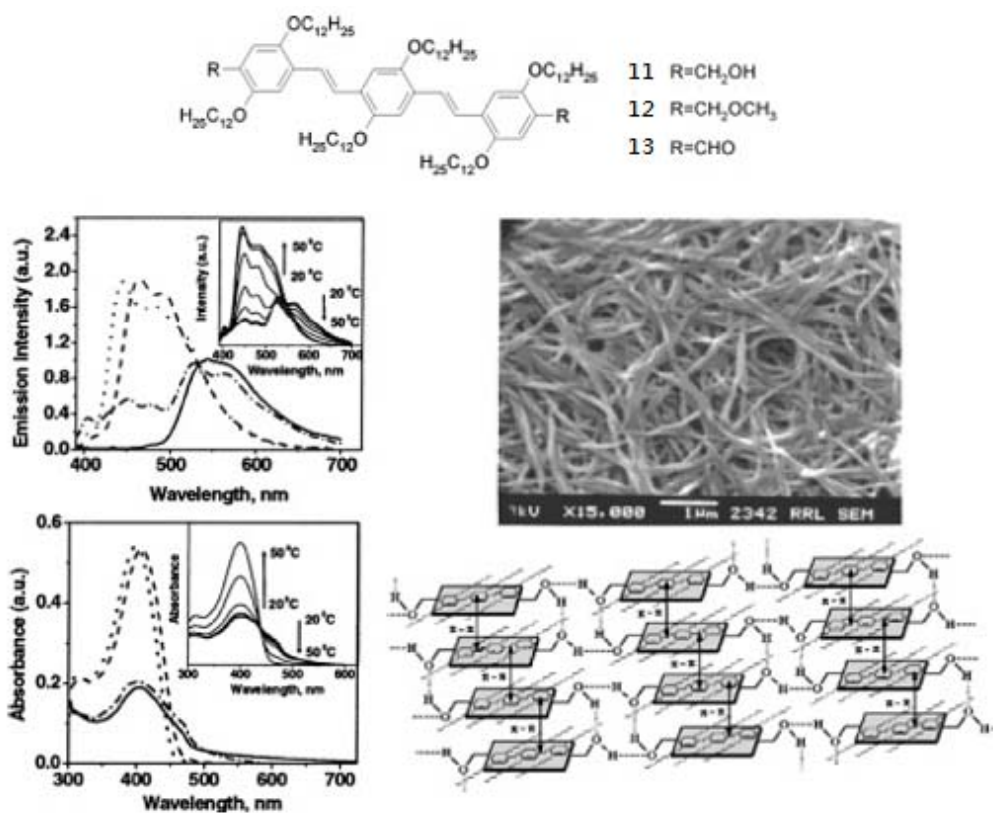
Figure 1.3.2 **OPV** derivatives **11-13** are able to gelate in hexane monitored by temperature-dependent absorption and emission spectra of **11**. For comparison, these spectra are also given in a good solvent like chloroform and as a film from hexane.

The SEM picture of a dried gel of **11** shows an entangled fibrillar network. The self-assembly of the gel is proposed in the scheme.

Supramolecular polymers are constructed from monomeric units that are glued together by reversible noncovalent hydrogen-bond interactions and as such comprise a special class of self-assembled systems. Recently Meijer et al. reported on supramolecular hydrogen-bonded **OPV** dimers (**14**) and polymers (**15**) in which the specific electronic and optical properties of conjugated **OPV** oligomers were combined with the material properties of polymers.[14,15] These polymeric systems are based on the dimerization of strong quadruple hydrogen-bonding ureidopyrimidinone units, resulting in a random coil polymer in solution lacking higher mesoscopic order. The supramolecular polymer could easily be processed, revealing smooth films, and photoinduced electron transfer was observed when blended with a C60 derivative. This blend could be successfully incorporated in a photovoltaic device. Hydrogen bonds have also been used to obtain liquid-crystalline phases. When nucleobases such as adenine and thymine are attached to known mesogens such as alkoxyphenylethynylenes **16-19**, no liquid crystal phase could be observed. However, the 1:1 blends of the complementary nucleobase derivatives resulted in formation of fairly stable lyotropic liquid-crystalline phases, Figure 1.3.3.
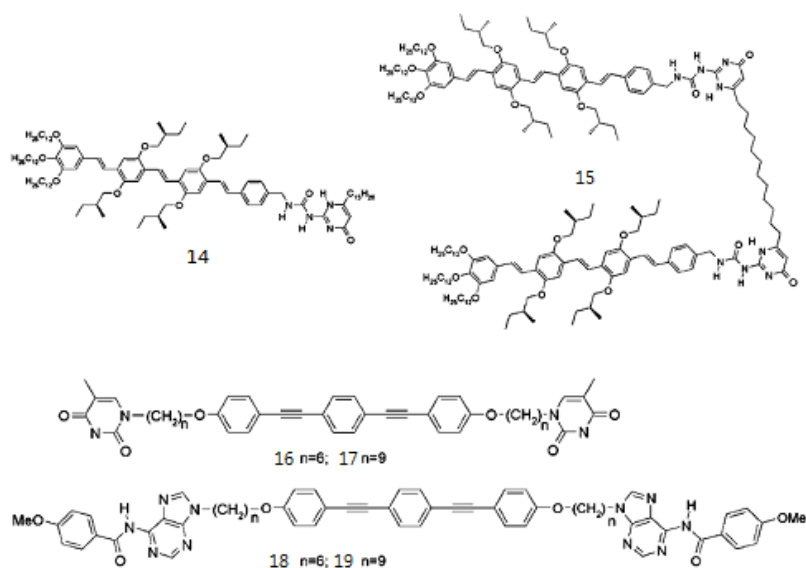
Figure 1.3.3 Conjugated oligomers provided with strong hydrogen-bonding interacting units.

1.4 Sensors and switches from supramolecular chemistry

Molecular recognition is one of the corner stones of supramolecular chemistry. Given any substrate (molecule, cation, or anion), the supramolecular approach is that an appropriate receptor, possessing structural and chemical features suitable for substrate recognition, can be designed. The keyword is shape. This concept is illustrated in Figure 1.4.1.[16]

signalling unit　　receptor　　substrate
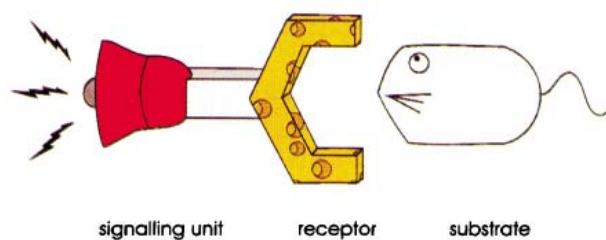
Figure 1.4.1 Designing a receptor for which the substrate has a specific affinity may not suffice; something should signal to the operator that recognition has occurred. Assembling a receptor and a signalling unit makes a sensor.

Most literature reports use fluorescence quenching as the readout mechanism for the sensor response. Very few involve a fluorescence "turn-on" response. Birck et. al. recently published an elegant example involving small molecule sensors that selectively identified iron cations by amplified fluorescence. The greatest advantage of fluorescence "turn-on" sensors related to "turn-off" sensors is the ease of measuring low-concentration contrast relative to a "dark" background. This reduces the likelihood of false positive signals and increases the sensitivity, as demonstrated by numerous studies. Poly[p-(phenyleneethynylene)-alt-(thienyleneethynylene)] (**PPETE**) with a *N,N,N*-trimethylethylenediamino receptor loaded on the thienylene ring (**tmeda-PPETE**) was synthesized on the basis of a strategy we advanced for a series of fluorescence "turn-on" chemosensors (see Figure 1.4.2).[17]

11
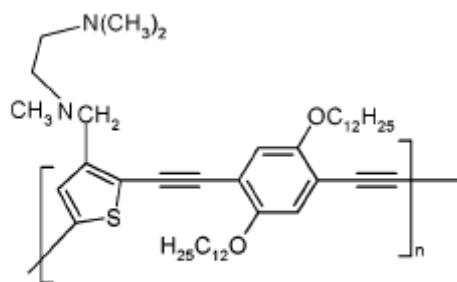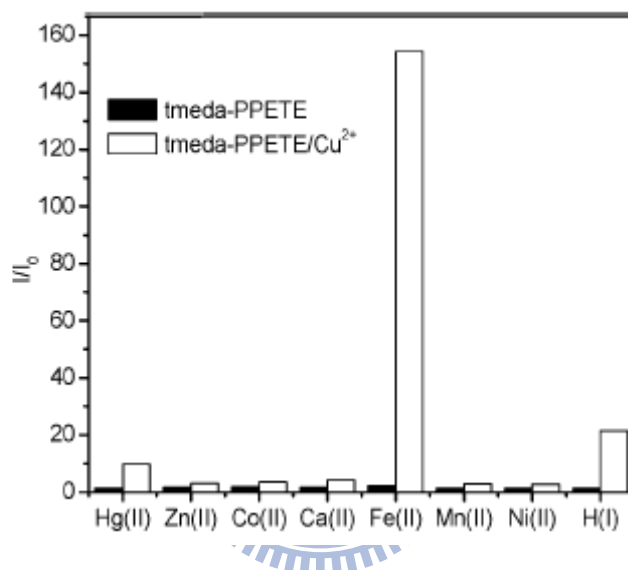
tmeda-PPETE

Figure 1.4.2 Fluorescence response of **tmeda-PPETE**/Cu^{2+} (white) or tmeda-

PPETE (black) to various 10 μM cations in room-temperature solution; the

concentrations of **tmeda-PPETE** (with respect to the repeat unit) and Cu^{2+} were fixed

at 5 μM.

In conventional fluorescent chemosensors, the recognition of the target by the

receptor unit affects the fluorescence properties of a single covalently coupled

fluorescent moiety. As shown in Figure 2.9, a suitable **TSQ** derivative is densely

grafted onto the surface of preformed silica nanoparticles electronic interactions

between the individual chemosensor units enable the free units to recognize the state

of the surrounding complexed ones. As a result, the fluorescence transduction is not

limited to the local site where binding occurs, but it involves a wider region of the

fluorophore network that is able to transfer its excitation energy to the complexed

units. Such behavior leads to an amplification of the fluorescence signal. What they

report here is the first example of amplification in the case an off-on chemosensor due

to its organization onto the surface of silica nanoparticles. They also describe a simple

general model to approach amplification in multifluorophoric systems based on the

localization of the excited states, which is valid for assemblies such as the

supramolecular ones where molecular interactions are weak and do not significantly

perturb the individual electronic states. The introduction of an amplification factor in

particular allows for a simple quantitative estimation of the amplification effects (see

Figure 1.4.3).[18]
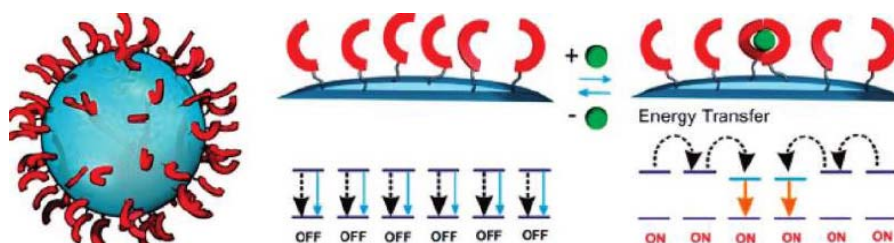
Figure 1.4.3 Schematic diagram of the excited states deactivation processes on the

surfaces of the nanoparticles.

1.5 AIM

In the present study, our strategy is to extend the π-conjugated system from H-acceptor emitters of small molecules to light-emitting H-acceptor polymers. A series of novel homopolymeric and random-copolymeric H-acceptor emitters containing carbazole moieties (to increase T_g values and hole-transporting properties of PLEDs) and three-conjugated aromatic rings, including one pendent pyridyl terminus (as the H-acceptor site) and two lateral methoxyl groups on the middle rings (to increase solubility after polymerization), were successfully synthesized. By incorporating with different generations of OXD dendritic H-donors bearing benzoic acids, the supramolecular side-chain copolymers (i.e., H-bonded dendritic complexes) were consecutively constructed. Hopefully, supramolecular dendrimers bearing light-emitting H-acceptor polymers (in comparison with small molecular emitters) will have a better film-forming property by the spin-coating process, which may eventually be more useful in PLED device applications.

In our previous work, the mesomorphic and photophysical properties of the H-bonded trimers and polymer networks can be easily adjusted by tuning the non-photoluminescent H-donor acids (or H-donor polymers) and fluorescent H-acceptors (small molecules) in the H-bonded complexes. Unique mesomorphic properties can be introduced to these supramolecular structures containing

non-mesogenic H-acceptor emitters. In the meanwhile, the emission properties of

bis-pyridyl H-acceptor emitters can be manipulated by their surrounding

non-photoluminescent proton donors. Moreover, new light-emitting H-bonded

side-chain dendritic complexes containing side-chain H-acceptor copolymers and

electron-transporting H-donor dendrimers have been developed recently, where

side-chain H-acceptor copolymers were composed of light-emitting H-acceptor and

hole-transporting (carbazole) moieties. In this report, H-bonded side-chain copolymer

and homopolymer complex networks containing non-photoluminescent H-donor

(benzoic acid) and fluorescent H-acceptor pendants, which involve three-conjugated

aromatic rings with pyridyl terminus and lateral methoxyl groups on the middle rings

(to increase solubility after polymerization), were successfully synthesized. The

copolymerization of H-donor (benzoic acid) and fluorescent H-acceptor monomers

with different molar ratios is to avoid the spontaneous aggregation of the π-conjugated

H-acceptor emitters and further to tune their emission colors. In addition, the

processes of blending H-donor and H-acceptor homopolymers to form H-bonded

homopolymer complexes are prepared for comparative purposes. Accordingly,

H-bonded effects on the mesomorphic, photophysical, and electro-optical properties

of these H-bonded polymer networks are investigated in the present work. Moreover,

herein we design and synthesize a side-chain conjugated polymer with pyridyl

pendant group as receptors for analyte matirals. The selectivity and sensitivity of polymer sensor, titration experiments were conducted with an addition of various metal ions. In addition, compare the sensitivity of polymer with its complementary monomer, PL-quenching characteristics toward Cu^{2+} ion were investigated.

Chapter 2

Study of Supramolecular Side-Chain Copolymers Containing Light-Emitting H-Acceptors and Electron-Transporting Dendritic H-Donors

2.1 Abstract

A novel light-emitting hydrogen-bonded (H-) acceptor **PBB** (**M1**) containing three conjugated aromatic rings, including one pyridyl terminus and two lateral methoxyl groups (on the middle ring), was successfully synthesized via Horner-Wadsworth-Emmons (HWE) olefination and Sonogashira coupling reaction. Moreover, different molar ratios of light-emitting H-acceptor monomer **PBB** (**M1**) and hole-transporting monomer **CAZ** (**M2**) bearing a carbazole unit were copolymerized through free radical polymerization to obtain light emitting and hole-transporting H-acceptor copolymers (**P1**-**P5**). H-acceptor copolymers **P3** and **P4** were complexed with different generations of dendritic H-donors (**G1COOH-G3COOH**) bearing 1,3,4-oxadiazole (**OXD**) dendrons and terminal benzoic acids via H-bonded self-assembly to form supramolecular side-chain copolymers (i.e., H-bonded dendritic complexes). In contrast to H-acceptor homopolymer **P1** (**HPBB**), H-acceptor copolymers **P2**-**P4** incorporated with

17

carbazole (**CAZ**) moieties effectively enhance the glass transition temperatures (T_gs) and minimize the interchain interations of the light-emitting H-acceptor units, and similar effects occur in their H-bonded dendritic complexes. In addition, red shifts of photoluminescence (PL) emissions in H-bonded dendritic complexes can be tuned up to 61 nm. Furthermore, H-bonded dendritic complexes excited at 305 nm of **OXD** absorption can create a stronger fluorescence than that excited at 397 nm of **PBB** absorption, indicating that the intensity of the sensitized emission of **PBB** (by energy transfer from **OXD** absorption at 305 nm) is even stronger than that of a direct emission of **PBB** (by merely **PBB** absorption at 397 nm). The **OXD** dendritic wedges in H-bonded dendritic complexes can lower the LUMO energy levels and provide a better electron injection property. H-acceptor polymer **P4** and its H-bonded dendritic complexes showed electroluminescence (EL) emissions in the range of 464-519 nm from blue to green. In addition, a PLED device containing H-bonded dendritic complex **P4/G1COOH** showed an EL emission of 519 nm under a turn-on voltage of 6.5 V, with a maximum luminance of 408 cd/m^2 at 18 V and a luminance efficiency of 0.39 cd/A at 100 mA/cm^2, respectively.

2.2 Introduction

In recent years, polymeric materials based on spontaneous formation of supramolecular architectures by self-assembly of various organic molecular components have attracted great attention in areas ranging from chemistry to materials science.[1,2] Simple association of two complementary compounds through specific noncovalent interactions, such as hydrogen-bonded (H-bonded),[2,19-26] ionic,[27,28] and metal-coordinative[29-32] interactions between molecular components, can give rise to unique properties and phase structures, which are not possessed by the individual components. Intensive researches have been directed toward functional supramolecular systems to control the dimensionality and shape of self-assembled structures through molecular design, but it remains a challenge driven by a wide variety of potential applications in the fields of catalyzes, microelectronics, nonlinear optics, sensors, and display technologies. Since the first polymeric light-emitting diode (PLED) based on poly(p-phenylenevinylene) (PPV) was reported by Burroughes et al.,[33] various kinds of conjugated main-chain and side-chain polymers have been developed for electroluminescent (EL) devices.[34-37] Future applications of PLEDs to full-color and large-area flat panel displays become possible due to their high luminescence efficiency, low cost, high flexibility, and easy fabrication of spin-coating technique.[38] However, the most important problem with the π-conjugated

systems is their tendency to form aggregates/excimers via π-π interactions in the solid

state, which will lead to red shifts or low-energy band gaps of emission spectra,

self-quenching of excitons, and reduction of fluorescence quantum efficiencies. To

overcome this problem, one of the approaches is to introduce dendritic architectures

into the π-conjugated systems so as to prevent close chains from packing and thus to

increase the polymer luminescent efficiency and reduce the tendency of aggregation.

For instance, Fréchet-type poly(aryl ether) dendrons attached to fluorene units were

reported by Carter et al.[39] to demonstrate the shielding effect by attaching dendritic

side chains to the conjugated polyfluorene backbones, which improved the

luminescence properties of these materials due to the reduction of both

aggregates/excimers in solution and solid states. Müllen et al.[40] prepared

polyfluorene-based conjugated polymers with bulky polyphenylene dendritic

substituents at C-9 position, which suppressed the formation of aggregates with long

wavelength emissions, and thus a pure blue emission was acquired. More recently, a

number of dendrimers have been reported for a wide variety of applications in such

EL device[41-51] and photovoltaic (PV) cell[52,53] materials. In our previous work,[54]

H-donor dendrimers with a benzoic acid terminus were singly/doubly H-bonded to

mono/bis-pyridyl H-acceptor emitters to form several series of novel supramolecular

dendrimers, whose emission colors could be easily adjusted by their

non-light-emitting H-donors. Moreover, the higher generation of dendritic sizes could afford stronger siteisolation and dendron-dilution effects, so better energy transfer along with higher fluorescence quantum efficiencies were achieved.

In the present study, our strategy is to extend the π-conjugated system from H-acceptor emitters of small molecules to light-emitting H-acceptor polymers. According to Scheme 1, a series of novel homopolymeric and random-copolymeric H-acceptor emitters containing carbazole moieties (to increase T_g values and hole-transporting properties of PLEDs) and three-conjugated aromatic rings, including one pendent pyridyl terminus (as the H-acceptor site) and two lateral methoxyl groups on the middle rings (to increase solubility after polymerization), were successfully synthesized. By incorporating with different generations of **OXD** dendritic H-donors bearing benzoic acids (see Figure 2.1), the supramolecular side-chain copolymers (i.e., H-bonded dendritic complexes) were consecutively constructed as shown in Figure 2.2. Hopefully, supramolecular dendrimers bearing light-emitting H-acceptor polymers (in comparison with small molecular emitters) will have a better film-forming property by the spin-coating process, which may eventually be more useful in PLED device applications. Accordingly, H-bonded effects on the thermal, photophysical, and photo-/electro-luminescent properties of these supramolecules in the solid state will be illustrated.
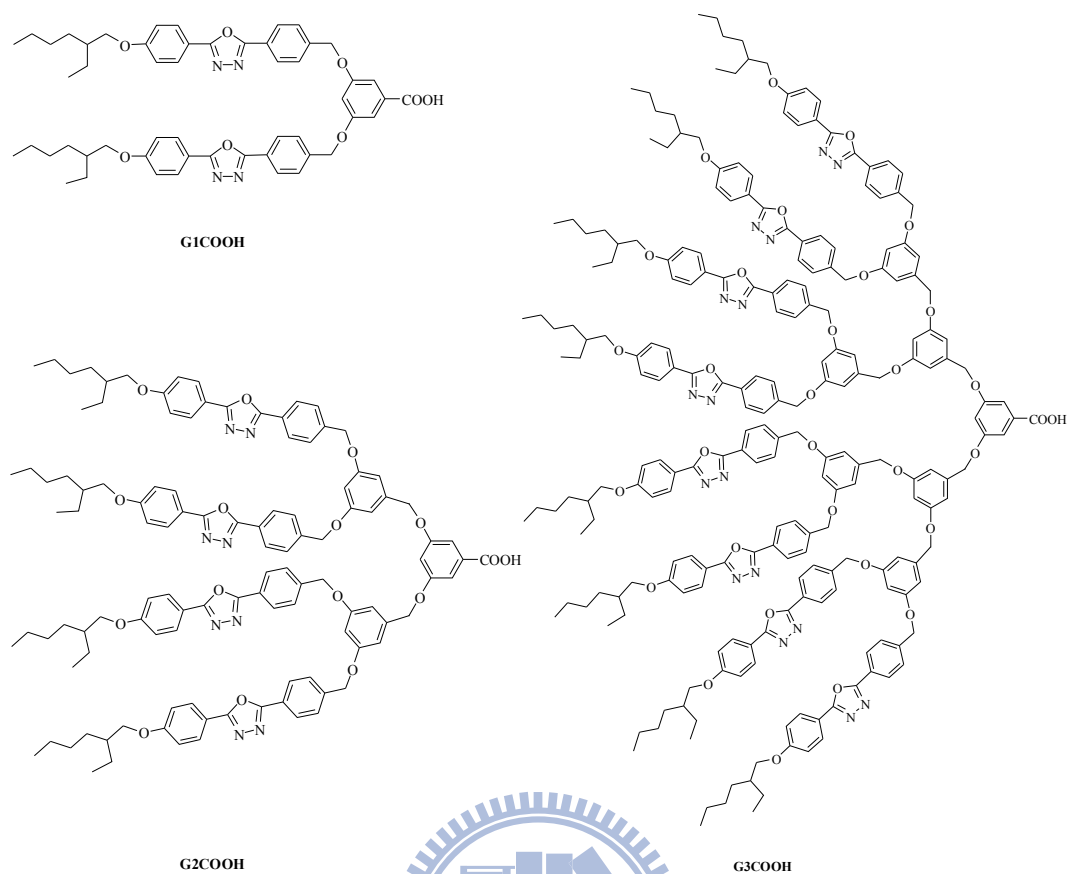
Figure 2.1 Different generations of dendritic H-donors (**G1COOH–G3COOH**) used in H-bonded side-chain dendritic complexes.
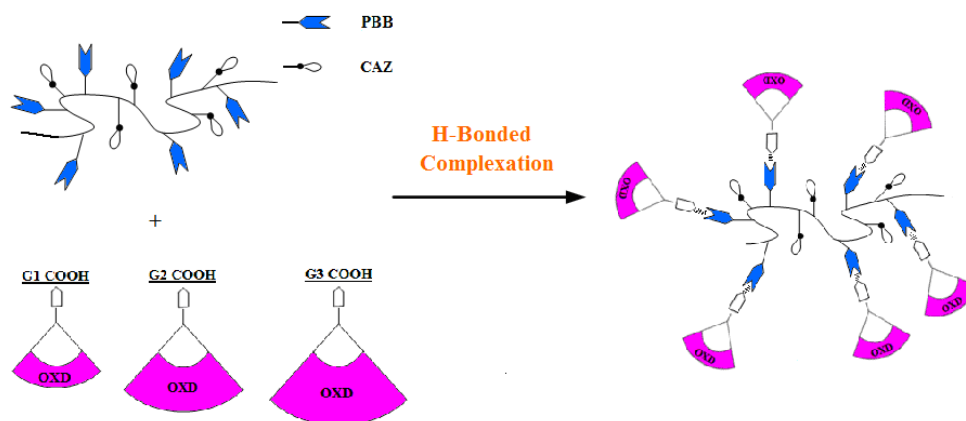
Figure 2.2 Schematic representation of H-acceptor copolymers and H-bonded side-chain dendritic complexes bearing different generations of dendritic H-donors (**G1COOH–G3COOH**).

2.3 Experimental Section

2.3.1 Measurements and Characterization

^{1}H NMR spectra were recorded on a Varian Unity 300 MHz spectrometer using $CDCl_3$ and DMSO-d_6 as solvents. Elemental analyses were performed on a HERAEUS CHN-OS RAPID elemental analyzer. High resolution electron impact mass data were obtained on a Finnigan-MAT-95XL. Phase transition temperatures were determined by differential scanning calorimetry (DSC, model: Perkin Elmer Diamond) under N_2 with a heating and cooling rate of 10 °C/min and polarizing optical microscope (POM, model: Leica DMLP) equipped with a hot stage. Thermogravimetric analyses (TGA) were carried out on a TA Instruments Q500 thermogravimetric analyzer at a heating rate of 20 °C/min under nitrogen. Gel permeation chromatography (GPC) analyses were conducted on a Water 1515 separation module using polystyrene as a standard and THF as an eluant. Fourier transform infrared (FTIR) spectra of samples (dispersed in KBr disks) were recorded on a Perkin-Elmer Spectrum 100 Series. Synchrotron powder X-ray diffraction (XRD) measurements were performed at the beamline BL17A of the National Synchrotron Radiation Research Center (NSRRC), Taiwan (for details of the XRD installation, see Supporting Information). UV-vis absorption spectra were recorded on a HP G1103A spectrophotometer, and photoluminescence (PL) spectra were obtained on a Hitachi

F-4500 spectrophotometer in dilute THF solutions (10^{-6} M). The PL quantum yields (Φ_{PL}) of polymers were measured with 9,10-diphenylanthracene as a reference (in cyclohexane, Φ_{PL} = 0.9).[55] Thin films in UV-vis and PL measurements were prepared by spin-coating of THF solutions (with a concentration of 10 mg/mL) at 3000 rpm on a quartz substrate. Cyclic voltammetry (CV) measurements were performed at a scanning rate of 100 mV/s in a solution of 0.1 M tetrabutylammonium hexafluorophosphate (Bu_4NPF_6) dissolved in acetonitrile at room temperature using an Autolab PGSTAT30 potentiostat/galvanostat with a standard three-electrode electrochemical cell. A platinum disk working electrode, a Pt wire counter electrode, and an Ag/AgCl reference electrode were used. The sample films were coated on the surface of a platinum disk by the solution-dipping process from THF solutions.

A series of electroluminescence (EL) devices with the configuration of ITO/PEDOT:PSS/polymer (**P4** or its H-bonded dendrimers complexes)/BCP/Alq_3/LiF/Al were made, where BCP (i.e., 2,9-dimethyl-4,7-diphenyl-1,10-phenanthroline) was used as a hole-blocking layer and Alq_3 (i.e., tris(8-hydroxyquinoline)aluminium) was used as an electron-transporting layer. ITO substrates, where glass substrates were coated with indium-tin oxide (ITO) having a sheet resistance of ~20 Ω/square and an effective individual device area of 3.14 mm^2, were routinely cleaned by ultrasonic treatments in

detergent solutions and diluted water, followed by rinsing with acetone and then

ethanol. After drying, ITO substrates were kept in oxygen plasma for 4 min before

being loaded into the vacuum chamber. The

poly(3,4-ethylenedioxythiophene):poly(styrenesulfonate) (PEDOT:PSS) films were

first deposited on pre-cleaned ITO substrates by spin-coating at 6000 rpm for 1 min

and subsequently cured in an oven at 120 °C for 1 h. Then, light-emitting polymers

(**P4** or its H-bonded side-chain dendritic complexes) in THF solutions (10 mg/mL)

were spin-coated onto the PEDOT:PSS layer at 4000–5500 rpm. The thicknesses of

PEDOT:PSS and LED polymers were measured by an Alfa Step 500 Surface Profiler

(Tencor). BCP and Alq$_3$ were thermally deposited at a rate of 1–2 Å/s under a

pressure of ~2 × 10^{-5} torr in an Ulvac Cryogenic deposition system. Under the same

deposition condition, one layer of LiF was thermally deposited as a cathode at a rate

of 0.1–0.2 Å/s, which was followed by capping with aluminum. The

current-voltage-luminescence characteristics were measured in ambient condition by

Keithley 2400 source meter and Newport 1835C optical meter equipped with 818ST

silicon photodiode.

Scheme 2.1   Synthetic Routes of H-Acceptor Monomer and Polymers (P1-P5)[a]

P1 (HPBB), x/y = 1/0
P2 (PBB-CAZ$_1$), x/y = 1/1
P3 (PBB-CAZ$_5$), x/y = 1/5
P4 (PBB-CAZ$_9$), x/y = 1/9
P5 (HCAZ), x/y = 0/1
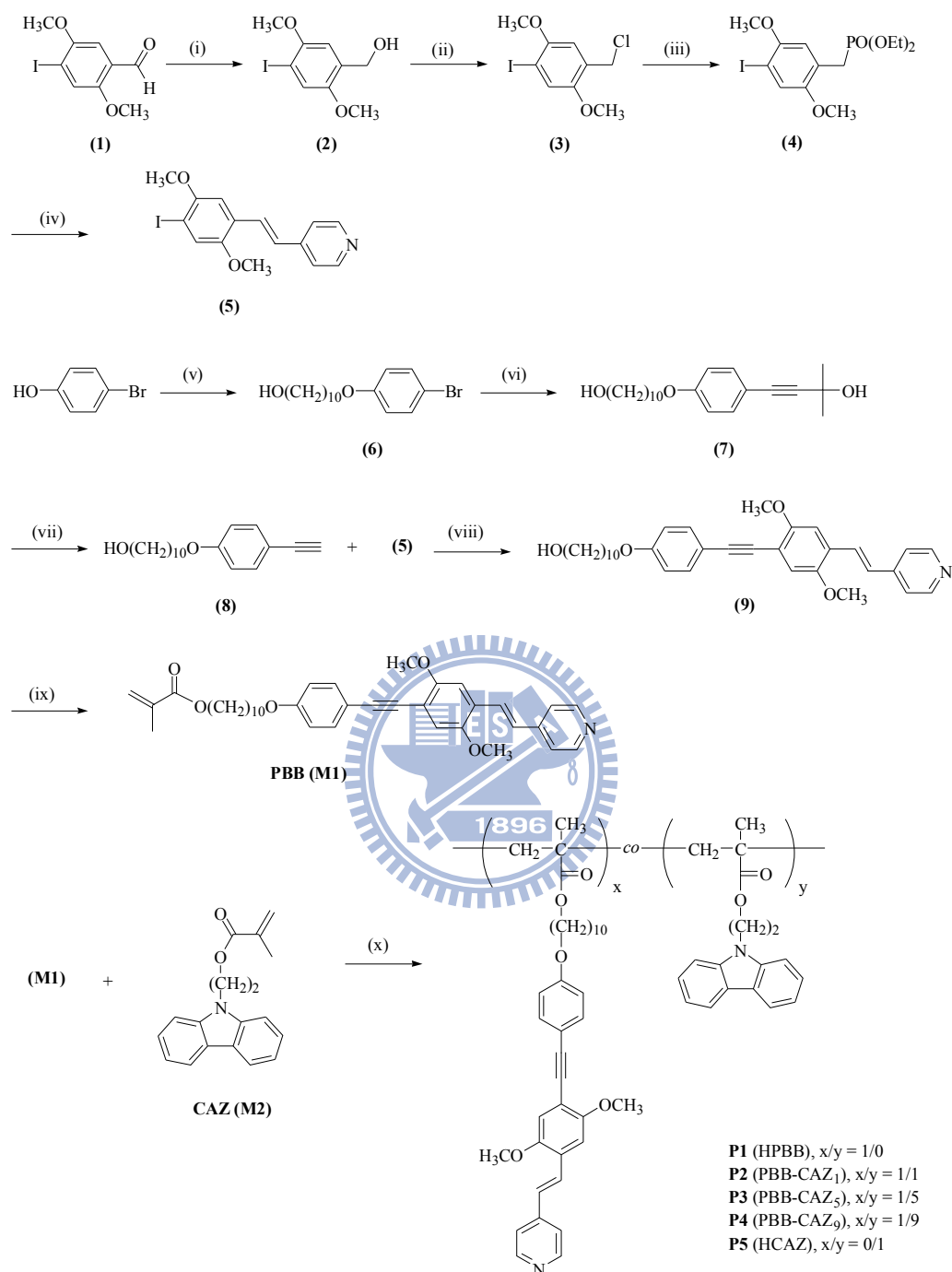
[a] Reagents and conditions: (i) NaBH$_4$, MeOH/THF, room temperature, 1 h; (ii) conc. HCl, dioxane, reflux, 10 h; (iii) P(OEt)$_3$, reflux, 12 h; (iv) pyridine-4-carboxaldehyde, t-BuOK, THF, room temperature, 12 h; (v) 10-bromodecanol, K$_2$CO$_3$, KI, acetone, reflux, 48 h; (vi) 2-methyl-3-butyn-2-ol, Pd(PPh$_3$)$_2$Cl$_2$, CuI, PPh$_3$, Et$_3$N, 70 °C, 12 h; (vii) KOH, dioxane, reflux, 3 h; (viii) Pd(PPh$_3$)$_2$Cl$_2$, CuI, PPh$_3$, Et$_3$N/THF, 50 °C, overnight; (ix) vinyl methacrylate, 1,3-dichloro-1,1,3,3-tetrabutyldistannoxane, 2,6-di-tert-butyl-4-methylphenol, THF, 50 °C, 48 h; (x) AIBN, THF, 60 °C, 24 h.

2.3.2 Materials

Chemicals and solvents were reagent grades and purchased from Aldrich, ACROS, TCI, and Lancaster Chemical Co. Tetrahydrofuran (THF) and triethylamine (Et$_3$N) were distilled to keep anhydrous before use. Azobisisobutyronitrile (AIBN) was recrystallized from methanol before use. The other chemicals were used without further purification. Different generations of dendritic H-donors (**G1COOH–G3COOH**), as shown in Figure 1, used in H-bonded side-chain dendritic complexes were reported in our previous work.[54] 10-Bromodecanol,[56] 1,3-dichloro-1,1,3,3-tetrabutyldistannoxane,[57] and monomer **CAZ (M2)**[58] were prepared by following the already published procedures.

4-Iodo-2,5-dimethoxybenyl alcohol (2). To a stirred solution of 4-iodo-2,5-dimethoxybenzaldehyde **1** (8.0 g, 27.4 mmol) in 200 mL of THF/MeOH (1:1), NaBH$_4$ (0.52 g, 13.7 mmol) was added very slowly to react at room temperature. After 1 h, the solution was cooled to 0 °C by ice bath, acidified with dilute HCl solution, and extracted with ethyl acetate. The resulting materials in organic phase were combined and washed with water. Afterward, the organic extracts were dried over Na$_2$SO$_4$ and evaporated. The purified residue was recrystallized from dichloromethane/2-propanol to give a colorless crystal. Yield: 7.6 g (95%). ^{1}H NMR (300 MHz, CDCl$_3$): δ (ppm) 7.25 (s, 1H), 6.85 (s, 1H), 4.65 (d, J = 6.3 Hz, 2H), 3.85

(s, 3H), 3.82 (s, 3H), 2.22 (t, $J = 6.6$ Hz, 1H).

1-Iodo--4-chloromethyl-2,5-dimethoxybenzene (3). To a stirred solution of **2** (7.0 g, 23.8 mmol) in 1,4-dioxane (200 mL), concentrated HCl (20 mL) was added to reflux for 10 h. After the reaction was completed, the crude mixture was added with water. The organic layer was extracted with ethyl acetate, dried over Na_2SO_4, and evaporated. The residual product was purified by flash column chromatography (silica gel, n-hexane/ethyl acetate 40:1) to give a white solid. Yield: 6.8 g (92%). ^{1}H NMR (300 MHz, CDCl$_3$): δ (ppm) 7.29 (s, 1H), 6.86 (s, 1H), 4.60 (s, 2H), 3.85 (s, 3H), 3.83 (s, 3H).

4-Iodo-2,5-dimethoxybenzyldiethylphosphonate (4). Compound **3** (6.0 g, 19.2 mmol) was mixed with an excess of triethyl phosphite (20 mL), and the mixture was heated to reflux and reacted for 12 h. The excess of triethyl phosphite was removed under reduced pressure, and the crude product was purified by washing with hot hexane to give a white solid. Yield: 7.2 g (90%). ^{1}H NMR (300 MHz, CDCl$_3$): δ (ppm) 7.25 (s, 1H), 6.9 (s, 1H), 4.08−3.99 (m, 4H), 3.83 (s, 3H), 3.80 (s, 3H), 3.20 (d, $J = 21.6$ Hz, 2H), 1.24 (t, 6.9 Hz, 6H).

1-Iodo-2,5-dimethoxy-4-[2-(4-pyridyl)ethenyl]benzene (5). To a solution of pyridine-4-carboxaldehyde (1.86 g, 17.4 mmol) in anhydrous THF (10 mL), a suspension of **4** (6.0 g, 14.5 mmol) and *t*-BuOK (2.93 g, 26.1 mmol) in anhydrous

THF (60 mL) under nitrogen was slowly added. The mixture was stirred to react at room temperature for 12 h. After the reaction was completed, it was quenched with water and extracted with dichloromethane. After that, the organic layer was dried over Na$_2$SO$_4$ and evaporated. The crude product was purified by column chromatography (silica gel, dichloromethane/acetone 30:1) to give a yellow solid. Yield: 3.2 g (60%).

^{1}H NMR (300 MHz, CDCl$_3$): δ (ppm) 8.55 (d, J = 4.5 Hz, 2H), 7.57 (d, J = 16.5 Hz, 1H), 7.37 (d, J = 4.5 Hz, 2H), 7.30 (s, 1H), 7.01 (d, J = 16.5 Hz, 1H), 7.00 (s, 1H), 3.88 (s, 3H), 3.84 (s, 3H).

10-(4-Bromophenoxy)-decan-1-ol (6). To a stirred solution of 4-bromophenol (4.0 g, 23.1 mmol) in acetone (200 mL), potassium carbonate (9.6 g, 69.3 mmol), 10-bromodecanol (6.6 g, 27.7 mmol), and a few amounts of potassium iodide (ca. 10 mg) were added to reflux for 48 h under nitrogen. After cooling to room temperature, the solvent was removed under reduced pressure, and the residue was taken up in water and extracted with ethyl acetate. Next, the organic layer was dried over Na$_2$SO$_4$ and evaporated. The crude product was purified by column chromatography (silica gel, n-hexane/ethyl acetate 3:1) to give a white solid. Yield: 6.1 g (80%). ^{1}H NMR (300 MHz, CDCl$_3$): δ (ppm) 7.33 (d, J = 9.0 Hz, 2H), 6.75 (d, J = 9.0 Hz, 2H), 3.89 (t, J = 6.3 Hz, 2H), 3.62 (t, J = 6.6 Hz, 2H), 1.78−1.69 (m, 2H), 1.59−1.50 (m, 2H), 1.41−1.29 (m, 12H).

4-[4-(10-Hydroxy-decyloxy)-phenyl]-2-methyl-3-butyn-2-ol (7). A solution of **6** (4.0 g, 12.1 mmol), PPh_3 (63.1 mg, 0.24 mmol), and CuI (45.6 mg, 0.24 mmol) in dry Et_3N (80 mL) was degassed with nitrogen for 5 min. Then, the solution was added with 2-methyl-3-butyn-2-ol (2.0 g, 24.2 mmol) and $Pd(PPh_3)_2Cl_2$ (84.1 mg, 0.12 mmol) at room temperature, and the reaction mixture was stirred to react at 70 °C for 12 h. The mixture was filtered and the solvent was removed in vacuum. The crude mixture was extracted using ethyl acetate, and the extract was washed with water, dried over Na_2SO_4, and then evaporated. Subsequently, the crude product was purified by column chromatography (silica gel, n-hexane/ethyl acetate 1:1) to give a light yellow solid. Yield: 3.14 g (78%). ^1H NMR (300 MHz, $CDCl_3$): δ (ppm) 7.31 (d, $J = 9.0$ Hz, 2H), 6.79 (d, $J = 9.0$ Hz, 2H), 3.92 (t, $J = 6.6$ Hz, 2H), 3.62 (t, $J = 6.6$ Hz, 2H), 1.77−1.70 (m, 2H), 1.60 (s, 6H), 1.58−1.50 (m, 2H), 1.42−1.29 (m, 12H).

4-Ethynyl-1-(10-hydroxydecan-1-yloxy)benzene (8). A stirred solution of **7** (2.5 g, 7.5 mmol) and finely powdered KOH (1.26 g, 22.5 mmol) in 1,4-dioxane (80 mL) was refluxed under nitrogen for 3 h. After cooling to room temperature, the solvent was removed under reduced pressure and the residue was taken up in water, and then the mixture was extracted with ethyl acetate and acidified with 3 N HCl (150 mL). The organic solution was washed with water, dried over Na_2SO_4, and then evaporated. Afterward, the crude product was purified by column chromatography (silica gel,

n-hexane/ethyl acetate 5:1) to give a light yellow solid. Yield: 1.75 g (85%). ^{1}H NMR

(300 MHz, CDCl$_3$): δ (ppm) 7.39 (d, J = 9.0 Hz, 2H), 6.80 (d, J = 9.0 Hz, 2H), 3.92 (t,

J = 6.6 Hz, 2H), 3.62 (t, J = 6.6 Hz, 2H), 2.97 (s, 1H), 1.80−1.70 (m, 2H), 1.57−1.50

(m, 2H), 1.42−1.29 (m, 12H).

1-{[4-(10-Hydroxy-decyloxy)-phenyl]-ethynyl}-2,5-dimethoxy-4-[2-(4-pyridyl)e

thenyl]benzene (9). A solution of **5** (1.0 g, 2.72 mmol), **8** (0.78 g, 2.85 mmol), and

PPh$_3$ (14.1 mg, 0.054 mmol) in 80 mL of dry Et$_3$N/THF (1:1) was degassed with

nitrogen for 5 min. Then, the solution was added with CuI (10.3 mg, 0.054 mmol) and

Pd(PPh$_3$)$_2$Cl$_2$ (19.1 mg, 0.027 mmol) at room temperature, and it was stirred to react

at 50 °C overnight. The mixture was filtered and the solvent was removed in vacuum.

The crude mixture was extracted using dichloromethane, and the extract was washed

with water, dried over Na$_2$SO$_4$, and then evaporated. After that, the crude product was

purified by column chromatography (aluminum oxide, dichloromethane/acetone 40:1)

to give a yellow solid. Yield: 1.28 g (92%). ^{1}H NMR (300 MHz, CDCl$_3$): δ (ppm)

8.56 (d, J = 4.5 Hz, 2H), 7.66 (d, J = 16.5 Hz, 1H), 7.50 (d, J = 9.0 Hz, 2H), 7.39 (d, J

= 4.5 Hz, 2H), 7.11 (s, 1H), 7.04 (d, J = 16.5 Hz, 1H), 7.04 (s, 1H), 6.87 (d, J = 9.0

Hz, 2H), 3.99 (t, J = 6.6 Hz, 2H), 3.97 (s, 3H), 3.89 (s, 3H), 3.62 (t, J = 6.6 Hz, 2H),

1.81−1.72 (m, 2H), 1.57−1.51 (m, 2H), 1.41−1.30 (m, 12H).

1-{[4-(10-Methacryloyloxy-decyloxy)-phenyl]-ethynyl}-2,5-dimethoxy-4-[2-(4-p

yridyl)ethenyl]benzene, PBB (M1). To a Schlenk tube, compound **9** (1.0 g, 1.95 mmol), vinyl methacrylate (0.55 g, 4.88 mmol), 1,3-dichloro-1,1,3,3-tetrabutyldistannoxane (43.12 mg, 0.078 mmol), and 2,6-di-tert-butyl-4-methylphenol (25.78 mg, 0.117 mmol) in dry THF (2 mL) were purged with nitrogen for 15 min at room temperature. The tube was sealed and heated with stirring at 50 °C for 2 days. After cooling to room temperature, the reaction mixture was extracted using dichloromethane, and the extract was washed with water, dried over Na_2SO_4, and then evaporated. The crude product was purified by column chromatography (aluminum oxide, n-hexane/dichloromethane 1:1) and then washed with hexane to give a light yellow solid. Yield: 0.97 g (85%). ^{1}H NMR (300 MHz, $CDCl_3$): δ (ppm) 8.57 (d, J = 4.5 Hz, 2H), 7.66 (d, J = 16.5 Hz, 1H), 7.50 (d, J = 9.0 Hz, 2H), 7.39 (d, J = 4.5 Hz, 2H), 7.11 (s, 1H), 7.04 (d, J = 16.5 Hz, 1H), 7.04 (s, 1H), 6.87 (d, J = 9.0 Hz, 2H), 6.10 (s, 1H), 5.55 (s, 1H), 4.14 (t, J = 6.6 Hz, 2H), 3.97 (t, J = 6.6 Hz, 2H), 3.96 (s, 3H), 3.89 (s, 3H), 3.62 (t, J = 6.6 Hz, 2H), 1.95 (s, 3H), 1.81−1.75 (m, 2H), 1.58−1.53 (m, 2H), 1.42−1.30 (m, 12H). HRMS (EI): calcd for $C_{37}H_{43}NO_5$, 581.3141; found 581.3146. Anal. Calcd for $C_{37}H_{43}NO_5$: C, 76.39; H, 7.45; N, 2.41. Found: C, 76.15; H, 7.37; N, 2.44.

General Procedure for the Syntheses of Homopolymers and Copolymers (P1-P5). All polymerization procedures were carried out according to the free radical

polymerization described by the following steps. To a Schlenk tube, 1.5 g of monomers **M1**, **M2,** or the mixture of **M1** and **M2** were dissolved in dry THF (7.5 mL) with 20 wt% of monomer concentration and AIBN (2 mol% of total monomer concentration) as an initiator. The solution was degassed by three freeze-pump-thaw cycles and then sealed off. The reaction mixture was stirred and heated at 60 °C for 24 h. After polymerization, the polymer was precipitated into diethyl ether. Then, the precipitated polymer was collected, washed with diethyl ether, and dried under high vacuum.

P1 (HPBB). ^{1}H NMR (300 MHz, DMSO-d_6): δ (ppm) 8.44 (br, 2H), 7.53−6.77 (br, 10H), 3.80 (br, 10H), 1.66−1.24 (br, 21H).

P2 (PBB-CAZ$_1$). ^{1}H NMR (300 MHz, DMSO-d_6): δ (ppm) 8.46 (br, 2H), 7.97−6.75 (br, 18H), 3.88 (br, 14H), 1.43−1.08 (br, 26H).

P3 (PBB-CAZ$_5$). ^{1}H NMR (300 MHz, DMSO-d_6): δ (ppm) 8.48 (br, 2H), 7.92−6.76 (br, 50H), 4.33−3.83 (br, 30H), 1.43−-0.06 (br, 46H).

P4 (PBB-CAZ$_9$). ^{1}H NMR (300 MHz, DMSO-d_6): δ (ppm) 8.48 (br, 2H), 7.88−6.76 (br, 80H), 4.34−3.83 (br, 45H), 1.43−-0.16 (br, 65H).

P5 (HCAZ). ^{1}H NMR (300 MHz, DMSO-d_6): δ (ppm) 7.89 (br, 2H), 7.32−7.00 (br, 6H), 4.34−3.94 (br, 4H), 0.99−-0.15 (br, 5H).

Sample Preparation of Supramolecular Side-Chain Copolymers (i.e.,

H-Bonded Side-Chain Dendritic Complexes). H-bonded side-chain dendritic complexes were made of appropriate (fully H-bonded) molar ratios of H-acceptor copolymers (**P3** and **P4**) and dendritic H-donors (**G1COOH–G3COOH**) in THF solutions, and then the solvent was removed by slow evaporation and followed by drying under vacuum at 50 °C.

2.4 Results and Discussion

2.4.1 Syntheses and Characterization of Polymers

The syntheticroutes of monomer **PBB** (**M1**) and polymers **P1-P5** are shown in Scheme 1. The starting material **1** (i.e., 4-iodo-2,5-dimethoxybenzaldehyde) was synthesized by following a reported procedure[59] via iodination of 2,5-dimethoxybenzaldehyde with iodine and silver nitrate in the presence of methanol. The aldehyde group of compound 1 was further reduced to a benzyl alcohol and then was transformed into a benzyl chloride group with hydrochloric acid in the presence of 1,4-dioxane to givecompound **3**, which was converted to the corresponding phosphonate ester **4** by Michaelis-Arbuzov reaction under the triethyl phosphite treatment with a yield of 90%.[60] Compound **5** was prepared by means of Horner-Wadsworth-Emmons (HWE) olefination reaction between compound **4** and pyridine-4-carboxaldehyde using potassium tert-butoxide as a base in THF to give 60% yield.[61] Compound **6** in 80% yield was obtained by reaction of 4-bromophenol

with 10-bromodecanol under Williamson etherification condition (K_2CO_3/acetone). The latter Sonogashira (Pd-catalyzed) coupling reaction of compound **6** with 2-methyl-3-butyn-2-ol afforded compound **7** in the presence of a catalytic amount (1 mol %) of Pd(PPh$_3$)$_2$Cl$_2$ in Et$_3$N with a yield of 78%,[62] which was then deprotected with KOH/1,4-dioxane to acquire compound **8** in 85% yield. Subsequently, the three-conjugated rings of compound **9** with a yield of 92% was prepared through a second Sonogashira coupling reaction between compounds **8** and **5** in Et$_3$N/THF (1:1). Finally, monomer **PBB** (**M1**) with a high yield of 85% was obtained by transesterification reaction[63] between compound **9** and an excess amount (2.5 equiv) of vinyl methacrylate in the presence of a higher concentration of 1,3-dichloro-1,1,3,3-tetrabutyldistannoxane as a catalyst and 2,6-di-tert-butyl-4-methylphenol as an inhibitor in THF. The yield is much better than that reported[64] by our previous esterification reaction. The final chemical structure of monomer **PBB** (**M1**) was confirmed by ^{1}H NMR spectroscopy, HRMS, and elemental analysis (see Experimental Section and Appendix A1).

The polymerization reactions with good yields (ranging 73-88%) were carried out in THF at 60 °C through free radical polymerization in the presence of azobis(isobutyronitrile) (AIBN) as an initiator. The feeding ratios of monomers **PBB** (**M1**) to **CAZ** (**M2**) were 1:0, 1:1, 1:5, 1:10, and 0:1, respectively, to acquire

H-acceptor polymers **P1-P5**. The chemical structures of polymers **P1-P5** in DMSO-d_6 were verified by ^{1}H NMR spectroscopy in comparison with those of their monomers **PBB** (**M1**) and **CAZ** (**M2**) (see Appendix A1). In the ^{1}H NMR spectra of polymers, the disappearance of proton peaks in the region of vinyl (methacrylate) groups with chemical shifts at 5.4-6.1 ppm indicated that all monomers were reacted. The copolymer compositions were estimated by comparing the relative integration areas of the peaks at 8.5 ppm (corresponding to two protons of α-pyridyl groups in **PBB**) and 6.7-7.9 ppm (corresponding to the other overlapped aromatic protons of **PBB** and **CAZ** units), respectively. Regarding the compositions of copolymers **P2-P4**, the actual compositions of **P2** and **P3** are very close to the feeding ratios of monomers, except that **P4** has a slightly lower molar ratio than that of feeding. All polymers are soluble in common organic solvents, such as THF, DMSO, and DMF. The weightaverage molecular weights (Mw) and polydispersity indexes (PDI) of polymers **P1-P5**, determined by gel permeation chromatography (GPC) with THF as the eluting solvent and polystyrene as standards, are in the range 14400-53100 g/mol and 1.72-3.69, respectively. The compositions (input and output molar ratio), molecular weights (Mw), PDI values, and yields of polymers **P1-P5** are summarized in Table 2.1.

Table 2.1   Composition, Yields, Molecular Weights, and Degradation Temperatures of Polymers P1-P5

| polymer | molar ratio | | yield (%) | M_w (g/mol)[b] | PDI (M_w/M_n)[b] | T_d (°C)[c] |
	feed monomer (PBB/CAZ)	polymers (x/y)[a]				
P1 (HPBB)	1/0	1/0	73	14400	1.72	357
P2 (PBB-CAZ₁)	1/1	1/1	88	38100	3.24	323
P3 (PBB-CAZ₅)	1/5	1/5	85	45600	2.99	305
P4 (PBB-CAZ₉)	1/10	1/8.75	81	53100	3.69	300
P5 (HCAZ)	0/1	0/1	75	47800	3.65	276

[a] Determined by ^{1}H NMR spectra.

[b] Weight-average molecular weight (M_w) and polydispersity index (PDI) determined by GPC in THF using polystyrene as a standard.

[c] Temperature (°C) at 5% weight loss measured by TGA at a heating rate of 20 °C min^{-1} under nitrogen.
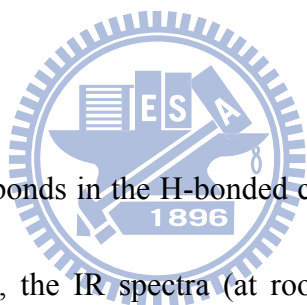
The existence of hydrogen bonds in the H-bonded complexes can be confirmed by FTIR spectroscopy. Therefore, the IR spectra (at room temperature) of H-acceptor polymer **P3**, H-donor **G1COOH**, and H-bonded side-chain dendritic complexes (side-chain copolymers with pendent dendrimers) **P3**/**G1COOH** shown in Figure 2.3 are compared to analyze the formation of hydrogen bonds between H-acceptor polymer **P3** and H-donor dendrimer **G1COOH**. In contrast to the O-H bands of pure H-donor (H-bonded dendritic dimer) **G1COOH** at 2627 and 2562 cm^{-1}, the weaker O-H bands observed at 1925 and 2500 cm^{-1} in the H-bonded side-chain dendritic complex **P3**/**G1COOH** are indicative of stronger hydrogen bonding between the pyridyl groups of polymer **P3** and the carboxylic acid of **G1COOH** in the H-bonded

complex. On the other hand, a stretching vibration of C=O at 1695 cm^{-1} in pure

G1COOH is shifted toward higher wavenumber and overlapped with the band of the

ester carbonyl groups at 1725 cm^{-1} in the H-bonded dendritic complex **P3**/**G1COOH**,

which shows that the carbonyl group was in a less associated state than that in the

pure H-bonded dimer state of H-donor **G1COOH**. These results suggest that

hydrogen bonds were formed between **P3** and **G1COOH** in the solid state of the

H-bonded dendritic complex **P3**/**G1COOH**. The other H-bonded complexes

discussed in this study should have similar consequences as the demonstrated

H-bonded complexes.[65]
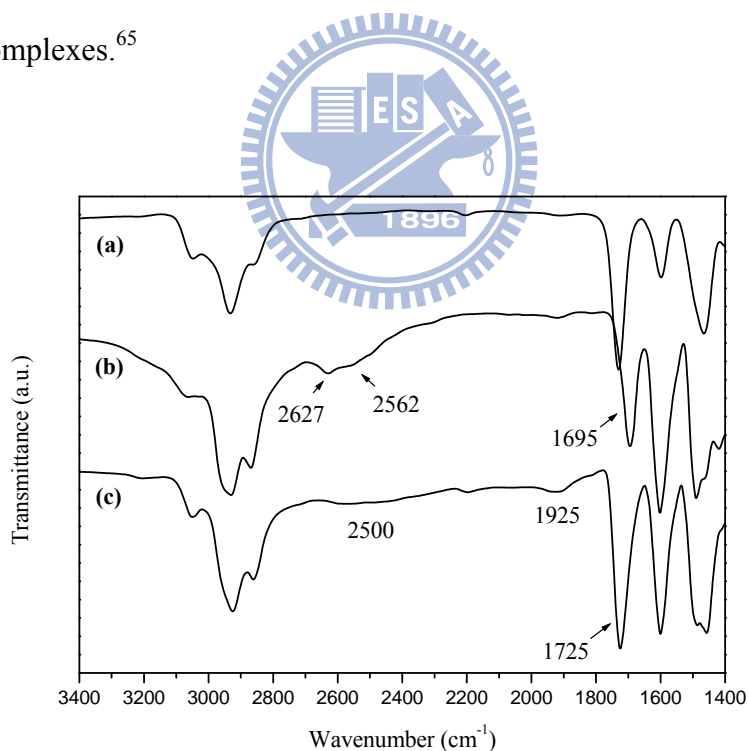
Figure 2.3 FTIR spectra of (a) H-acceptor polymer **P3 (PBB-CAZ$_5$)**, (b)

dendritic H-donor **G1COOH**, and (c) H-bonded side-chain dendritic complexes

P3/**G1COOH** at room temperature.

2.4.2 Thermal Properties

The thermal stabilities of polymers **P1-P5** were evaluated by thermogravimetric analyses (TGA), and their corresponding data are also summarized in Table 2.1. The TGA analyses indicate that the degradation temperatures (T_d) of polymers with 5% weight loss (under nitrogen) are between 276 and 357 °C, and T_d values decrease with increasing the molar ratio of monomer **CAZ** (**M2**) monotonically. Hence, homopolymers **P1** (**HPBB**) and **P5** (**HCAZ**) have the highest and lowest thermal stabilities, respectively, which means that the carbazole unit of monomer **CAZ** (**M2**) is less stable than the light-emitting unit of **PBB** (**M1**) in polymers **P1-P5** (see Supporting Information). The phase transition temperatures of polymers **P1-P5** and H-bonded side-chain dendritic complexes containing H-acceptor polymers **P2** (**PBB-CAZ1**), **P3** (**PBB-CAZ5**), and **P4** (**PBB-CAZ9**), which were determined by differential scanning calorimetry (DSC) under nitrogen, are summarized in Table 2. Polymers **P1-P5** only show glass transition temperatures (T_gs), but without any melting and crystallization peaks. The T_g values of polymers **P1-P5** (ranging 63-142 °C) gradually increase as the **CAZ** (**M2**) molar ratio increases. Hence, higher T_g values of copolymers with higher **CAZ** contents can be originated from the contribution of the bulky carbazole pendent groups, where the mobility of polymeric chains are restricted due to the steric hindrance and rigidity of carbazole units.

Table 2.2 Glass Transition Temperatures of Polymers (P1–P5) and H-Boned Side-Chain Dendritic Complexes Containing H-Acceptor Polymers P3 and P4

polymer or H-bonded complex	T_g (°C)
P1 (HPBB)	63
P2 (PBB-CAZ$_1$)	88
P3 (PBB-CAZ$_5$)	117
P4 (PBB-CAZ$_9$)	125
P5 (HCAZ)	142
P3/G1COOH	81
P3/G2COOH	86
P3/G3COOH	83
P4/G1COOH	88
P4/G2COOH	99
P4/G3COOH	89

During the heating run of polarizing optical microscopy (POM) study in the glassy state of polymers, homopolymer **P1 (HPBB)** exhibited weak birefringent behavior (up to the clearing point of 125 °C) corresponding to a characteristic mesophase at 90 °C (see Appendix A2 and 3), which was further confirmed by powder X-ray diffraction (XRD). The diffraction pattern has two diffuse halos in the small- and wide-angle regions, respectively, indicating the absence of any positional order as a smectic or highly ordered phase.[66] Hence, these results suggest that the mesogenic homopolymer **P1** showed the nematic phase [glassy (64 °C) nematic (125 °C) isotropic]. However, only homopolymer **P1** formed the nematic phase, and the other polymers **P2**-**P5** do not have any mesogenic properties, which is probable that the incorporation of the bulky carbazole groups into the copolymer system will disturb the self-assembly of rigid rods in **PBB** units and thus to prohibit from their mesogenic

behavior.

To elucidate the H-bonding effect on the thermal properties of supramolecular side-chain dendritic complexes, **OXD** dendritic H-donors (bearing benzoic acids) were introduced to be H-bonded with light-emitting H-acceptor copolymers **P2** (**PBB-CAZ$_1$**), **P3** (**PBB-CAZ$_5$**), and **P4** (**PBB-CAZ$_9$**), where **P2/G3COOH** is omitted due to the possible unstabilized H-bonded structures originated from the highest steric hindrance between the highest generation of dendrimer **G3COOH** and the denser H-acceptor units in **P2**. As shown in Table 2, both series of H-bonded side-chain dendritic complexes containing H-acceptor polymers **P3** and **P4** show only a single T_g, which suggests good miscibilities between **OXD** dendritic H-donors (i.e., **G1COOH-G3COOH**) and H-acceptor polymers (i.e., **P3** and **P4**). Besides, since no melting and crystallization were observed in the DSC measurements, it suggests that these H-bonded dendritic complexes possess amorphous characteristics. Moreover, neither phase separation nor mesogenic properties were observed in the POM measurements. However, the T_g values of supramolecular side-chain dendritic complexes (containing **P3** and **P4**) are notably lower than those of their H-acceptor copolymers (i.e., **P3** and **P4**). This result may be explained by that the free volumes of the H-bonded side-chain dendritic complexes were enhanced by the bulky dendritic structures of the **OXD** H-donors.

In comparison with different generations of H-bonded sidechain dendritic complexes containing **P3** and **P4** (i.e., **P3/G1COOH-G3COOH** and **P4/G1COOH-G3COOH**), both series of T_g values increase initially with enlarging the generation number of the **OXD** dendron from **G1** to **G2**, reaching the highest values at dendrimer **G2** (i.e., **P3/G2COOH** and **P4/G2COOH**). With the further increase of the generation number to dendrimer **G3**, both series of T_g values begin to decrease. The initial increase in the T_g value is probably due to the increase of the molecular weight in a larger dendron (from **G1** to **G2**), which is similar to the phenomena observed in our previous study of H-bonded dendrimers.[67] However, the further decrease in the T_g value of the highest generation number (**G3**) is due to the free volume effect (increasing with enlarging the size of the dendritic **OXD** wedges so as to decrease the adjacent polymeric chain interactions) being more dominant than the molecular weight effect, which was also described in our previous polyfluorene polymers containing **OXD** dendritic pendants.[54] Therefore, the competition between the free volume effect and the molecular weight effect influenced the T_g values of H-bonded side-chain dendritic complexes containing **P3** and resulted in the following order: **P3/G2COOH** > **P3/G3COOH**> **P3/G1COOH**. A similar tendency was also observed in analogous H-bonded dendritic complexes containing **P4**. However, there were some possibilities for unstabilized H-bonded structures of complexes made from

the highest generation of dendrimer **G3COOH** and the denser H-acceptor units in **P1**

and **P2** due to the steric hindrance within the higher generations of dendrimers and

hence to induce the incomplete H-bonded complexes. Therefore, the decrease of T_g

values in the complexes might be also attributed to the plasticizing effect of the

non-H-bonded dendrimers, which were homogeneously dispersed in the complexes.

2.4.3 Optical Properties

The absorption and photoluminescence (PL) spectra of H-acceptor monomer **M1**

(**PBB**) and polymers **P1-P5** were measured in both solution and solid states, and their

photophysical properties are summarized in Table 2.3. As shown in Figure 2.4, the

absorption intensities of copolymers **P2-P4** at 294, 328, and 342 nm (in THF

solutions) increase dramatically by raising the **CAZ** content, which are attributed to

the absorption bands of the **CAZ** moieties. The additional absorption bands of

polymers **P1-P4** at ca. 320 and 385 nm are assigned to the light-emitting **PBB**

segments of the H-acceptor moieties. The copolymers do not demonstrate any new (or

shifted) bands in the absorption spectra, indicating no interaction between the **CAZ**

and **PBB** moieties in the ground state.
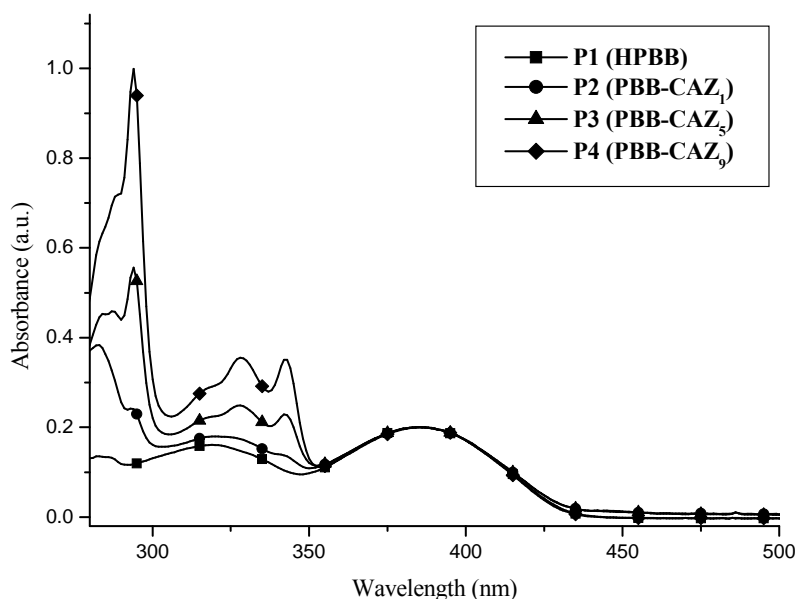
Figure 2.4 Absorption spectra of H-acceptor polymers **P1**−**P4** in THF solutions,

normalized at the maximum absorption peak of the light-emitting **PBB** segments at

385 nm.
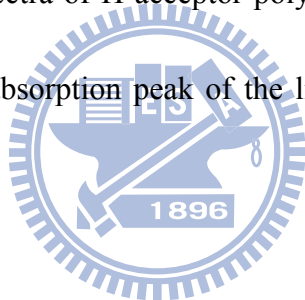
Table 2.3 Absorption and PL Emission Spectral Data of Polymers (P1−P5) in THF Solutions and Solid Films

polymer	$\lambda_{abs,sol}{}^{a}$ (nm)	$\lambda_{PL,sol}{}^{a,b}$ (nm)	$\lambda_{PL,film}{}^{b}$ (nm)	$\Phi_{PL,sol}{}^{b,c}$
P1 (HPBB)	320, 385	449	496	0.49
P2 (PBB-CAZ₁)	294, 320, 342, 385	447	487	0.68
P3 (PBB-CAZ₅)	294, 328, 342, 385	445	469	0.83
P4 (PBB-CAZ₉)	294, 328, 342, 385	444	466	0.94
P5 (HCAZ)	294, 328, 343	348, 364	352, 367	

[a] Measured in dilute THF solutions.

[b] Excited at the maximum absorption of **PBB** units.

[c] Solution fluorescence quantum efficiencies were measured in THF, relative to 9,10-diphenylanthracene (Φ_{PL} = 0.90).

The absorption spectra of the polymers in solid films are similar except for 5-7 nm of red shifts in contrast to those in THF solutions (see Appendix A4). The PL emission spectra of polymers **P1-P4** in solid films show 22-47 nm of significant red shifts, i.e., **P1** (47 nm) > **P2** (40 nm) > **P3** (24 nm) > **P4** (22 nm), in comparison with their corresponding dilute solutions (see Table 2.3), which is due to the formation of π-π stacking and molecular aggregation in solid state. Furthermore, compared with copolymers **P2-P4** in solid films as shown in Figure 2.5, homopolymer **P1** exhibits the largest red shift, i.e., 47 nm, in PL spectra. With the increase of **CAZ** contents in copolymers **P2-P4**, the PL peaks are blue-shifted from 487 nm in **P2** to 466 nm in **P4**. This result clearly indicates that the dilution effect by the **CAZ** moieties can be incorporated into the copolymers to suppress the intermolecular π-π stacking and the aggregation of the light-emitting **PBB** units in polymers and thus to reduce the red shifts (by aggregation) in the PL emission spectra. As listed in Table 2.3, the PL quantum yields (Φ_{PL}) of polymers **P1-P4** in solutions were in the order of **P1** < **P2** < **P3** < **P4**, where **P4** has the largest quantum yield ($\Phi_{PL} = 0.94$) due to the highest content of **CAZ** moieties. This consequence indicates that the dilution effect of **CAZ** units in the copolymers will reduce the aggregation and self-quenching of the **PBB** segments to acquire higher PL quantum yields.
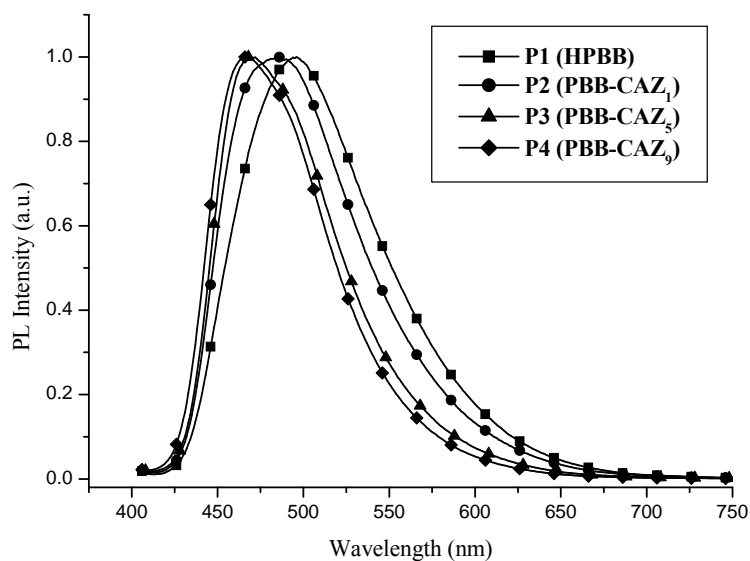
Figure 2.5 Normalized PL spectra of H-acceptor polymers **P1**–**P4** excited at the

maximum absorption (397 nm) of the light-emitting **PBB** segments in solid films.

In order to investigate the generation effect of **OXD** dendrons on the absorption

spectra of H-bonded side-chain dendritic complexes (in solid films), the absorption

spectra of model compound **1** (containing an **OXD** unit, which is illustrated in the

Appendix A5) in THF solution and H-acceptor polymer **P3** in solid state are

compared.[54] As shown in the absorption spectra of Figure 2.6, the maximum

absorption wavelength $\lambda_{max,abs}$ of model compound **1** in THF solution is ca. 305 nm

(from **OXD** units) and that of H-acceptor polymer **P3** in solid state is ca. 296 nm

(from **CAZ** units). Nevertheless, the major absorption bands of H-bonded side-chain

dendritic complexes containing **P3** in solid films are dominated at ca. 296 nm (from

CAZ units) with a shoulder at ca. 315 nm (from **OXD** units), which are originated

from the combined absorption band of the **OXD** and **CAZ** moieties. The longer

absorption band at ca. 397 nm is attributed to the characteristic absorption of the

light-emitting **PBB** units. By increasing the generation number of the dendritic

H-donors in the H-bonded side-chain dendritic complexes, the intensity of the

absorption band in the **OXD** moieties at ca. 305-315 nm is proportional to the

generation number of the H-donor dendrimers. The photophysical properties of

H-bonded side-chain dendritic complexes containing H-acceptor monomer **M1** (**PBB**)

and polymers **P2-P4** in solid films are summarized in Table 2.4, where **M1/G3COOH**

and **P2/G3COOH** are omitted due to the possible unstabilized H-bonded structures

originated from the highest steric hindrance between the highest generation of

dendrimer **G3COOH** and the denser H-acceptor units in **M1** and **P2**. From the results

of Table 2.4, the least red-shifted PL emissions of $\Delta\lambda_{PL}$ in **P2/G1COOH** and

P2/G2COOH have the evidence of the possible unstabilized H-bonded structures of

complexes made from **P2**. Therefore, the possible unstabilized H-bonded structures of

complexes made from **P2** will be similar to those made from **P1**, in which the

H-bonded structures are possibly unsteady due to the steric hindrance between the

denser H-acceptor units in **P1** (as well as **P2**) and the higher generation of dendrimers,

especially for the highest generation of H-bonded complexes containing **G3COOH**.
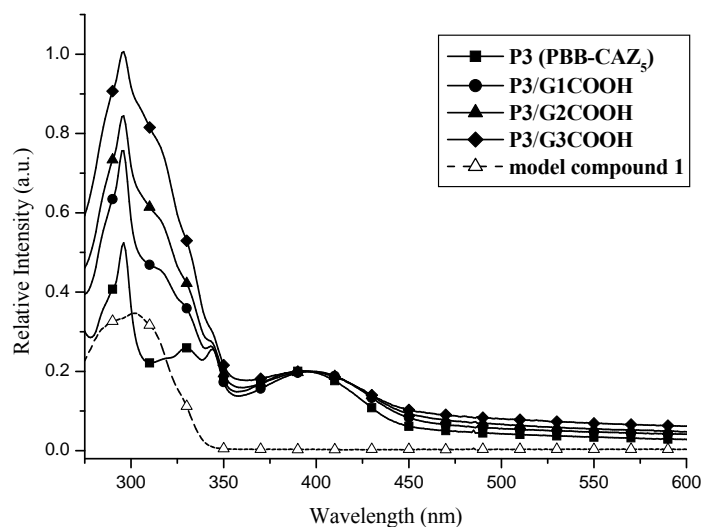
Figure 2.6 Absorption spectra of H-acceptor polymer **P3** and its H-bonded side-chain dendritic complexes in solid films normalized at the maximum absorption (397 nm) of the light-emitting **PBB** cores along with model compound **1** (containing an **OXD** unit with the maximum absorption around 305 nm in THF solution).

Table 2.4 **Photophysical Properties of H-Boned Side-Chain Dendritic Complexes Containing H-Acceptor Polymers P3 and P4**

H-bonded complex	$\lambda_{PL,\ film}$ (nm)	$\triangle\lambda_{PL}{}^{a}$ (nm)	RFI^{b}
P3/G1COOH	530	61	1.56
P3/G2COOH	520	51	2.16
P3/G3COOH	509	40	3.14
P4/G1COOH	523	57	2.09
P4/G2COOH	512	46	2.44
P4/G3COOH	498	32	4.45

^{a} Different degrees of red-shifted PL emissions between the H-boned side-chain dendrimers and their corresponding acceptor copolymers.

^{b} Relative fluorescent intensities (RFI) were calculated by the ratios of the core emission intensities excited at the absorption peaks of the **OXD** units (305 nm) and the **PBB** cores (397 nm).

The photophysical properties of both series of H-bonded sidechain dendritic complexes containing H-acceptor polymers **P3** and **P4** in solid films (see Table 2.4) are evaluated accordingly. Compared with H-acceptor polymer **P3** (**PBB-CAZ5**) in Figure 2.7, the supramolecular side-chain dendritic complexes **P3**/**G1COOH-G3COOH** (excited at the maximum absorption of the light-emitting **PBB** units) exhibit red-shifted PL emissions with λmax values at 530, 520, and 509 nm, respectively. This result is similar to our previous work[68] that red shifts of PL emissions are expected in the H-bonded structures, where the nonphotoluminescent H-donors bearing benzoic acids (as solid solvents) were H-bonded to the photoluminescent H-acceptors containing pyridyl groups. Therefore, analogous H-bonded sidechain dendritic complexes containing different generations of dendritic H-donors appeared to have different degrees of red shifted PL emissions in comparison with H-acceptor polymer **P3**. The red shifts of PL emissions in H-bonded side-chain dendritic complexes **P3**/**G1COOH-G3COOH** are 61, 51, and 40 nm, respectively, where the higher generation of the H-bonded side-chain dendritic complex has a smaller red-shifted PL emission than the lower generation of the H-bonded sidechain dendritic complex. It clearly indicates that the larger dendritic wedges on the side chains have a larger site isolation or dendritic dilution effect than the smaller dendritic ones, so the higher generations of dendrimers efficiently

minimize the interchain interaction and lower the aggregation extent between the

light-emitting **PBB** units.
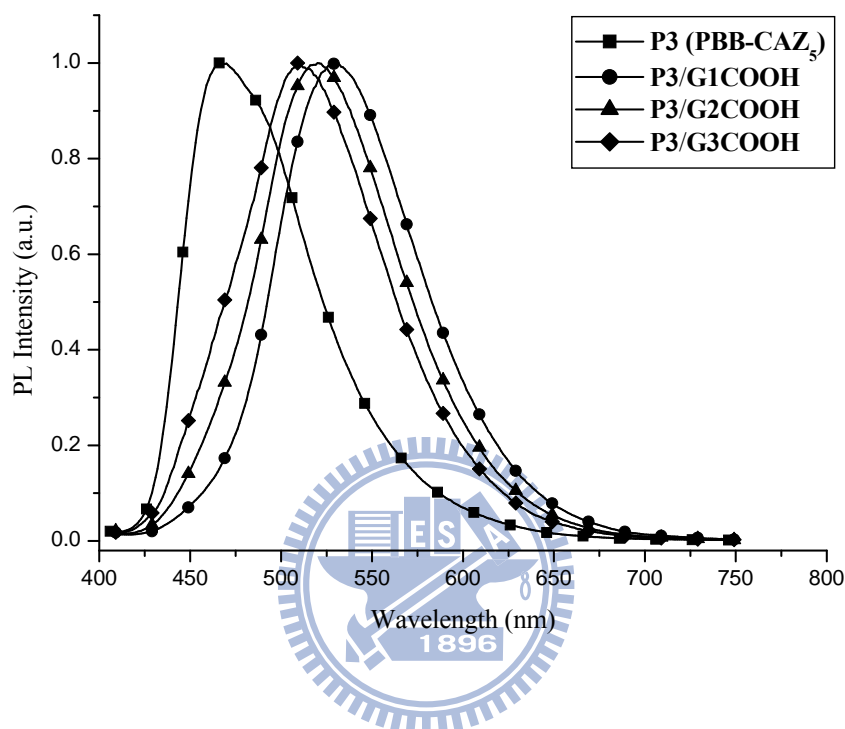
Figure 2.7 Normalized PL spectra of H-acceptor polymer **P3** and its H-bonded

side-chain dendritic complexes excited at the maximum absorption (397 nm) of the

light-emitting **PBB** cores in solid films.

The PL emission data of H-bonded dendritic dendrimers containing **P4** are also

summarized in Table 2.4, which demonstrate similar trends as those of H-bonded

dendritic dendrimers containing **P3**. However, in contrast to the same generation of

OXD dendron, H-bonded dendritic complexes containing **P4** have smaller degrees of

red-shifted PL emissions than H-bonded dendritic complexes containing **P3** (see Table

4). This might be due to the larger dilution effect of **CAZ** units in **P4** (**PBB-CAZ$_9$**)

with higher **CAZ** contents than that in **P3** (**PBB-CAZ$_5$**), where a higher **CAZ** molar

ratio of **P4** reduces the interchain interaction between the light-emitting PBB units in

these H-bonded side-chain dendritic complexes.

Because of the significant spectral overlap in the absorption spectrum of

homopolymer **P1** and the emission spectra of model compound **1** (containing an **OXD**

unit) and homopolymer **P5** (as shown in the Appendix A5), the energy transfer from

the **OXD** dendritic wedges and **CAZ** pendant groups to the light-emitting **PBB** cores

can be expected. This effect was also probed by photoluminescent excitation (**PLE**)

and absorption spectra of H-bonded side-chain dendritic complexes containing **P4**

(see Figure 2.8). Similar spectral features of PLE spectra appear to match those of

their corresponding absorption spectra, where PLE spectra were monitored at the

corresponding maximum PL emission. This result indicates that the existing sites of

CAZ pendent groups, peripheral **OXD** dendritic wedges, and light-emitting **PBB**

cores (ca. 296, 305, and 397 nm, respectively) in such supramolecular side-chain

dendrimers provide the characteristics of light-harvesting capability, i.e., antenna

effect. Since only the energy transfer of the dendritic **OXD** units in the H-bonded

side-chain dendritic complexes is concerned, the excitation wavelength of 305 nm

was chosen at the maximum absorption of the dendritic **OXD** units.
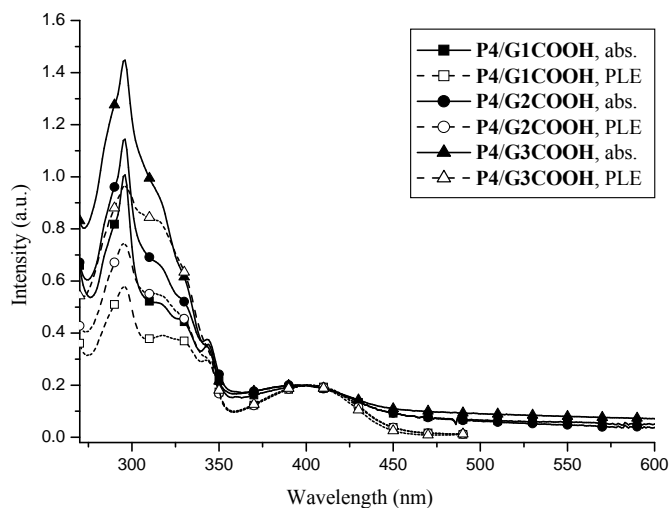
Figure 2.8 UV spectra and PLE spectra of H-acceptor polymer **P4** and its H-bonded side-chain dendritic complexes in solid films normalized at the light-emitting **PBB** units (397 nm), where PLE spectra were monitored at the corresponding maximum PL emissions.

As shown in Figure 2.9, different generations of H-bonded dendritic complexes containing **P4** (**P4/G1COOH-G3COOH**) have PL emissions at wavelengths of 545, 539, and 522 nm, respectively. Upon excitation of the dendritic **OXD** units at 305 nm, H-bonded dendritic complexes apparently generated identical predominant emission peaks as those excited at the maximum absorption of the **PBB** cores. Whereas, no major PL emission from **OXD** dendrons was detected, and thus an efficient energy

transfer from the peripheral **OXD** units to the **PBB** cores is confirmed. Furthermore, the functionalized **OXD** dendritic units or the light-emitting **PBB** cores can be independently addressed by changing the excitation wavelengths in PL experiments. By excitation of the electron-transporting dendrons and the lightemitting cores selectively, it provides a window to study the photoinduced energy transfer between proton donors and acceptors.

In addition, different generations of **OXD** dendritic H-donors were investigated to evaluate their antenna effect in the supramolecular side-chain dendrimers. Thus, the values of relative fluorescent intensities (RFI) in H-bonded side-chain dendritic complexes were calculated from the intensity ratios of their PBB core emissions by respective excitations at the maximum absorption peaks of the **OXD** dendrons (by the sensitized absorption at 305 nm and then energy transfer to **PBB** core emissions) and the maximum absorption peaks of the **PBB** cores (by the direct core absorption at 397 nm), respectively. The RFI values of H-bonded side-chain dendrimers containing H-acceptor copolymer **P4** and H-donor dendrimers **G1COO**H to **G3COOH** are 2.09, 2.44, and 4.45, respectively (as shown in Figure 2.9 and Table 2.4), which indicates that the intensity of the sensitized emission (by the energy transfer from **OXD** dendritic absorption at 305 nm) is even stronger than that of the direct **PBB** core emission (by the direct core absorption at 397 nm) in the H-bonded side-chain

dendrimers. Therefore, the RFI values are much enhanced in the higher generations of

H-bonded dendritic complexes (with the maximum values in both series of H-bonded

side-chain dendritic complexes bearing the highest generation of H-donor dendrimer

G3COOH), which is attributed to the higher absorptions by the larger numbers of

OXD units in the higher generations of dendritic wedges as well as the further

reduced aggregation of the light-emitting **PBB** cores by the more bulky sizes of

dendrons in the higher generations of **OXD** H-donors.
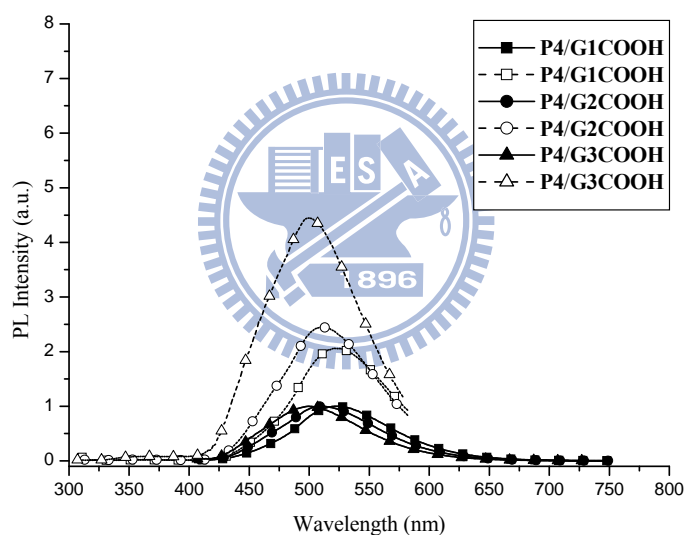
Figure 2.9 PL spectra of H-acceptor polymer **P4** and its H-bonded side-chain

dendritic complexes in solid films, which were excited at the dendritic peripheral

OXD units (at 305 nm for open symbols) and at the maximum absorption of the

light-emitting **PBB** cores in H-bonded side-chain dendritic complexes containing

dendritic H-donors (ca. 397 nm for solid symbols).

2.4.4 Electrochemical Properties

The electrochemical behavior of H-acceptor copolymer **P4** and its H-bonded side-chain dendritic complexes were investigated by cyclic voltammetry (CV), and the results are summarized in Table 2.5. The highest occupied molecular orbital (HOMO) and lowest unoccupied molecular orbital (LUMO) levels were calculated according to the following equation: $E_{HOMO}/E_{LUMO} = -e(E_{ox/onset}/E_{red/onset} + 4.4)$ (eV).[69] The onset potentials were determined from the intersections of two tangents drawn at the rising and background currents of the CV curves. Since the onsets of the oxidation potentials (i.e. $E_{ox/onset}$) for H-acceptor copolymer **P4** and its H-bonded dendritic complexes were obtained from the CV measurements, the HOMO (i.e. E_{HOMO}) values were calculated from the previous equation, i.e., $E_{HOMO} = -e(E_{ox/onset} + 4.4)$ (eV),, where Eox/onset is the onset oxidation potential versus the saturated calomel electrode (SCE). H-acceptor copolymer **P4** and its H-bonded dendritic complexes show the onset potentials of oxidation between 1.24 and 1.27 V in the anodic scans (see Table 2.5). The reduction potential peaks of H-acceptor copolymer and H-bonded side-chain dendrimers were not observed in the CV measurements, so crude estimations of LUMO values in the reduction processes of H-acceptor copolymer **P4** and its H-bonded side-chain dendrimers were made by the deduction of optical band gap values from HOMO values. The optical band gaps estimated from the absorption

onsets of H-acceptor copolymer **P4** and its H-bonded side-chain dendritic complexes in solid films are also listed in Table 2.5, which reveals that H-acceptor copolymer **P4** has a larger band gap than its H-bonded side-chain dendrimers. Comparing the H-bonded sidechain dendritic complexes with various generations of **OXD** dendritic wedges, their LUMO values are not remarkably changed. However, it seems that the H-bonded side-chain dendritic complexes have slightly lower LUMO values than H-acceptor copolymer **P4** similar to a previously reported consequence.[67a]

Table 2.5   Electrochemical Properties of H-Acceptor Polymer P4 and Its H-Bonded Side-Chain Dendritic Complexes

polymer or H-bonded complex	optical band gap[a] (eV)	$E_{ox/onset}$[b] (V)	HOMO (eV)	LUMO[c] (eV)
P4 (PBB-CAZ₉)	2.79	1.24	-5.64	-2.85
P4/G1COOH	2.75	1.26	-5.66	-2.91
P4/G2COOH	2.76	1.27	-5.67	-2.91
P4/G3COOH	2.77	1.27	-5.67	-2.90

[a] Estimated from the onset wavelength of optical absorption in solid films.

[b] The onset oxidation potential vs. SCE.

[c] LUMO values were estimated by the deduction of optical band gaps from HOMO values.

2.4.5 Electroluminescence (EL) Properties

The electrochemical properties as well as the HOMO and LUMO energy levels of H-acceptor copolymer **P4** and its H-bonded side-chain dendritic complexes are crucial parameters for the device configuration and further confine the electron-hole recombination zone to the emission layer sufficiently. Therefore, H-acceptor polymer **P4** and its H-bonded dendritic complexes were fabricated into four-layer PLED devices, with a configuration of ITO/PEDOT:PSS (50 nm)/polymer (**P4** or its H-bonded dendritic complexes) (55-70 nm)/BCP (10 nm)/Alq3 (30 nm)/LiF (1 nm)/Al (150 nm) using standard procedures of spin-coating and vacuum deposition methods, where polymer (**P4** or its H-bonded dendritic complexes) was used as the emission layer and PEDOT:PSS as the hole transporting layer (anode buffer). Besides, BCP (HOMO = -6.70 eV, LUMO = -3.20 eV), Alq_3 (HOMO = -6.00 eV, LUMO = -3.30 eV), and LiF/Al were employed as a hole-blocking layer, an electron-transporting layer, and a bilayer cathode, respectively. As shown in Figure 2.10, under forward bias voltages, the electroluminescence (EL) spectra of H-acceptor polymer **P4** and its H-bonded dendritic complexes show EL emissions in the range of 464-519 nm, indicating that the emission color can be effectively tuned from blue to green by incorporating light-emitting H-acceptor copolymer **P4** with various generations of **OXD** dendritic donors into the supramolecular side-chain polymer

structures. These EL features are similar to those observed with corresponding PL

emissions of the respective solid films.
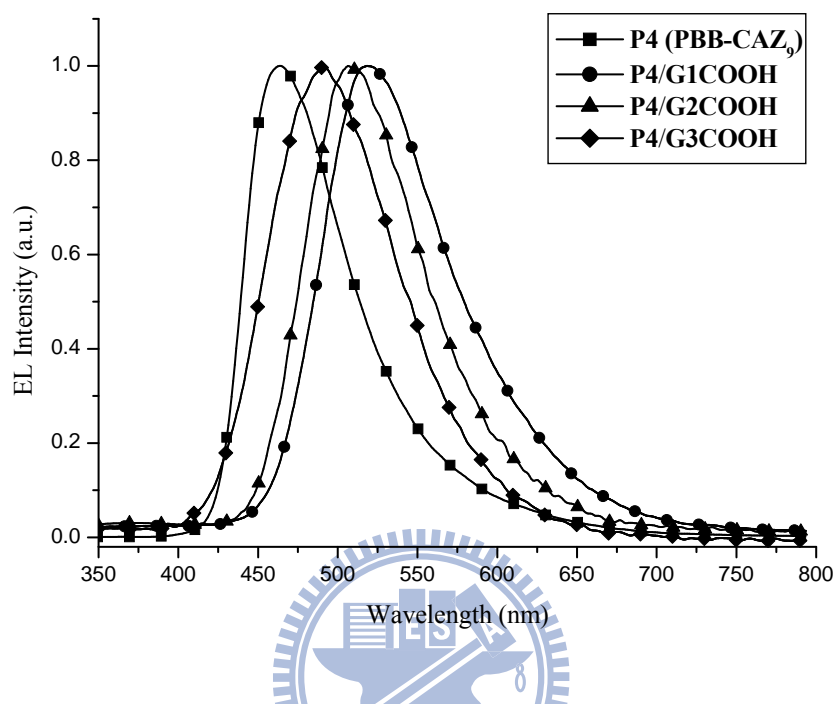
Figure 2.10 Normalized EL spectra of PLED devices with the configuration of

ITO/PEDOT:PSS/polymer (**P4** or its H-bonded side-chain dendritic

complexes)/BCP/Alq$_3$/LiF/Al.

The electroluminescence (EL) properties of the PLED devices are summarized in

Table 2.6, and their current-voltage and luminescence-voltage characteristics are

displayed in Figure 2.11. A comparison of their turn-on voltages, the PLED device

bearing H-bonded dendritic complex **P4/G1COOH**, has a lower turn-on voltage than

that bearing H-acceptor **P4**. From this result, it can be concluded that the integration

of **OXD** dendritic wedges (electron transporting) into the supramolecular structures can remarkably improved device performance with a reduced turn-on voltage (though with a lower power efficiency). However, with higher generations (from **G1COOH** to **G3COOH**) of **OXD** dendritic wedges in the supramolecular H-bonded dendritic complexes, the turn-on voltages and power efficiencies of the PLED devices become worse (higher). This may be due to the intrinsic insulation properties of the higher generations of the **OXD** dendritic wedges with more 2-ethylhexyloxy end groups (as a shielding effect for electron and hole transporting) which consequently deteriorate the charge-carrier transporting properties and lead to higher turn-on voltages.[70] In addition, the PLED device bearing H-bonded dendritic complex **P4/G1COOH** has the best EL performance characteristics with a maximum luminance and luminous efficiency of 408 cd/m^2 at 18 V and 0.39 cd/A at 100 mA/cm^2, respectively, which are generally better than those of corresponding PLED devices bearing H-bonded dendritic complexes **P4/G2COOH** and **P4/G3COOH**. This could be presumably attributed to the larger dendron shells of the higher generations of **OXD** H-donors, which have a larger influence on the carrier mobility and trapping process.[67a,71]
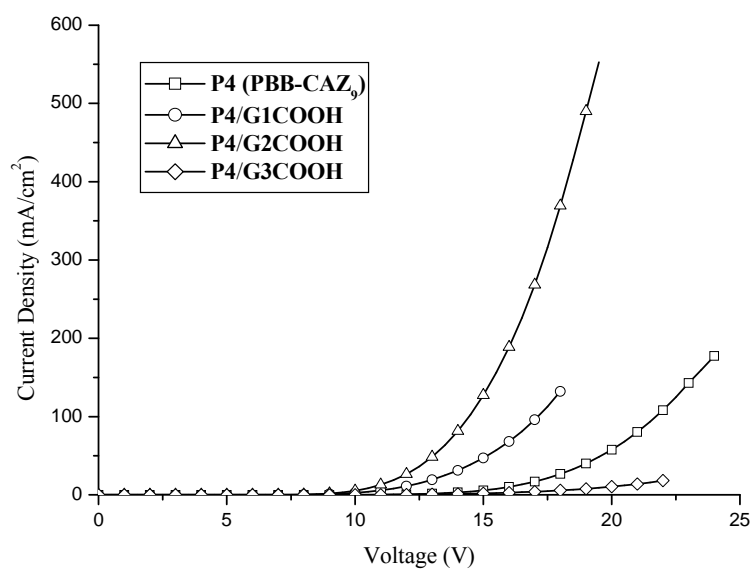
(a)
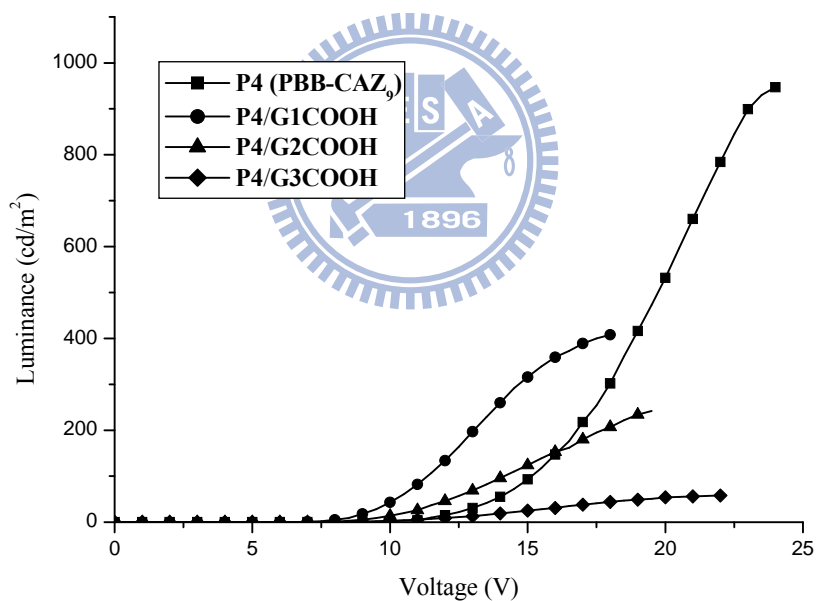
(b)

Figure 2.11   (a) Current density-voltage (*I-V*) curves and (b) luminance-voltage

(*L-V*) curves of PLED devices with the configuration of ITO/PEDOT:PSS/polymer

(**P4** or its H-bonded side-chain dendritic complexes)/BCP/Alq$_3$/LiF/Al.

Table 2.6 Electroluminescence (EL) Device Performance Characteristics of H-Acceptor Polymer P4 and Its H-Boned Side-Chain Dendritic Complexes[a]

polymer or H-bonded complex	$\lambda_{EL, film}$ (nm)	V_{on}[b] (V)	luminance efficiency[c] (cd/A)	power efficiency[c] (lm/W)	max. luminance (cd/m²) (V)
P4 (PBB-CAZ₉)	464	8.5	0.75	0.109	947 (24)
P4/G1COOH	519	6.5	0.39	0.070	408 (18)
P4/G2COOH	506	7	0.11	0.034	242 (19.5)
P4/G3COOH	492	8.5	-[d]	-[d]	58 (22)

[a] Device configuration: ITO/PEDOT:PSS/polymer (**P4** or its H-bonded side-chain dendritic complexes)/BCP/Alq₃/LiF/Al.

[b] V_{on}: the turn on voltage of light.

[c] Measured at 100 mA/cm².

[d] Undetectable (less than 100 mA/cm²).

2.5 Conclusion

A series of novel H-bonded acceptor copolymers containing different molar ratios of hole-transporting carbazole (**CAZ**) units and light-emitting **PBB** moieties (bearing three conjugated aromatic rings and a terminal H-acceptor), were successfully synthesized. By the complementary surroundings via the complexation with different generations of **OXD** dendritic donors (**G1COOH−G3COOH**), the emission wavelengths of H-acceptor copolymers can be easily adjusted in their self-assembled structures of H-bonded side-chain dendritic complexes. As a result, all light-emitting, hole-transporting, and charge-transporting groups possessing novel photophysical and thermal properties are obtained in the supramolecular side-chain copolymers (i.e., H-bonded side-chain dendritic complexes). Moreover, the incorporation of carbazole

units in the acceptor copolymers shows higher glass transition temperatures than the acceptor homopolymer itself and the emission wavelengths of H-acceptor polymers can be tuned (up to 61 nm of red-shift) by H-bonds. In addition, the larger dendritic size (i.e., the higher generation) of H-donors can afford stronger site-isolation and dendron-dilution effects, and thus better energy-transfer phenomena can be achieved. The PLED devices with the configuration of ITO/PEDOT:PSS/(**P4** or its H-bonded dendritic complexes)/BCP/Alq$_3$/LiF/Al were fabricated, and the emission colors from blue to green can be effectively tuned by incorporating various generations of **OXD** dendritic donors in the supramolecular side-chain polymer structures.

Chapter 3

H-Bonded Liquid Crystalline Polymer Networks Self-Assembled from Side-Chain Copolymers and Homopolymer Complexes Containing Fluorescent H-Acceptor and Non-Photoluminescent H-Donor Pendants

3.1 Abstract

A series of H-bonded side-chain mesogenic copolymer networks containing different molar ratios of light-emitting proton (H-) acceptor **PBB (M1)** and proton (H-) donor **BA (M2)** were synthesized via free radical polymerization. In addition, analogous H-bonded polymer networks were prepared from fully H-bonded polymer complexes of H-donor and H-acceptor homopolymers. The H-bonded copolymer networks **P2−P4** have higher glass transition temperatures (T_gs) than the individual hompolymers **P1** and **P5**, which is due to the promoted interchain interations by H-bonds. Both H-bonded copolymer and homopolymer complex networks show mesomorphic behavior with the smectic A phase. The isotropization temperatures (T_is) and S_A phase stabilities of the H-bonded copolymer networks increase as the molar ratios of H-donor **BA** units increase. Furthermore, the red-shifts of PL emissions in H-bonded copolymer and homopolymer complex networks can be tuned up to 39 nm

in contrast to H-acceptor homopolymer **P1**. The PL quantum yields (Φ_{PL}) of polymers **P1−P4** in solid films were enhanced by increasing the molar ratios of H-donor **BA** unit. The electroluminescence (EL) and photoluminescence (PL) results of H-acceptor homopolymer **P1** and its fully H-bonded cross-linking copolymer **P2** show emission colors varying from c.a. 496-500 nm (greenish-blue) to 531-537 nm (green), respectively. Overall, H-bonded effects on the mesomorphic, photophysical, and electro-optical properties of these H-bonded polymer networks are investigated.

3.2 Introduction

Supramolecular chemistry is concerned with self-assembly of distinct molecules using secondary chemical interactions rather than covalent bonding, which particularity offers opportunities for engineering novel features, functions, and properties into supramolecular assemblies through different molecular components.[72-74] Simple association of two complementary compounds through specific non-covalent interactions, such as hydrogen bonding,[75-79] π–π stacking,[80-83] and metal-coordinative interaction,[84-87] can be applied to build new dynamically functional materials. Especially, the use of hydrogen bonding in self-assembly of liquid crystals (LCs) is a powerful tool for stabilization and induction of mesomorphism, even for compounds with structures largely deviated from a proper

design in molecular interactions and shapes, such as classical calamitic (rod-like),[88,89]

discotic,[90,91] and bent-core[92] LCs.

The main advantage of hydrogen-bonded (H-bonded) mesogens is that their LC properties can be tuned easily by changing the components and ratios of the H-bonded moieties, i.e., proton donors and acceptors (H-donors and H-acceptors). Following the work reported by Kato and Fréchet in 1989,[93] a number of H-bonded systems containing pyridyl groups (H-acceptors) and carboxyl groups (H-donors) have been extensively investigated for the applications in side-chain, main-chain, and cross-linking LC polymers.[94-104]

In the past decade, conjugated polymers with novel semi-conducting properties, such as poly(p-phenylenevinylene) (PPV), poly(fluorene) (PF), and their derivatives, have received considerable attention and emerged as the most interesting materials due to their unique properties and potential applications in optoelectronic devices, including polymeric light-emitting diodes (PLEDs)[105-107] and photovoltaic (PV) cells.[108,109] However, the light-emissions from the π-conjugated polymers are limited by several important factors, for instance the packing distance (π–π interaction) of chromophores, aggregate/excimer formation, and self-quenching in the solid state, which lead to red-shifted and less-efficient emissions. To minimize the tendency of aggregation, numerous attempts have been exploited by using bulky

substituents,[110,111] copolymerization techniques,[112-114] and dendrimer attachments.[115]

Among these approaches, copolymerization has been widely utilized in the preparation of conjugated polymers to achieve specific electronic and physical properties as well as their high fluorescence efficiencies. As illustrated previously in the H-bonded structural applications of LC materials, the supramolecular organization of π-conjugated systems has recently become a new research direction to offer designed materials with extremely valuable properties.[116,117] Moreover, the H-bonded self-assembly processes of π-conjugated supramolecules also play a crucial role in facilitating energy and electron-transfer processes in electro-optical devices.[118-123]

In our previous work, the mesomorphic and photophysical properties of the H-bonded trimers and polymer networks can be easily adjusted by tuning the non-photoluminescent H-donor acids (or H-donor polymers) and fluorescent H-acceptors (small molecules) in the H-bonded complexes. Unique mesomorphic properties can be introduced to these supramolecular structures containing non-mesogenic H-acceptor emitters. In the meanwhile, the emission properties of bis-pyridyl H-acceptor emitters can be manipulated by their surrounding non-photoluminescent proton donors. Moreover, new light-emitting H-bonded side-chain dendritic complexes containing side-chain H-acceptor copolymers and electron-transporting H-donor dendrimers have been developed recently, where

side-chain H-acceptor copolymers were composed of light-emitting H-acceptor and hole-transporting (carbazole) moieties. In this report, H-bonded side-chain copolymer and homopolymer complex networks (as shown in Figure 3.1) containing non-photoluminescent H-donor (benzoic acid) and fluorescent H-acceptor pendants, which involve three-conjugated aromatic rings with pyridyl terminus and lateral methoxyl groups on the middle rings (to increase solubility after polymerization), were successfully synthesized. The copolymerization of H-donor (benzoic acid) and fluorescent H-acceptor monomers with different molar ratios is to avoid the spontaneous aggregation of the π-conjugated H-acceptor emitters and further to tune their emission colors. In addition, the processes of blending H-donor and H-acceptor homopolymers to form H-bonded homopolymer complexes are prepared for comparative purposes. Accordingly, H-bonded effects on the mesomorphic, photophysical, and electro-optical properties of these H-bonded polymer networks are investigated in the present work.

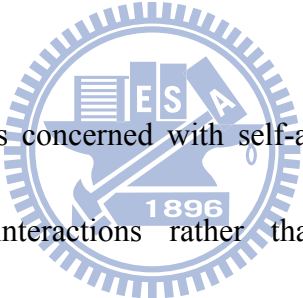**Figure 3.1** Simplified schematic illustration of idealized H-bonded liquid crystalline polymer networks self-assembled from side-chain copolymers and homopolymer complexes containing fluorescent H-acceptor **PBB** and non-photoluminescent H-donor **BA** pendants.

3.3 Experimental Section

3.3.1 Measurements and Characterization

^{1}H NMR spectra were recorded on a Varian Unity 300 MHz spectrometer using

CDCl$_3$ and DMSO-d_6 as solvents. Elemental analyses were performed on a HERAEUS CHN-OS RAPID elemental analyzer. High resolution electron impact mass data were obtained on a Finnigan-MAT-95XL. Phase transition temperatures were determined by differential scanning calorimetry (DSC, model: Perkin Elmer Diamond) under N$_2$ with a heating and cooling rate of 10 °C/min and polarizing optical microscope (POM, model: Leica DMLP) equipped with a hot stage. Thermogravimetric analysis (TGA) was carried out with a TA Instruments Q500 thermogravimetric analyzer at a heating rate of 20 °C/min under nitrogen. Gel permeation chromatography (GPC) analysis was equipped with a Waters HPLC pump 510 connected to a Waters 410 differential refractmeter and three Ultrastyragel columns using polystyrene as a standard and DMF as an eluant. Fourier transform infrared (FTIR) spectra were recorded on a Perkin-Elmer Spectrum 100 Series and sample films were cast from THF solutions directly on KBr plates and dried in a vacuum at 50 °C for 2 days. Synchrotron powder X-ray diffraction (XRD) measurements were performed at the beamline BL 17A of the National Synchrotron Radiation Research Center (NSRRC), Taiwan (for detail of the XRD installation, see Appendix). The theoretical molecular length is estimated from CS Chem3D Ultra 7.0 software. UV-vis absorption spectra were recorded on a HP G1103A spectrophotometer, and photoluminescence (PL) spectra were obtained on a Hitachi

F-4500 spectrophotometer in dilute THF solutions (10^{-6} M). Thin films of UV-vis and

PL measurements were spin-coated on a quartz substrate from THF solutions with a

concentration of 10 mg/mL at 3000 rpm. Cyclic voltammetry (CV) was performed

using an Autolab PGSTAT30 potentiostat/galvanostat with a standard three-electrode

electrochemical cell in a solution of 0.1 M tetrabutylammonium hexafluorophosphate

(Bu_4NPF_6) dissolved in acetonitrile (CH_3CN) at room temperature at a scanning rate

of 100 mV/s. A platinum disk working electrode, Pt wire counter electrode, and an

Ag/AgCl reference electrode were used. The sample films were coated on the surface

of the platinum disk by a solution-dipping process from THF solutions.

A series of electroluminescence (EL) devices with the configuration of

ITO/PEDOT:PSS/polymer (**P1** or its full H-bonded networks)/BCP/Alq$_3$/LiF/Al were

made, where BCP (2,9-dimethyl-4,7-diphenyl-1,10-phenanthroline) was used as a

hole-blocking layer and Alq$_3$ (tris(8-hydroxyquinoline)aluminium) was used as

electron transporting layer. Substrates used were indium-tin oxide (ITO) coated glass

with a sheet resistance of ~20 Ω/square and an effective individual device area of 3.14

mm^2. ITO substrates were routinely cleaned by ultrasonic treatments in detergent

solutions and diluted water, followed by rinsing with acetone and then ethanol. After

drying, ITO substrates were kept in oxygen plasma for 4 min before being loaded into

the vacuum chamber. The poly(3,4-ethylenedioxythiophene):poly(styrenesulfonate)

(PEDOT:PSS) films were first deposited on pre-cleaned ITO substrates by spin-coating at 6000 rpm for 1 min and subsequently cured in an oven at 120 °C for 1 h. Then, polymers in THF solutions (10 mg/mL) were spin-coated onto the PEDOT:PSS layer at 4000–5500 rpm. The thicknesses of PEDOT:PSS and polymers were measured by an Alfa Step 500 Surface Profiler (Tencor). BCP and Alq$_3$ were thermally deposited at a rate of 1–2 Å/s under a pressure of $\sim 2 \times 10^{-5}$ Torr in an Ulvac Cryogenic deposition system. Under the same deposition condition, one layer of LiF was thermally deposited as a cathode at a rate of 0.1–0.2 Å/s, which was followed by capping with aluminum. The current-voltage-luminescence characteristics were measured in ambient condition by Keithley 2400 source meter and Newport 1835C optical meter equipped with 818ST silicon photodiode.
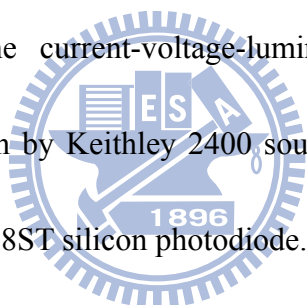
Scheme 3.1   Synthetic Routes of Homopolymers and Copolymers

AIBN

THF, 60 °C, 24hr

BA (M2) R = H
or
BAMe (M3) R = Me

PBB (M1)

P1 (HPBB), x/y = 1/0
P2 (PBB-BA₁), x/y = 1/1   R = H
P3 (PBB-BA₄), x/y = 1/4   R = H
P4 (PBB-BA₁₂), x/y = 1/12   R = H
P5 (HBA), x/y = 0/1   R = H
P6 (PBB-BAMe₁), x/y = 1/1   R = Me
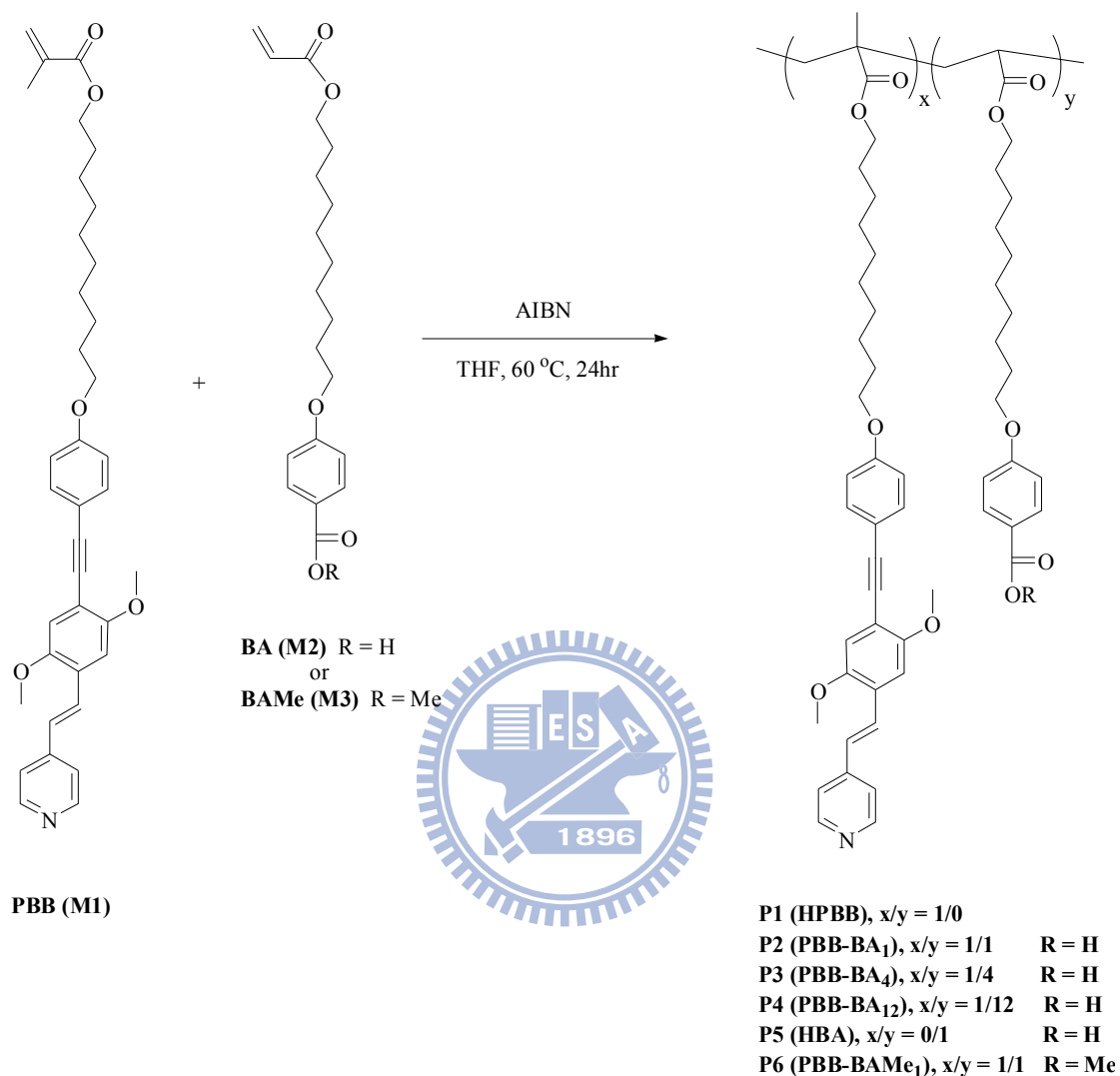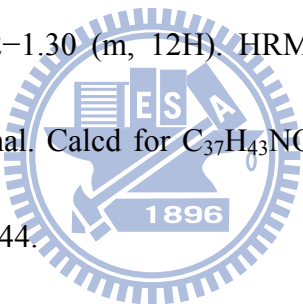
3.3.2 Materials

Chemicals and solvents were reagent grades and purchased from Aldrich, Acros, TCI,

and Lancaster Chemical Co. Tetrahydrofuran (THF) and triethylamine (Et₃N) were

distilled to keep anhydrous before use. Azobisisobutyronitrile (AIBN) was

recrystallized from methanol before use. The other chemicals were used without

further purification. The monomers of **PBB** (**M1**), **BA** (**M2**), and **BAMe** (**M3**) were prepared following the already published procedure.

1-{[4-(10-Methacryloyloxy-decyloxy)-phenyl]-ethynyl}-2,5-dimethoxy-4-[2-(4-pyridyl)ethenyl]benzene, PBB (M1). Yield: 85%. ^{1}H NMR (300 MHz, CDCl$_3$): δ (ppm) 8.57 (d, J = 4.5 Hz, 2H), 7.66 (d, J = 16.5 Hz, 1H), 7.50 (d, J = 9.0 Hz, 2H), 7.39 (d, J = 4.5 Hz, 2H), 7.11 (s, 1H), 7.04 (d, J = 16.5 Hz, 1H), 7.04 (s, 1H), 6.87 (d, J = 9.0 Hz, 2H), 6.10 (s, 1H), 5.55 (s, 1H), 4.14 (t, J = 6.6 Hz, 2H), 3.97 (t, J = 6.6 Hz, 2H), 3.96 (s, 3H), 3.89 (s, 3H), 3.62 (t, J = 6.6 Hz, 2H), 1.95 (s, 3H), 1.81−1.75 (m, 2H), 1.58−1.53 (m, 2H), 1.42−1.30 (m, 12H). HRMS (EI): calcd for C$_{37}$H$_{43}$NO$_5$, 581.3141; found 581.3146. Anal. Calcd for C$_{37}$H$_{43}$NO$_5$: C, 76.39; H, 7.45; N, 2.41. Found: C, 76.15; H, 7.37; N, 2.44.

4-(10-Acryloyloxy-decyloxy)benzoic Acid, BA (M2). Yield: 75%. ^{1}H NMR (300 MHz, DMSO-d_6): δ (ppm) 12.58 (br, 1H), 7.86 (d, J = 8.7 Hz, 2H), 6.98 (d, J = 8.7 Hz, 2H), 6.30 (dd, J = 17.4 Hz, J = 1.8 Hz, 1H), 6.17 (dd, J = 17.4 Hz, J = 10.2 Hz, 1H), 5.91 (dd, J = 10.2 Hz, J = 1.8 Hz, 1H), 4.08 (t, J = 6.6 Hz, 2H), 4.01 (t, J = 6.6 Hz, 2H), 1.75−1.66 (m, 2H), 1.65−1.50 (m, 2H), 1.27−1.20 (m, 12H). HRMS (EI): calcd for C$_{20}$H$_{28}$O$_5$, 348.1937; found 348.1940. Anal. Calcd for C$_{20}$H$_{28}$O$_5$: C, 68.94; H, 8.10. Found: C, 68.67; H, 8.13.

Methyl 4-(10-Acryloyloxy-decyloxy)benzoate, BAMe (M3). Yield: 80%. ^{1}H

NMR (300 MHz, CDCl$_3$): δ (ppm) 7.88 (d, J = 9.0 Hz, 2H), 7.01 (d, J = 9.0 Hz, 2H), 6.30 (dd, J = 17.4 Hz, J = 1.8 Hz, 1H), 6.15 (dd, J = 17.4 Hz, J = 10.2 Hz, 1H), 5.91 (dd, J = 10.2 Hz, J = 1.8 Hz, 1H), 4.08 (t, J = 6.6 Hz, 2H), 4.02 (t, J = 6.6 Hz, 2H), 3.79 (s, 3H), 1.73−1.66 (m, 2H), 1.64−1.51 (m, 2H), 1.26−1.21 (m, 12H). HRMS (EI): calcd for C$_{21}$H$_{30}$O$_5$, 362.2093; found 362.2094. Anal. Calcd for C$_{21}$H$_{30}$O$_5$: C, 69.59; H, 8.34. Found: C, 69.39; H, 8.39.

General Procedure for the Synthesis of Homo- and Copolymers, P1−P6. All of the polymerizations were carried out by the free radical polymerization described as follows. To a Schlenk tube, 1.0 g of monomers **M1**, or **M2**, or **M1** and **M2**, or **M1** and **M3** mixture were dissolved in dry THF (7.5 mL) with 20 wt% of monomer concentration and AIBN (2 mol% of total monomer concentration) as an initiator. The solution was degassed by three freeze-pump-thaw cycles and then sealed off. The reaction mixture was stirred and heated at 60 °C for 24 h. After polymerization, the polymer was precipitated into diethyl ether for **P1−P4** and **P6**, and methanol for **P5**. The precipitated polymer was collected, washed with diethyl ether, and dried under high vacuum.

P1 (HPBB). ^{1}H NMR (300 MHz, DMSO-d_6): δ (ppm) 8.44 (br, 2H), 7.53−6.77 (m, 10H), 3.80 (br, 10H), 1.66−1.24 (br, 21H).

P2 (PBB-BA$_1$). ^{1}H NMR (300 MHz, DMSO-d_6): δ (ppm) 12.58 (br, 1H), 8.47 (br,

2H), 7.80−6.81 (m, 14H), 3.80 (br, 14H), 2.16 (br, 1H), 1.56−1.16 (m, 39H).

P3 (PBB-BA₄). ^{1}H NMR (300 MHz, DMSO-d_6): ^{1}H NMR (300 MHz, DMSO-d_6): δ (ppm) 12.56 (br, 4H), 8.49 (br, 2H), 7.83−6.85 (m, 58H), 3.83 (br, 25H), 2.17 (br, 4H), 1.60−1.18 (m, 88H).

P4 (PBB-BA₁₂). ^{1}H NMR (300 MHz, DMSO-d_6): δ (ppm) 12.55 (br, 12H), 8.49 (br, 2H), 7.83−6.86 (m, 58H), 3.87 (br, 60H), 2.18 (br, 12H), 1.60−1.18 (m, 244H).

P5 (HBA). ^{1}H NMR (300 MHz, DMSO-d_6): δ (ppm) 12.56 (br, 1H), 7.83 (d, 2H), 6.90 (br, 2H), 3.92 (br, 4H), 2.20 (br, 1H), 1.62−1.21 (m, 18H).

P6 (PBB-BAMe₁). ^{1}H NMR (300 MHz, DMSO-d_6): δ (ppm) 8.54 (br, 2H), 7.88−6.96 (m, 14H), 3.90 (br, 17H), 2.18 (br, 1H), 1.58−1.40 (m, 39H).

Sample Preparation.

*Full H-bonded polymer networks **P1/P5***: The full H-bonded polymer networks blend(**P1/P5**)s prepared by proton acceptor homopolymer **P1** and donor homopolymer **P5** (1:1 stoichiometric mixture of pyridyl and carboxylic acid groups to form H-bonded polymer networks) was dissolved in THF solution, and the solvent was removed by slow evaporation, followed by drying in a vacuum at 50 °C.

Fibers: Fibers were manually drawn from the mesogenic state at 100 °C using a tweezers withdrawn from a 30−50 mg pool of mesogenic melt state and quenched to room temperature for X-ray experiments.

3.4 Results and Discussion

3.4.1 Synthesis and Properties of Polymers

The chemical structures and the synthetic approaches of the designed polymers are shown in Scheme 1. The key three-conjugated rings of acceptor emitter monomer **PBB (M1)** was elaborated through multiple-step reaction routes with a good yield as our previously reported, and synthesized via Horner–Wadsworth–Emmons (HWE) olefination reaction and Sonogashira (Pd-catalyzed) coupling reaction. The non-photoluminescent proton donor of monomer **BA** (**M2)** and monomer **BAMe** (**M3)** (i.e., benzoic acid derivative by esterification with methyl group) were prepared following the modified procedures in the literature method. The chemical structures and purity of the final monomers **PBB (M1)**, **BA (M2)**, and **BAMe (M3)** were confirmed by ^{1}H NMR spectroscopy, HRMS, and elemental analysis, as listed in the Experimental Section.

All the polymers were synthesized using the well-known free radical polymerization method in the presence of azobisisobutyronitrile (AIBN) as an initiator at 60 °C in THF. The feeding ratios of monomers **PBB (M1)** to **BA (M2)** in the present work were 1:0, 1:1.5, 1:5, 1:10, and 0:1 (i.e., **P1−P5**), respectively. The chemical structures of polymers **P1−P6** in DMSO-d_6 were verified in comparison with those of their monomers **PBB (M1)**, **BA (M2)**, and **BAMe (M3)** by ^{1}H NMR

spectroscopy (see Appendix A6 and 7). In the ^{1}H NMR spectra of polymers, the completely disappearance of proton peaks in the region of vinyl proton (methacrylate and acrylate) group with chemical shifts at 5.5−6.3 ppm indicated that no monomers were present. As an example, the copolymer compositions were estimated by comparing the relative integration areas of the peaks at 8.5 ppm (corresponding to two protons of α-pyridyl in **PBB** groups) and 6.7−7.9 ppm (corresponding to overlapped aromatic protons of other **PBB** groups and **BA** groups), respectively. For copolymer compositions of **P2−P4** and **P6**, the actual compositions of **P2**, **P3**, and **P6** have slightly lower molar ratio of monomers than that of feeding ratio, but that **P4** showed much higher molar ratio than the feeding. The polymers **P1−P6** were obtained in 49−73% yields after purification and could also be readily dissolved in common organic solvents, e.g., THF, DMSO, and *N,N*-dimethylformamide (DMF). The weight-average molecular weights (M_w) and polydispersity indexes (PDI) of polymers **P1−P6**, determined by gel permeation chromatography (GPC) with DMF as the eluting solvent and polystyrene as standards, were in the range 8700−13600 and 1.25−2.16, respectively. The compositions, molecular weights, and yields of polymers **P1−P6** are summarized in Table 3.1.

Table 3.1 Compositions, Yields, Molecular Weights, Polydispersity Index (PDI), and Degradation Temperatures of Homopolymers and Copolymers

polymer	molar ratio		yield (%)	M_w (g/mol)[c]	PDI (M_w/M_n)[c]	T_d (°C)[d]
	feeding (PBB/BA)	output (PBB/BA)[b]				
P1 (HPBB)		1/0	73	13600	1.67	357
P2 (PBB-BA₁)	1/1.5	1/1	49	9400	1.45	352
P3 (PBB-BA₄)	1/5	1/3.7	57	10700	1.86	352
P4 (PBB-BA₁₂)	1/10	1/12.3	61	9100	1.30	351
P5 (HBA)		0/1	65	8700	1.25	357
P6 (PBB-BAMe₁)	1/1.2[a]	1/1	54	11900	2.16	335

[a] Feeding monomer: PBB/BAMe.

[b] Determined by ^{1}H NMR spectra.

[c] Weight-average molecular weight (M_w) and polydispersity index (PDI) determined by GPC in DMF using polystyrene as the standard.

[d] Temperature (°C) at 5% weight loss measured by TGA at a heating rate of 20 °C min^{-1} under nitrogen.
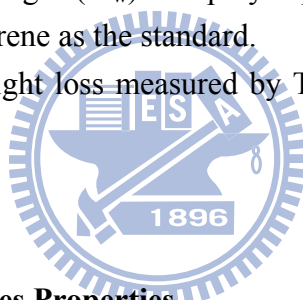
3.4.2 Thermal and Mesophases Properties

The thermal stability of polymers **P1−P6** was evaluated by thermogravimetric analysis (TGA), and their corresponding data are also summarized in Table 3.1. The TGA analyses indicate that the degradation temperatures (T_ds) of all polymers with 5% weight loss (under nitrogen) were ranged from 335 to 357 °C. The T_ds of hompolymers **P1** and **P5** are slightly higher than its analogous H-bonded copolymer networks, which due to the polymeric chains in the random copolymer system was disturbed lead to a decrease T_ds values of copolymers. However, these copolymers showed nearly the same the T_ds values (except **P6** with the lowest).

To investigate the H-bonding effect on the thermal properties of H-bonded copolymers networks, introduction of benzoic acid (**BA**) donors with various molar ratios comprising H-bonded networks with light-emitting acceptor **PBB** moieties were studied. Phase transition temperatures and associated enthalpies of polymers **P1**−**P6** and full H-bonded polymers networks **P1/P5**, determined by a combination differential scanning calorimetry (DSC) under nitrogen and polarizing optical microscopy (POM) measurements are summarized in Table 3.2. Polymers **P1**−**P5** only show glass transition temperatures (T_gs) and are in the range of 63−73 °C. The T_gs of copolymers **P2**−**P4** are higher than that of the individual hompolymers **P1** and **P5**. This result is attributed to the contribution of the intermolecular H-boned between the pyridyl and carboxylic acid groups interactions, which not only extend conformations of pendant units and enhance stiffness of pendant units, but further lead to restrict the rotational freedom and motion of polymeric chains and influence a T_g. However, when the BA content was increased, among the T_g values of copolymers **P2**−**P4** were not significantly different; so the T_g values will not depend on BA content. For comparison reasons, the H-bonded effect on the enhanced of the T_g value within H-bonded copolymer networks, without H-bonds of analogous copolymer **P6** were prepared by emitting acceptor **PBB** and **BAMe**. As expected, the T_g value of the lack of H-bonds copolymer **P6** are much lower in comparison with those of H-bonded

copolymer networks. Comparison with the full H-bonded polymers networks **P1/P5**, the full H-bonded copolymer networks **P2** exhibit higher the T_g value. This may be ascribed to well-distribution of configurations arrangement of comonoeric units of the backbone in full H-bonded copolymer networks **P2** was more effective in stabilizing the backbone, which was not easier cooperative motion of polymeric chains. The full H-bonded polymer networks **P1/P5** detects only a T_g, which typically implies the miscibilities of homopolymers **P1** and **P5**.

Table 3.2   Thermal Properties of Polymers P1−P6 and Fully H-Bonded Homopolymer Complex P1/P5[a]

polymer or H-bonded networks	phase transition temperature (°C) and enthalpy (ΔH/J g^{-1})	
	heating	cooling
P1 (HPBB)	g 63.3 N 125.0[b] I	I 123.0[b] N 63.1 g
P2 (PBB-BA$_1$)	g 72.6 S$_A$ 110.4 (3.2) I	I 108.2 (-2.9) S$_A$ 70.7 g
P3 (PBB-BA$_4$)	g 73.4 S$_A$ 117.4 (3.8) I	I 115.3.0 (-3.7) S$_A$ 72.1 g
P4 (PBB-BA$_{12}$)	g 72.7 (S$_A$)[c] S$_C$ 150.2 (0.9) I	I 145.0 (-0.7) S$_C$ (S$_A$)[c] 71.7 g
P5 (HBA)	g 65.7 S$_C$ 161.9 (14.7) I	I 156.9 (-13.9) S$_C$ 64.6 g
P6 (PBB-BAMe$_1$)	g 26.6 I	I 26.2 g
P1/P5	g 62.9 S$_A$ 137.6 (5.2) I	I 132.17 (-4.8) S$_A$ 62.6 g

[a] Measured by DSC during the second heating and first cooling rate of 10 °C min^{-1} under nitrogen. Abbreviations: g = glassy state; S$_C$ = smectic C phase; S$_A$ = smectic A phase; N = nematic phase; I = isotropic state.

[b] Determined by POM observation.

[c] **PBB-BA** polymer complex network domain in **P4**: S$_A$ 133.5 (3.6) I and I 130.0 (-3.3) S$_A$ upon heating and cooling, respectively; **BA** polymer domain in **P4**: S$_C$ 150.2 (0.9) I and I 145.0 (-0.7) S$_C$ upon heating and cooling, respectively.

Furthermore, polymers **P1−P5** and the full H-bonded polymers networks **P1/P5**

show enantiotropic mesomorphic behavior until the temperature of freezing of mesophase into their glassy states. Therefore, these polymers can be retained the mesogenic arrangement at room temperature. Only analogous copolymer **P6** does not exhibit any mesomorphism and possesses an amorphous nature (e.g. without any melting and crystallization peaks), which due to the lack of H-bonded effect. In the case of H-bonded copolymer networks containing different molar ratios of emitting acceptor **PBB** moieties and donor **BA** moieties are favored the formation of smectic A (S_A) phase, which may be attributed to the stabilization of the assembly of the S_A phase by H-bonded crosslinks. The isotropization temperatures (T_is) and temperature ranges of the S_A phase of H-bonded copolymer networks **P2−P4** were gradually increase as the molar ratio of the **BA** moieties increases (see Table 3.2). For example, the highest **BA** contents in H-bonded copolymer networks **P4** is owing to the highest T_i and the S_C phase formation (during cooling from the isotropic state to 130 °C) as a result of a more excess of the BA moieties of copolymers crosslinking within themselves and formation of acid dimmers. Subsequent further cooling in the temperature below 130 °C, **P4** is revealing to the wider temperature range and the coexistence of the two S_A phases which would gradually induce the formation of the S_A phase and further help sustain the S_A phase stability in the H-bonded copolymer networks (the phases transition process is further confirmed as shown below X-ray

part). However, the S_A phase stability of H-bonded copolymer networks **P3** not only substantially decreased but also no S_C phase was observed by DSC measurements. This is probably due to a little excess of the **BA** moieties of copolymers crosslinking within themselves (acid dimmers), in which the BA moieties is more disordered whereas decreased the stability of the S_A phase as comparison with H-bonded copolymer networks **P4**. On the other hand, the full H-bonded polymers networks **P1/P5** is notably higher T_i and wider temperature ranges of the S_A phase than that of full H-bonded polymer networks **P2**. These results are probably that the full H-bonded polymer networks **P1/P5** has coherent packing of H-bonded networks lead to more ordered arrangement.

In polarizing optical microscopy (POM) study during heating from the glassy state, the acceptor homopolymer **P1** displays the nematic phase formation of a weak birefringent regions at 90 °C (see Figure 3.2a), which was further identified in our previous work by powder one-dimensional X-ray diffraction (1D-XRD). Upon cooling form the isotropic state, the donor homopolymer **P5** displays two characteristic non-specific small fragment and schlieren textures of the mesophase at 135 °C (see Figure 3.2b) resulting from the dimerization of their carboxylic acids via H-bonded. In addition, the full H-bonded copolymer networks **P2** and full H-bonded polymers networks **P1/P5** show a colorful birefringent texture, as shown Figure 3.2c

(at 95 °C) and Figure 3.2d (at 115 °C), respectively. In general, the viscous polymers do not easily form a typical mesogenic textures, so the results of POM do not provide clear clues for us to identify the nature of their mesophases (further confirmed by X-ray measurements, see below).

(a)

(b)

(c)

(d)
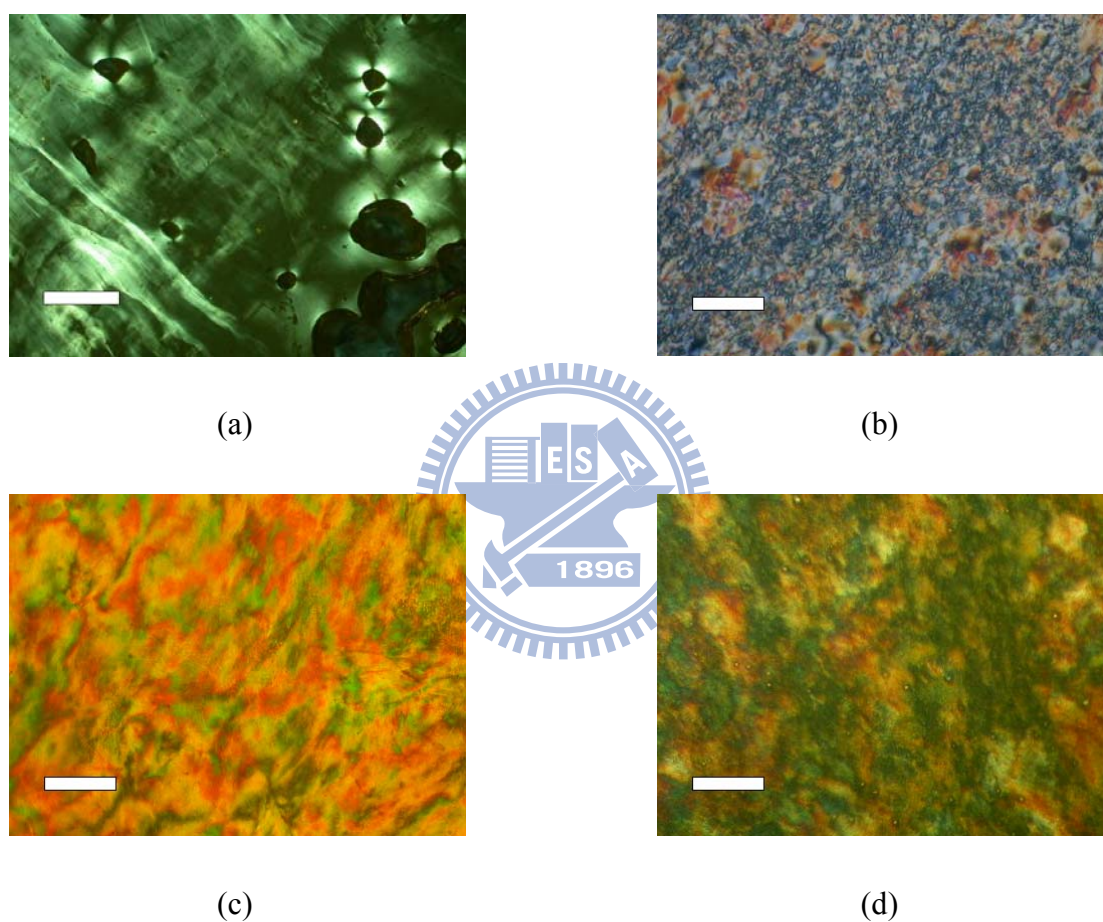
Figure 3.2 Optical micrographs of liquid crystalline textures (from POM with crossed polarizers): (a) H-acceptor homopolymer **P1** at 90 °C (cooling), (b) H-donor homopolymer **P5** at 135 °C (cooling), (c) fully H-bonded copolymer **P2** at 95 °C (cooling), and (d) fully H-bonded homopolymer complex **P1/P5** at 115 °C (cooling). The scale bars all correspond to 100 μm.

3.4.3 XRD Studies

To investigate the molecular arrangements of the mesophases by XRD measurements, the XRD studies were carried out at the temperature ranges of mesophases for polymers **P1−P5** and full H-bonded polymer networks **P1/P5**. Their XRD experimental results and theoretical molecular lengths are listed in Table 3. The layer d spacing was detected by XRD based on first-order reflection as indexed (100) for all samples. The theoretical values of the full extended molecular length for the H-bonded networks are calculated by the sum of molecular projection lengths of the two H-boned components along the rigid cores though molecular modeling, where we assumes that all molecular structures are coplanar and the alkoxy chain spacers are in the fully extended all-*trans* conformation.

The XRD analysis of donor homopolymer **P5** showed two reflection peaks corresponding to d spacings of 32.8 and 16.2 Å with a reciprocal spacing ratio of 1:2 that cab be indexed as the (100) and (200) reflections of a smectic phase. The layer d spacing of 32.8 Å is much smaller than twice of the calculated theoretical molecular lengths (41.4 Å), indicating a tilted arrangement of bilayer smectic structure, i.e., bilayer S_C phase with tilt angle of 38° along the layer normal direction (see Table 3.3). As shown in Figure 3.3, the XRD pattern of both the full H-bonded copolymer networks **P2** and full H-bonded polymers networks **P1/P5** at 85 °C show two

reflection peaks corresponding to the first and second orders of diffraction (with a reciprocal spacing ratio of 1:2), consistent with a smectic structure in the small-angle region and a diffuse halo at about 4.5 Å associated with the liquid-like order of the average lateral spacing distances between side chain of extended mesogenic units in the wide-angle region. The layer d spacing value of the full H-bonded copolymer networks **P2** and full H-bonded polymers networks **P1/P5** are 51.2 and 50.7 Å, respectively, and corresponding approximately to the calculated theoretical molecular lengths is 51.6 Å, suggest the formation of the S_A mesophase within a monolayer structure.
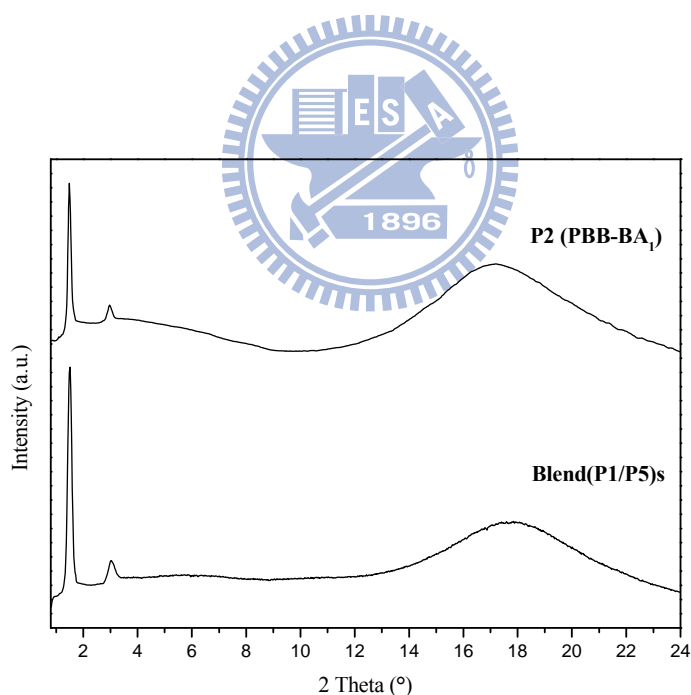
Figure 3.3 One-dimensional powder X-ray diffraction (1D-XRD) patterns (intensity against angle profiles) obtained in the S_A phase of the fully H-bonded copolymer **P2** and fully H-bonded homopolymer complex **P1/P5** at 85 °C (cooling).

Table 3.3   The *d* Spacing Values and Theoretical Molecular Lengths of Polymers P1−P5 and Fully H-Bonded Homopolymer Complex P1/P5[a,b]

polymer or H-bonded networks	temp[c] (°C)	phase	obtained *d* spacing value (*hkl*)[d]	theoretical molecular length
P1 (HPBB)	90	N	--[e]	30.9
P2 (PBB-BA$_1$)	85	S$_A$	51.2 (100), 25.5 (200)	41.4−51.6
P3 (PBB-BA$_4$)	85	S$_A$	52.9 (100)	41.4−51.6
P4 (PBB-BA$_{12}$)	85	S$_A$	58.0 (100), 41.1 (100)	41.4−51.6
P5 (HBA)	130	S$_C$	32.8 (100), 16.2 (200)	20.7
P1/P5	85	S$_A$	50.7 (100), 25.1 (200)	51.6

[a] The obtained *d*-spacing values (Å) and theoretical molecular lengths (Å) are the observed from XRD measurements and calculated from molecular modeling, respectively.

[b] All samples exhibited a diffuse halo at around 4.5−4.3 Å.

[c] Determined by cooling samples from isotropic temperature.

[d] *hkl* is the indexation of the reflection.

[e] No observed diffraction peak.
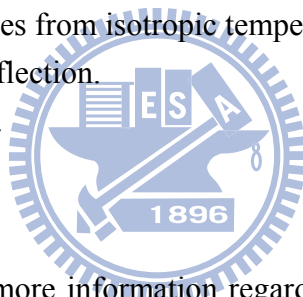
In order to further acquire more information regarding the molecular organization of the S$_A$ mesophase in the full H-bonded copolymer networks **P2**, two-dimensional X-ray diffraction (2D-XRD) pattern was performed by drawing sample to fiber at room temperature. As shown in Figure 3.4a, the X-ray incident beam is perpendicular to the fiber direction that is along the equator. In this pattern, the diffraction pattern including two symmetric intense spots in the small-angle region on the equator and other two broad halos in the wide-angle region on the meridian, concentrated at the azimuthal angle of 90° between two regions (see Figure 3.4b), indicates clearly that the layer normal is perpendicular to the meridian of the pattern and the layer

reflections lie at the equator.

(a)

(b)
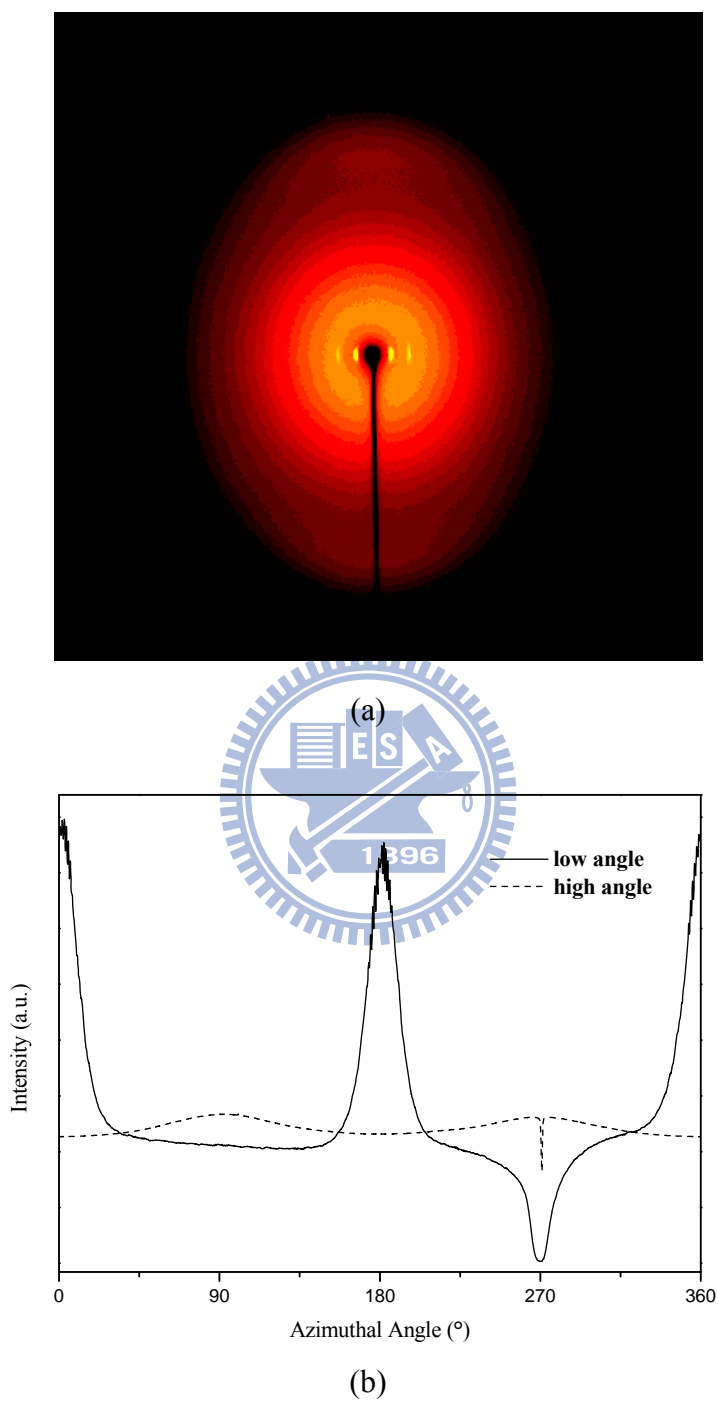
Figure 3.4 (a) Two-dimensional X-ray diffraction (2D-XRD) pattern obtained from the as-drawn fiber of H-bonded copolymer **P2** at room temperature and (b) azimuthal scan of low and high angle reflections. Fiber direction is horizontal axis.

In other words, the side chain of extended mesogenic units is perpendicular to the backbone and aligns along the fiber direction. These results substantiate the formation of orthogonal arrangement of monolayer S_A structure with a layer d spacing of 51.4 Å (approximately equal to the calculated theoretical molecular lengths is 51.6 Å).

From the DSC result, H-bonded polymers networks **P4** exhibits two mesophases. The detail of this phenomenon is studied by temperature-dependent XRD experiments. As shown in Figure 3.5 between isotropic temperature and 155 °C, due to predominant of H-bonded crosslinkings between the **BA** moieties in the copolymer system at a certain temperature, one reflection peak of 35.2 Å can be observed corresponding to an S_C mesophase of the **BA** moieties contrast to the layer d spacing of homopolymer **P5** (see Table 3.3). However, the reflection peak shifts toward to a lower angle with decreasing temperature. Below 130 °C, a pair of reflection peak at higher angle develops corresponding to twice of the calculated theoretical molecular lengths (41.4 Å) of the **BA** moieties. It is assumed that predominant crosslinking between the **BA** moieties themselves in the bilayer S_C mesophase is induced and transforms into a bilayer S_A mesophase. A pair of reflection peak at lower angle appears a lager layers d spacing value, longer than that of calculated theoretical molecular lengths of H-bonded networks (51.6 Å), indicating H-bonded networks from between **PBB** and **BA** moieties the formation of the interdigitated bilayer S_A

phase. These layers *d* spacing data may result from a coexistence of bilayer S_A

(between 40.2 and 42.7 Å) and interdigitated bilayer S_A (between 57.7 and 61.0 Å)

phases in the H-bonded polymers networks **P4**.
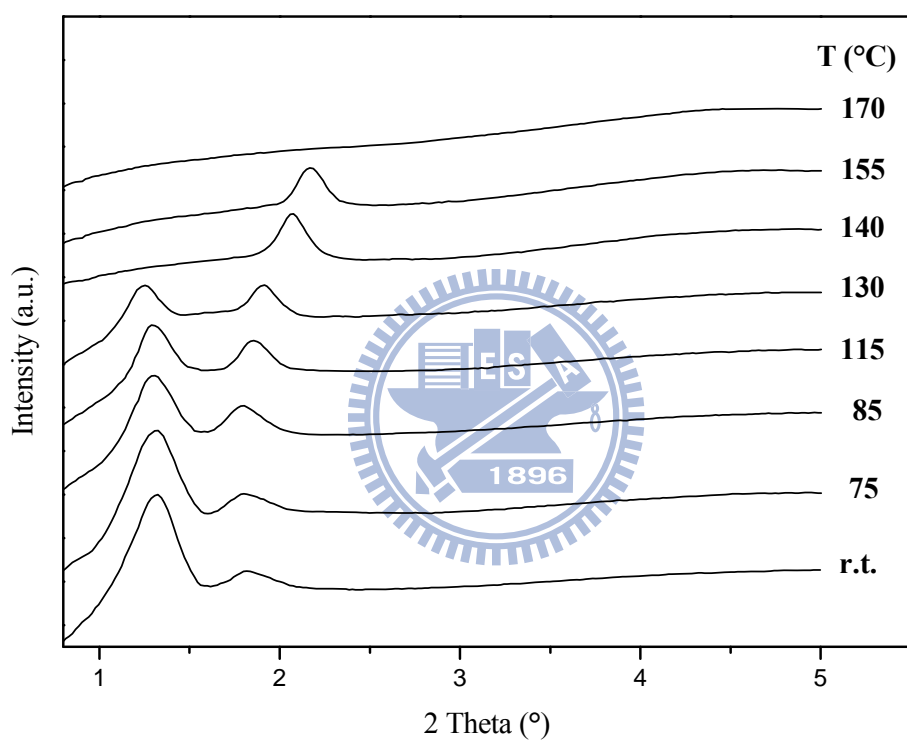
Figure 3.5 Temperature-dependent one-dimensional powder X-ray diffraction

(1D-XRD) pattern in the low angle region of H-boned copolymer **P4** recorded during

the cooling process from the isotropic state to room temperature.

3.4.4 FTIR Studies

The existence of hydrogen bonds in the H-bonded networks can be proved by temperature-various FTIR spectroscopy, as shown in Figure 3.6. At room temperature (glassy state), In contrast to the O-H bands of pure donor homopolymer **P5** (H-bonded dimer) at 2627 and 2562 cm^{-1}, two new broad O-H bands centered at 1920 and 2515 cm^{-1} were observed in the full H-bonded copolymer networks **P2** is indicative of stronger hydrogen bonding between the pyridyl and the carboxylic acid groups in the H-bonded networks. On the other hand, a shoulder can be seen in the main peak located at 1730 cm^{-1}. This is attributed to a stretching vibration of C=O at 1683 cm^{-1} in pure donor homopolymer **P5** which shifts toward higher wavenumber and overlaps with the band of the ester carbonyl groups at 1730 cm^{-1} in the full H-bonded copolymer networks **P2**, which show the carbonyl group was in a less associated state than that in pure donor homopolymer **P5** (H-bonded dimer). These phenomenons can be explained that hydrogen bonds were formed between **PBB** and **BA** units in the solid film state of the full H-bonded copolymer networks **P2**. When the temperature rises to 100 °C (S$_A$ phase), the carbonyl band only becomes broader. Other characteristic have similar consequences as the room temperature (glassy state). Besides, Upon heating above isotropic state at 170 °C, two broad O-H bands centered at 1920 and 2515 cm^{-1} still persist and become weak, which is attributed to the

hydrogen bonds is stable enough to some extent. In addition, the shoulder (C=O

stretching vibration) of the main peak located at 1730 cm^{-1} was further shifted toward

higher wavenumber and combined with the band of the ester carbonyl groups at 1730

cm[-1] as a result of the formation carbonyl band of the monomeric **BA**. These results

suggest that the stability of the hydrogen bonds is decreased in the isotropic state.
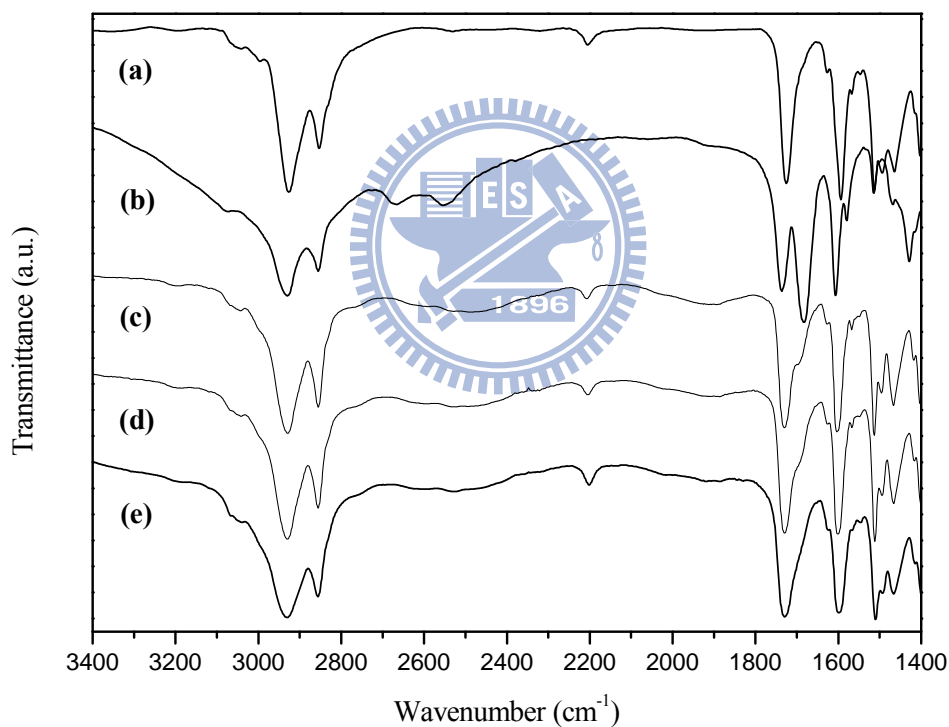
Figure 3.6   FT-IR spectra recorded for (a) pure H-acceptor homopolymer **P1** and

(b) pure H-donor homopolymer **P5** at room temperature, and (c) fully H-bonded

copolymer **P2** at (c) room temperature (glassy state), (d) 100 °C (S$_A$ phase), and (e)

170 °C (isotropic state).

3.4.5 Optical Properties

The absorption and PL spectra of polymers **P1−P4** and **P6** were measured in both solutions and solid states, and full H-bonded polymer networks **P1/P5** in solid state. Their photophysical properties are summarized in Table 4. As shown in Figure 3.7, the absorption bands of polymers **P1−P4**, **P6**, and full H-bonded polymer networks **P1/P5** in solid states at c.a. 324 and 395 nm are assigned to the light-emitting PBB segments of the acceptor moieties. The absorption spectra of polymers **P1−P4** and **P6** in solid films are similar except for 9−11 nm of red-shifts in absorption maximum in contrast to those in THF solutions (see Table 3.4). As shown in Figure 8, the emission spectra of polymers **P1−P4** and **P6** in solid films show 43−83 nm of significant red-shifts in comparison with their corresponding dilute solutions, which was due to the formation of π-π stacking and molecular aggregation in solid state. Compared with acceptor homopolymer **P1** in Figure 3.8, the H-bonded copolymer networks **P2−P4** exhibit red-shifted PL emissions were excited at the maximum absorption of emitter PBB with values of λ_{max} at 531, 523, and 517 nm, respectively. This result is similar to our previous work,[68] where red shifts of PL emissions are expected in the H-bonded structures. The non-photoluminescent proton donors bearing benzoic acids (as solid solutions) are H-bonded to the photoluminescent proton acceptors containing pyridyl groups. Therefore, H-bonded copolymer networks containing acceptor emitter

PBB and different the molar ratios of proton donors (benzoic acids) appeared to have different degrees of red-shifted PL emissions between acceptor homopolymer **P1** and its analogous H-bonded copolymer networks. The red-shifts of PL emissions in H-bonded copolymer networks **P2−P4** are 35, 27, and 21 nm, respectively, i.e., H-bonded copolymer networks with higher benzoic acid contents have a smaller degrees of red-shifted PL emissions than the lower benzoic acid contents ones. It clearly indicates that the higher benzoic acid contents in H-bonded copolymer networks have higher dilution effect than lower benzoic acid contents in H-bonded copolymer networks, so the higher benzoic acid contents efficiently minimize interchain interaction and lower the aggregation extent between emitter **PBB** cores.

To further evaluate the both dilution effect and H-bonded effect in H-bonded copolymer networks, the monomers of **BAMe** and **BA** were copolymerized with acceptor emitter PBB in molar ratio of 1:1 to construct the without H-bonded copolymer **P6** and H-bonded copolymer **P2**, respectively. In contrast to the acceptor homopolymer **P1**, the analogous copolymer **P6** without H-bonds exhibits 6 nm blue-shifted PL emission due to dilution effect and the full H-bonded copolymer networks **P2** exhibits 35 nm red-shifted PL emission due to H-bonded effect. This result can be explained that in H-bonded copolymer networks system, the benzoic acids play both roles as solid solvents and H-bonded donors at the same time. Thus,

the dilution effect of the acids (as solid solvents) to induce blue-shift of PL and the H-bonded effect of the acid donors to cause red-shift of PL are coexistence and competitive. As a consequence, in the cases of H-bonded copolymer networks **P2−P4**, it seems that the H-boned effect of red-shifted PL emissions is more dominant than the dilution effect.
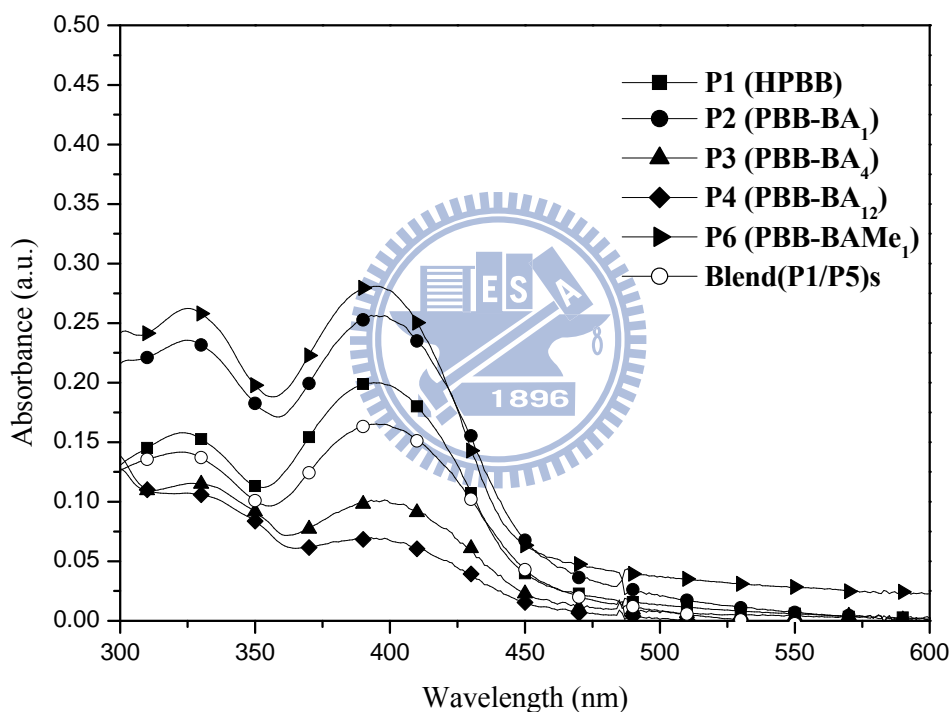
Figure 3.7 Absorption spectra of polymers **P1−P4**, **P6**, and fully H-bonded homopolymer complex **P1/P5** in solid films.
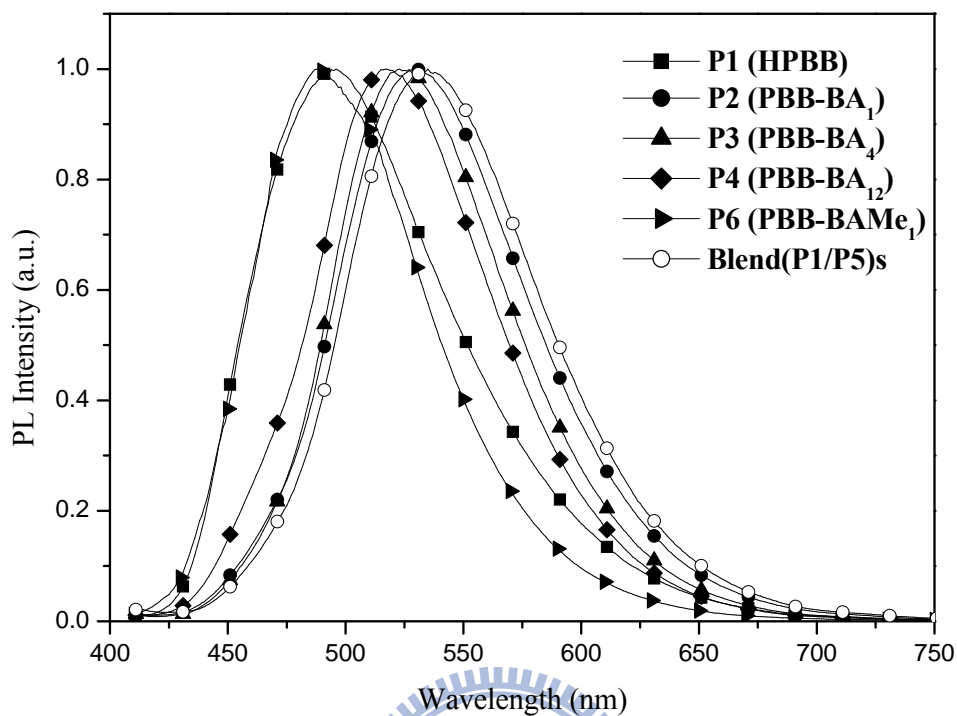
Figure 3.8 Normalized PL spectra of polymers **P1**−**P4**, **P6**, and fully H-bonded

homopolymer complex **P1/P5** were excited at the maximum absorption of

light-emitting H-acceptor PBB segments in solid films.

In addition, the full H-bonded copolymer networks **P2** has smaller degrees of

red-shift in PL emission than the full H-bonded polymers networks **P1/P5** (see Figure

3.8 and Table 3.4) due to the well-distribution with configurations arrangement of

comonoeric units of the backbone in full H-bonded copolymer networks **P2**, which

lead to resist interchain interaction in the copolymer and form relatively disordered

aggregates. On the contrary, the full H-bonded polymers networks **P1/P5** is more ordered assemblies consist of the H-bonds and tend to form the stronger aggregation, which created the larger degrees of red-shift in PL emission in solid films. Besides, as listed in Table 3, the PL quantum yields (Φ_{PL}) of polymers **P1−P4** and **P6** in dilute THF solutions were in the range of 0.49−0.71, which depends on the content of the BA moieties. The Φ_{PL} vales of polymers **P1−P4**, **P6**, and full H-bonded polymer network **P1/P5** in solid films were in the range of 0.11−0.53 and the same trend is also observed in their solution counterparts. The results clearly indicate that the dilution effect by the BA moieties was incorporated into the copolymers to inhibit the interchain aggregation/quenching, and hence the copolymers exhibit an enhanced Φ_{PL} values as the molar ratio of the **BA** moieties increases.
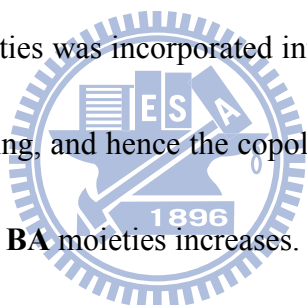
Table 3.4 **Absorption and PL Emission Spectral Data of Polymers P1−P4, P6, and Fully H-Bonded Homopolymer Complex P1/P5 in THF Solutions and Solid Films**

polymer or H-bonded networks	$\lambda_{abs,sol}{}^{a}$ (nm)	$\lambda_{abs,film}$ (nm)	$\lambda_{PL,sol}{}^{a,b}$ (nm)	$\lambda_{PL,film}{}^{b}$ (nm)	$\triangle\lambda_{PL}{}^{c}$ (nm)	$\Phi_{PL,sol}{}^{b,d}$	$\Phi_{PL,film}{}^{b,e}$
P1 (HPBB)	320, 385	324, 395	449	496	--	0.49	0.11
P2 (PBB-BA$_1$)	321, 385	327, 396	448	531	35	0.52	0.15
P3 (PBB-BA$_4$)	322, 385	327, 395	446	523	27	0.59	0.24
P4 (PBB-BA$_{12}$)	325, 385	326, 395	444	517	21	0.71	0.53
P6 (PBB-BAMe$_1$)	321, 385	325, 394	447	490	-6	0.60	0.18
P1/P5		323, 396		535	39		0.12

[a] Measured in dilute THF solutions.

[b] Excited at the maximum absorption of acceptor emitter PBB segments.

[c] Different degrees of red-shifted (or "-" indicated blue-shifted) PL emissions between the acceptor homopolymer and its analogous copolymers.

[d] Solution fluorescence quantum efficiency were measured in THF, relative to 9,10-diphenylanthracene ($\Phi_{PL} = 0.90$).

[e] PL quantum efficiency were estimated relative to 9,10-diphenylanthracene in poly-(methyl methacrylate) as a standard ($\Phi_{PL} = 0.83$).

3.4.6 Electrochemical Properties

The electrochemical behavior of acceptor homopolymer **P1** and its full H-bonded networks were probed by cyclic voltammetry (CV), and the results are summarized in Table 5. The highest occupied molecular orbital (HOMO) and lowest unoccupied molecular orbital (LUMO) levels were calculated according to the following equation:

$E_{HOMO}/E_{LUMO} = -e(E_{ox/onset}/E_{red/onset} + 4.4)$ (eV),[69] where $E_{ox/onset}$ and $E_{red/onset}$ were the onset potentials for the oxidation and reduction processes of the sample versus the saturated calomel electrode (SCE). The onset potentials were determined from the

intersection of two tangents drawn at the rising and background currents of the CV curve. The acceptor homopolymer **P1** and its full H-bonded networks show the onset potentials of oxidation between 0.99 and 1.28 V in anodic scans (see Table 3.5). The reduction potential peaks of acceptor homopolymer **P1** and its full H-bonded networks were not observed in the CV measurements, so crude estimations of LUMO values in reduction processes of acceptor homopolymer **P1** and its full H-bonded networks were deduced from the HOMO values and the optical band gaps. The optical band gaps estimated from absorption onset of acceptor homopolymer **P1** and its full H-bonded networks in solid films are also listed in Table 5 and were calculated to be in the range of 2.67−2.73eV, which reveals that acceptor homopolymer **P1** has a larger band gap than that of its full H-bonded networks. However, it seems that the full H-bonded networks show lower HOMO and LUMO levels than acceptor homopolymer **P1**, which is probably ascribed to the presence of **BA** moieties in H-bonded networks through H-bonded self-assembly. The lower LUMO levels of full H-bonded networks will a significant enhance the electron injection from cathode to the emitter layer.

Table 3.5   Electrochemical Properties of H-Acceptor Homopolymer P1 and Its Fully H-Boned Copolymer P2 and Homopolymer Complex P1/P5

polymer or H-bonded networks	optical band gap[a] (eV)	$E_{ox/onset}$[b] (V)	HOMO (eV)	LUMO[c] (eV)
P1 (HPBB)	2.73	0.99	-5.30	-2.57
P2 (PBB-BA$_1$)	2.69	1.26	-5.66	-2.97
P1/P5	2.67	1.28	-5.68	-3.01

[a] Estimated from the onset wavelength of optical absorption in solid films.
[b] The onset oxidation potential vs SCE reference.
[c] LUMO energy levels were deduced from HOMO values and optical band gaps.

3.4.7 Electroluminescence Properties

The acceptor homopolymer **P1** and its full H-bonded networks were fabricated into four-layer PLED devices, with a configuration of ITO/PEDOT:PSS (50 nm)/polymer (**P1** or its full H-bonded networks) (55−70 nm)/BCP (10 nm)/Alq$_3$ (30 nm)/LiF (1 nm)/Al (150 nm) using standard procedures of spin-coating and vacuum deposition methods, where polymer (**P1** or its full H-bonded networks) were used as the emission layer and PEDOT:PSS as the hole transporting layer (anode buffer). Besides, the BCP, Alq$_3$, and LiF/Al were used as hole-blocking layer, electron-transporting layer, and bilayer cathodes, respectively. As shown in Figure 3.9, under forward bias voltages, the EL spectra of acceptor homopolymer **P1**, full H-bonded copolymer networks **P2**, and full H-bonded polymer networks **P1/P5** show the maximum emission at 500, 537, and 540 nm, respectively, indicating that this can

effectively tune the emission color from greenish-blue to green by the incorporation

of **BA** donors in the supramolecular structures containing acceptor emitter copolymer

or polymers blend. The electroluminescence (EL) emission peaks of all PLED devices

were very similar with their corresponding PL emission peaks of the solid films

within only a slight red-shift.
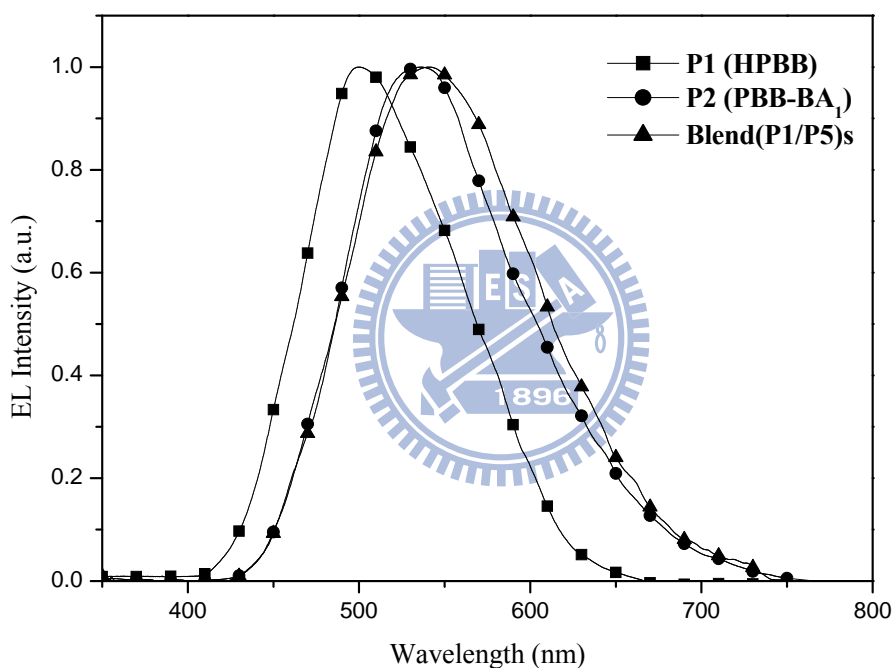
Figure 3.9 Normalized EL spectra of PLED devices with configurations of
ITO/PEDOT:PSS/polymer (H-acceptor **P1** or its fully H-bonded cross-linking
copolymer **P2** and homopolymer complex (**P1/P5**))/BCP/Alq$_3$/LiF/Al.

The current-voltage and luminescence-voltage characteristics are displayed in

Figure 3.10 and the EL properties are collected in Table 3.6. A comparison of the turn-on voltages of all PLED devices, full H-bonded networks devices is higher turn-on voltage than acceptor homopolymer **P1** devices. This may be due to the intrinsic insulation properties of nonconjugated segments of **BA** donors with long alkoxy side chains in H-bonded networks which consequently deteriorate the charge-carrier transporting properties, lead to increases the turn-on voltage. In addition, the device performance characteristics of full H-bonded copolymer networks **P2** device with a maximum luminance and luminous efficiency of 268 cd/m^2 at 22 V and 0.152 cd/A at 100 mA/cm^2, respectively, are better than that of full H-bonded polymer networks **P1**/**P5** devices. This presumably could be attributed that the full H-bonded polymer networks **P1**/**P5** device has a strong interchain interactions increases and the probability of interchain exciton quenching thus lead to deteriorate device performance.

Table 3.6 Electroluminescence (EL) Device Performance Characteristics of H-Acceptor Homopolymer P1 and Its Fully H-Boned Copolymer P2 and Homopolymer Complex P1/P5[a]

polymer or H-bonded networks	$\lambda_{EL, film}$ (nm)	V_{on}[a] (V)	luminous efficiency[b] (cd/A)	power efficiency[b] (lm/W)	max. luminance (cd/m^2) (V)
P1 (HPBB)	500	7.5	0.261	0.040	693 (28)
P2 (PBB-BA$_1$)	537	8.5	0.152	0.031	268 (22)
P1/P5	542	8.5	0.112	0.020	157 (23)

[a] V_{on} is the turn on voltage of light.

[b] Measured at 100 mA/cm^2.
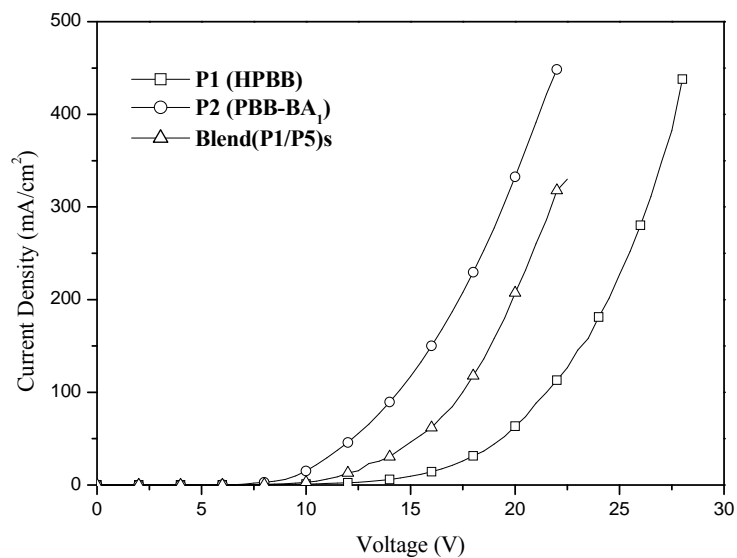
(a)
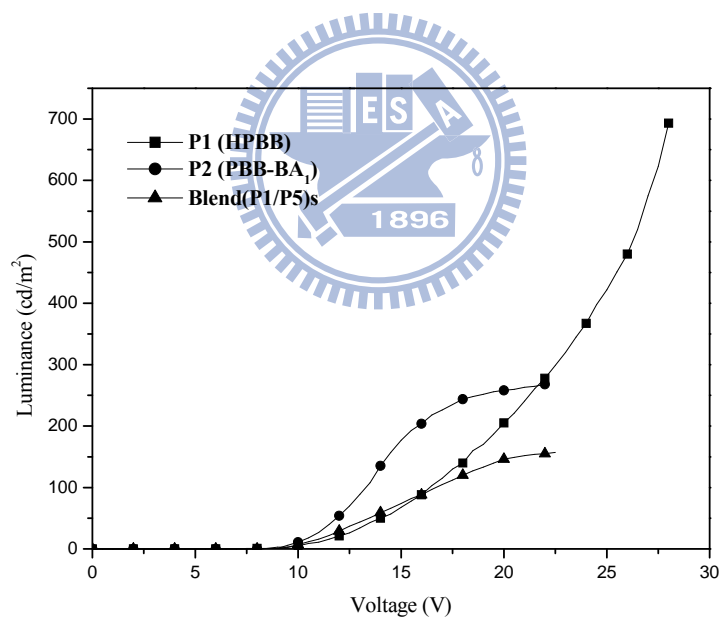
(b)

Figure 3.10 (a) Current density-voltage (*I-V*) curves and (b) luminance-voltage (*L-V*) curves of PLED devices with configurations of ITO/PEDOT:PSS/polymer (H-acceptor **P1** or its fully H-bonded cross-linking copolymer **P2** and homopolymer complex (**P1/P5**))/BCP/Alq$_3$/LiF/Al.

3.5 Conclusion

A series of well-defined H-bonded side chain mesogenic copolymer networks containing proton acceptor emitter **PBB** with different molar ratios of proton donor benzoic acid (**BA**) were successfully synthesized. The polymers **P1−P5** and full H-bonded polymers networks **P1/P5** show enantiotropic mesomorphic behavior and give rise to mesomorphic glasses at room temperature. Compared with acceptor homopolymer **P1**, the H-bonded copolymer networks **P2−P4** exhibit red-shifted PL emissions that due to H-boned effect. In addition, the higher benzoic acid contents in H-bonded copolymer networks have higher dilution effect than lower benzoic acid contents one, thereby the higher benzoic acid contents can be efficiently minimize interchain interaction and lower the aggregation extent between emitter **PBB** cores. So the benzoic acids play both roles as solid solvents and H-bonded donors at the same time in H-bonded copolymer networks system. The four-layer PLED devices with the configuration of ITO/PEDOT:PSS/(**P1** or its H-bonded networks)/BCP/Alq$_3$/LiF/Al were fabricated, and effectively tuned the emission color from greenish-blue to green by the incorporation **BA** moieties donors in the H-bonded networks containing acceptor emitter **PBB** through a H-bonded self-assembly process. In addition, a multilayered PLED device containing fully H-bonded cross-linking copolymer **P2** showed EL emission of 537 nm under a turn-on voltage of 8.5 V, with

a maximum luminance of 268 cd/m^2 at 22 V and a luminance efficiency of 0.152 cd/A

at 100 mA/cm^2.

Chapter 4

Novel chemosensory materials based on Side-Chain Polymer Containing Fluorescent Receptor Pendants Functionalized with Pyridyl Groups

4.1 Abstract

A novel light-emitting receptor **PBBD** (**M1**) containing three conjugated aromatic rings, including one pyridyl terminus and two lateral methoxyl groups (on the middle ring), was successfully synthesized via Wittig and Pd-catalyzed Heck coupling reactions. Homopolymer **P1** shows a glass transition temperature (T_g) of 60 °C and melting transition temperature (T_i) up to 150 °C. In CH$_3$COOH solution, homopolymer **P1** exhibits a pH-tunable photoluminescence with emission maximum varies from 460 to 605 nm. The fluorescence of **P1** was efficiently quenched upon addition of transition metal ions due to facile energy migration within the pendant groups of the polymer. **P1** exhibits an extraordinary sensory selectivity for Ni^{2+} over other transition metal ions as a result of the stronger binding ability of the Ni^{2+} onto polymer **P1** than other transition metals ions. Stern-Volmer constant for the Ni^{2+} ion sensing was determined through concentration dependent studies as 5.65×10^6 M^{-1}. In addition, the ON-OFF-ON fluorescent switch behavior upon the addition of

PMDTA to the **P1**-Cu^{2+} complexes demonstrates a superior reusability of this chemosensor which is important for the practical use.

4.2 Introduction

Supramolecular chemistry approaches have generated a great variety of multicomponent architectures which typically organized into higher-order functional structures through the virtue of noncovalent interactions. Examples such as supramolecular assemblies system have attracted continuing interest due to their fascinating properties and potential uses in electronics, optics, catalysts, sensors, and other fields in which synthetic self-assembling systems allow control of material properties and are a valuable contribution to the field of materials engineering.

In recent years, conjugated polymers (CPs) are successfully proven for use in suitability for a variety of practical applications because their well-defined chemical structure facilitates tuning of electronic properties, which include polymer light-emitting diodes (PLEDs), thin film transistors (TFTs), and photovoltaics (PVs). Nonetheless, a new development of fluorescence sensors based on CPs materials are emerging after the discovery of some polymers exhibit high fluorescence sensitivity to pH, chemical or biological environments, as demonstrated by the large number of scientific publications in this area. Mechanisms of those fluorescence sensors have

been reported which utilize photophysical changes phenomena such as photoinduced electron transfer (PET),[124-126] photoinduced charge transfer (PCT),[127-129] excimer/exciplex formation, and electronic energy transfer (EET), etc.

Of various kinds of sensors, chemosensors, i.e., those sensors that transform chemical response into analytically detectable signal, are of paramount importance. They have, in fact, already found a wide application in many fields, such as environmental monitoring, process control, food analysis, medical diagnosis, and, lately, toxic gases and explosives detection. Among different target analytes, a special interest is devoted into the development of chemosensors to detect transition metal ions of trace amounts. A promising candidate for a chemosensor should meet the need of being selective, sensitive and reusable. The simplest approach to this requirement consists in using fluorescent moieties that are at the same time metal ion receptors, such as hydroxyquinoline, bipyridyl derivatives.[130] The applicability and the characteristics of these species are mostly well established. Specifically, the formation of a complex through a pyridyl-N-metal coordination and the detection of the corresponding fluorescent properties provide a guide for us to construct a model of a conjugated polymer-based chemosensor for recognizing metal ions.

In addition, there have been numerous fluorescent chemosensors reported by the virtue of the formation of organic/inorganic nanocomposite.[131,132] Especially, the gold

nanoparticles (AuNPs) based chemosensor has attracted many interests in bioanalysis in recent years. AuNP offers unique optical properties from their surface plasmon resonance (SPR) absorption, high surface area to volume ratio and biocompatibility for the amplified optical detection. Herein we design and synthesize a side-chain conjugated polymer with pyridyl pendant group as receptors for analyte matirals. The selectivity and sensitivity of polymer **P1** sensor, titration experiments were conducted with an addition of various metal ions. In addition, compare the sensitivity of polymer **P1** with its complementary monomer **M1**, PL-quenching characteristics toward Cu^{2+} ion were investigated.

4.3 Experimental Section

4.3.1 Measurements and Characterization

^{1}H NMR spectra were recorded on a Varian Unity 300 MHz spectrometer using $CDCl_3$ and DMSO-d_6 as solvents. Elemental analyses were performed on a HERAEUS CHN-OS RAPID elemental analyzer. High resolution electron impact mass data were obtained on a Finnigan-MAT-95XL. Phase transition temperatures were determined by differential scanning calorimetry (DSC, model: Perkin Elmer Diamond) under N_2 with a heating and cooling rate of 10 °C/min and polarizing optical microscope (POM, model: Leica DMLP) equipped with a hot stage.

Thermogravimetric analysis (TGA) was carried out with a TA Instruments Q500 thermogravimetric analyzer at a heating rate of 20 °C/min under nitrogen. Gel permeation chromatography (GPC) analysis was equipped with a Waters HPLC pump 510 connected to a Waters 410 differential refractmeter and three Ultrastyragel columns using polystyrene as a standard and THF as an eluant. UV-vis absorption spectra were recorded on a HP G1103A spectrophotometer, and photoluminescence (PL) spectra were obtained on a Hitachi F-4500 spectrophotometer in dilute THF solutions (10^{-6} M). Thin films of UV-vis and PL measurements were spin-coated on a quartz substrate from THF solutions with a concentration of 10 mg/mL at 3000 rpm.

Scheme 4.1 Synthetic Route of Monomer and Polymer

4.3.2 Materials

Chemicals and solvents were reagent grades and purchased from Aldrich, ACROS, TCI, and Lancaster Chemical Co. Tetrahydrofuran (THF) and triethylamine (Et$_3$N) were distilled to keep anhydrous before use. Azobisisobutyronitrile (AIBN) was recrystallized from methanol before use. The other chemicals were used without further purification.

4-(10-Hydroxydecyloxy)benzaldehyde (1) 4-Hydroxybenzaldehyde (2.0 g, 16.4 mmol) was dissolved in butan-2-one (200 mL), and then potassium carbonate (4.5 g, 32.8 mmol), 10-bromodecanol (4.7 g, 19.7 mmol) and a few amounts of potassium iodide (ca. 10 mg) were added. The reaction mixture was refluxed for 24 h under nitrogen. After cooling to room temperature, the solvent was removed under reduced pressure, and the residue was taken up in water and extracted with CH$_2$Cl$_2$. The organic layer was dried over Na$_2$SO$_4$ and the solvent evaporated under reduced pressure. The crude product was purified by column chromatography (silica gel, n-hexane/ethyl acetate 3:1) to give a white solid. Yield: 4.2 g (91%). ^{1}H NMR (300 MHz, CDCl$_3$): δ (ppm) 9.88 (s, 1H), 7.83 (d, J = 9.0 Hz, 2H), 7.01 (d, J = 8.7 Hz, 2H), 4.04 (t, J = 6.6 Hz, 2H), 3.65 (t, J = 6.6 Hz, 2H), 1.84−1.72 (m, 2H), 1.60−1.50 (m, 2H), 1.41−1.25 (m, 12H).

4-[10-(*tert*-Butyldimethylsilanyloxy)decyloxy]benzaldehyde **(2)**

tert-Butyldimethylsilyl chloride (TBDMSCl, 2.24 g, 16.6 mmol) was added to a solution of **1** (4.2 g, 15.1 mmol) and imidazole (1.33 g, 19.6 mmol) in anhydrous CH_2Cl_2 (200 mL) under nitrogen at 0 °C. The reaction was allowed to warm to room temperature and was stirred overnight. The resulting mixture was poured into water and extracted with CH_2Cl_2. The organic layer was dried over Na_2SO_4 and the solvent evaporated under reduced pressure. The crude product was purified by flash column chromatography (silica gel, n-hexane/ethyl acetate = 25:1) to give a colorless oil. Yield: 5.4 g (95%). ^{1}H NMR (300 MHz, CDCl$_3$): δ (ppm) 9.85 (s, 1H), 7.80 (d, J = 9.0 Hz, 2H), 6.96 (d, J = 9.0 Hz, 2H), 4.01 (t, J = 6.6 Hz, 2H), 3.57 (t, J = 6.6 Hz, 2H), 1.83−1.74 (m, 2H), 1.50−1.28 (m, 14H), 0.88 (s, 9H), 0.01 (s, 6H).

1-[10-(*tert*-Butyldimethylsilanyloxy)decyloxy]-4-vinylbenzene (3) A solution of **2** (5.4 g, 13.8 mmol), potassium *tert*-butoxide (*t*-BuOK, 2.0 g, 17.9 mmol), and methyltriphenylphosphonium bromide (6.39 g, 17.9 mmol) in anhydrous THF (80 mL) was stirred under nitrogen at room temperature for 4 h. Then, the reaction was quenched with water and extracted with dichloromethane. The organic layer was dried over Na_2SO_4 and the solvent evaporated under reduced pressure. The crude product was purified by flash column chromatography (silica gel, n-hexane/ethyl acetate = 40:1) to give a colorless oil. Yield: 4.8 g (89%). ^{1}H NMR (300 MHz, CDCl$_3$): δ (ppm) 7.33 (d, J = 9.0 Hz, 2H), 6.84 (d, J = 8.7 Hz, 2H), 6.65 (dd, J = 17.6 Hz, J = 10.8 Hz,

1H), 5.59 (dd, J = 17.6 Hz, J = 0.9 Hz, 1H), 5.10 (dd, J = 10.8 Hz, J = 0.9 Hz, 1H),

3.95 (t, J = 6.3 Hz, 2H), 3.60 (t, J = 6.6 Hz, 2H), 1.85−1.72 (m, 2H), 1.53−1.30 (m,

14H), 0.90 (s, 9H), 0.02 (s, 6H).
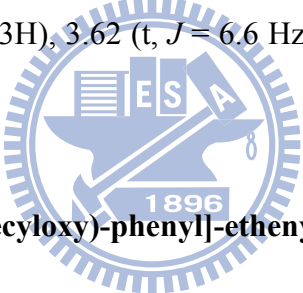
1-{[4-(10-   *tert*-**Butyldimethylsilanyloxy**

-decyloxy)-phenyl]-ethenyl}-2,5-dimethoxy-4-[2-(4-pyridyl)ethenyl]benzene (5) A

solution of **3** (4.8 g, 12.3 mmol), **4** (4.5 g, 12.3 mmol), tri(*o*-tolylphosphine)

(P(*o*-tolyl)₃, 0.22 g, 0.74 mmol), and palladium acetate (Pd(OAc)₂, 83.0 mg, 0.37

mmol) in 100 mL of anhydrous Et3N/THF (1:1, v/v) was heated to 100 °C under

nitrogen for 12 h. After cooling, the reaction solution was filtered and the solvent was

removed in vacuum. The crude mixture was extracted with CH_2Cl_2, and the extract

was washed with water, dried over Na_2SO_4, and then evaporated under reduced

pressure. The crude product was purified by column chromatography (aluminum

oxide, n-hexane/CH_2Cl_2 1:2) to give a light yellow solid. Yield: 6.8 g (86%). ^{1}H NMR

(300 MHz, CDCl₃): δ (ppm) 8.54 (d, J = 5.7 Hz, 2H), 7.70 (d, J = 16.2 Hz, 1H),

7.48−7.42 (m, 4H), 7.32 (d, J = 16.5 Hz, 1H), 7.12−7.06 (m, 3H), 7.02 (d, J = 16.5 Hz,

1H), 6.87 (d, J = 8.7 Hz, 2H), 3.96 (t, J = 6.6 Hz, 2H), 3.93 (s, 3H), 3.90 (s, 3H), 3.58

(t, J = 6.6 Hz, 2H), 1.82−1.72 (m, 2H), 1.49−1.28 (m, 14H), 0.88 (s, 9H), 0.03 (s, 6H).

10-(4-{2-[2,5-Dimethoxy-4-(2-pyridin-4-yl-vinyl)-phenyl]-vinyl}-phenoxy)-decan-

1-ol A mixture of **5** (4.0 g, 6.3 mmol) and THF (50 mL) was added with 12.6 mL
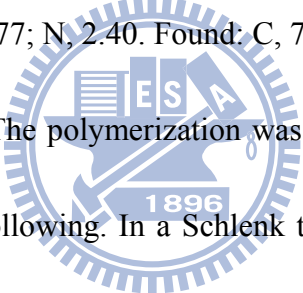
(12.6 mmol) of tetra-*n*-butylammonium floride (TBAF, 1M solution in THF) at room temperature. The resulting solution was stirred overnight and then was poured into water. The product was extracted with CH_2Cl_2, washed with water, dried over Na_2SO_4 and then evaporated under reduced pressure. The crude product was purified by column chromatography (aluminum oxide, CH_2Cl_2/acetone 40:1) to give a light yellow solid. Yield: 3.2 g (90%). ^{1}H NMR (300 MHz, $CDCl_3$): δ (ppm) 8.53 (d, *J* = 5.7 Hz, 2H), 7.73 (d, *J* = 16.2 Hz, 1H), 7.48−7.45 (m, 4H), 7.32 (d, *J* = 16.5 Hz, 1H), 7.12−7.06 (m, 3H), 7.03 (d, *J* = 16.5 Hz, 1H), 6.87 (d, *J* = 8.7 Hz, 2H), 3.96 (t, *J* = 6.6 Hz, 2H), 3.93 (s, 3H), 3.90 (s, 3H), 3.62 (t, *J* = 6.6 Hz, 2H), 2.12 (br, 1H), 1.82−1.72 (m, 2H), 1.44−1.30 (m, 14H).

1-{[4-(10-Methacryloyloxy-decyloxy)-phenyl]-ethenyl}-2,5-dimethoxy-4-[2-(4-pyridyl)ethenyl]benzene (M1) In a Schlenk tube, a mixture of compound **5** (2.0 g, 3.88 mmol), vinyl methacrylate (1.09 g, 9.7 mmol), 1,3-dichloro-1,1,3,3-tetrabutyldistannoxane (85.72 mg, 0.155 mmol), and 2,6-di-tert-butyl-4-methylphenol (51.26 mg, 0.233 mmol) in dried THF (4 mL) were purged with nitrogen for 15 min at room temperature. The tube was sealed and heated with stirring at 50 °C for 2 days. After cooling to room temperature, the reaction mixture was extracted with CH_2Cl_2, and the extract was washed with water, dried over Na_2SO_4, and then evaporated under reduced pressure. The crude product was purified

by column chromatography (aluminum oxide, n-hexane/dichloromethane 1:3) and then washed with hexane to give a light yellow solid. Yield: 1.88 g (83%). ^{1}H NMR (300 MHz, CDCl$_3$): δ (ppm) 8.56 (d, J = 6.0 Hz, 2H), 7.68 (d, J = 16.2 Hz, 1H), 7.48 (d, J = 8.7 Hz, 2H), 7.39 (d, J = 6.0 Hz, 2H), 7.34 (d, J = 16.5 Hz, 1H), 7.13 (s, 1H), 7.12 (s, 1H), 7.09 (d, J = 16.5 Hz, 1H), 7.02 (d, J = 16.5 Hz, 1H), 6.89 (d, J = 8.7 Hz, 2H), 6.09 (s, 1H), 5.54 (s, 1H), 4.14 (t, J = 6.6 Hz, 2H), 3.98 (t, J = 6.6 Hz, 2H), 3.94 (s, 3H), 3.92 (s, 3H), 1.94 (s, 3H), 1.84−1.74 (m, 2H), 1.72−1.63 (m, 2H), 1.46−1.25 (m, 12H). HRMS (EI): calcd for C$_{37}$H$_{45}$NO$_5$, 583.32977; found 583.3297. Anal. Calcd for C$_{37}$H$_{43}$NO$_5$: C, 76.13; H, 7.77; N, 2.40. Found: C, 76.02; H, 7.77; N, 2.54.

Synthesis of polymer P1. The polymerization was carried out by the free radical polymerization described as following. In a Schlenk tube, 1.0 g (20 wt%) monomer **M1** was dissolved in dried THF (7.5 mL) and AIBN (2 mol% of total monomer concentration) was added as an initiator. The acquired solution was degassed by three freeze-pump-thaw cycles and then the Schlenk tube was sealed off. The reaction mixture was stirred and heated at 60 °C for 24 h. After polymerization, the polymer was precipitated with diethyl ether. The precipitated polymer was collected, washed with diethyl ether, and dried in a vacuum. ^{1}H NMR (300 MHz, DMSO-d_6): δ (ppm) 8.44 (br, 2H), 7.53−6.77 (m, 12H), 3.80 (br, 10H), 1.66−1.24 (br, 21H).

4.3.3 Metal ion titration

Each metal ion titration experiment was started with 150 mL of polymer in THF solution with a known concentration (5.0×10^{-6} M). Solutions of metal salt (chlorate salts 1×10^{-3} M in THF containing 3% H_2O) were used for the titration. The fluorescence titration was take data for 7 min prior to measuring fluorescence spectra, which allows the complete formation of the complex between the ion and the polymer.

4.4 Results and Discussion

4.4.1 Syntheses and Characterization of Polymers

The synthetic routes and structures of monomer **PBBD (M1)** was synthesized following several reactions as outlined in Scheme 4.1. The important key three-conjugated rings of receptor emitter monomer **PBBD (M1)** was designed on the basis of the Wittig and Pd-catalyzed Heck coupling reactions. Compound **2** was protected at one hydroxyl group of terminus decyloxy chain with TBDMSCl to give compound **3**. The aldehyde group of compound **3** was further converted to the corresponding vinyl group derivative by Wittig reaction under the methyl triphenylphosphonium bromide treatment. Compound **4** was obtained by a six-step synthetic path from 2,5-dimethoxybenzaldehyde as reported in our previous paper. Compound **5** was prepared by means of Pd-catalyzed Heck coupling reaction between compound **3** and **4** with $Pd(OAc)_2$ as a catalyst in the presence of $P(o\text{-tolyl})_3$ in Et_3N/THF (1/1, v/v) , which was then deprotected with TBAF in the THF to acquire compound **6**. Finally, monomer **PBBD (M1)** was obtained by transesterification reaction between compound **6** and an excess amount (2.5 equiv) of vinyl methacrylate in the presence of a higher concentration of 1,3-dichloro-1,1,3,3-tetrabutyldistannoxane as a catalyst and 2,6-di-tert-butyl-4-methyl phenol as an inhibitor in THF. The final chemical structure

of monomer **PBBD (M1)** was confirmed by ^{1}H NMR spectroscopy, HRMS, and elemental analysis (see Experimental Section and Supporting Information).

The homopolymerization of monomer **1** was performed by a conventional free radical polymerization approach in THF at 60 °C with azobisisobutyronitrile (AIBN) as the initiator. The polymer **P1** obtained is an orange-yellow solid in 65% yield after purification and can be readily soluble in organic solvents, such as THF, DMSO, and *N,N*-dimethylformamide (DMF). A number-average molecular weight (M_n) of 11200 g/mol of **P1** was determined by gel permeation chromatography (GPC) in THF eluent using a calibration curve of polystyrene standards, corresponding to degree of polymerization of about 19, with a polydispersity index (PDI) of 1.7.

The chemical structure of polymer **P1** in DMSO-d_6 was verified by ^{1}H NMR spectroscopy. The ^{1}H NMR spectra of polymer **P1** is here compared with that of its monomer **(M1)** to illustrate polymer **(P1)** structure. The coupling constants of two vinyl protons in monomers **(M1)** are in the range of 16.2–16.5 Hz, which is consistent with expected value for an all-*trans* configuration. The chemical shifts of polymer **P1** are characterized as the same position as the monomer, except for a broadening of the peaks and a disappearance of peaks at 5.4−6.1 ppm, say, the vinyl (methacrylate) groups, indicating that the unreacted monomer was removed completely after homopolymerization.

4.4.2 Thermal Properties

The thermal stability of **P1** was evaluated by thermogravimetric analysis (TGA) in nitrogen. The TGA analyses indicate that the degradation temperature (T_d) of **P1** with 5% weight loss around 356 °C. Thermally induced phase transition behavior was investigated with differential scanning calorimetry (DSC). P1 shows a glass transition temperature (T_g) of 60 °C and melting transition temperature (T_m) up to 150 °C. On the basis of polarizing optical microscopy (POM) observation, these transitions were attributed to the melting of the material from birefringent solid to isotropic liquid, and were further confirmed by powder X-ray diffraction (XRD). These results suggest that the mesogenic homopolymer **P1** exhibits a nematic phase.
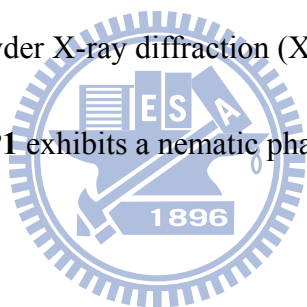
4.4.3 Optical Properties

The UV−vis absorption and photoluminescence (PL) spectra of monomer **M1** and polymers **P1** were measured in different solvents and solid film, and their photophysical properties are summarized in Table 4.1. As shown in Figure 4.1, the absorption bands of polymers **P1** at ca. 332 and 400 nm (in THF solution) are assigned to the light-emitting **PBBD** segments of the receptor moieties. The absorption spectra of the polymer **P1** in solid films are similar except for 7 nm of red-shifts in contrast to those in THF solutions. The PL emission spectra of polymers

P1 in solid films show significant red-shifts of 38 nm in comparison with its corresponding dilute solutions (see Table 4.1). This can be explained as the enhancement of the interchain interaction leading to the formation of π–π stacking and molecular aggregation in solid state.

Table 4.1   Absorption and PL emission of P1 for Different Solvents and Film

compound (solvent or film)	λ_{abs} (nm)	λ_{PL} (nm)[a]	$\triangle\lambda_{PL}$ (nm)	$\Phi_{PL,sol}$[a,b]
M1 (THF)	332, 400	460, 484	-7	1.0
P1 (THF)	332, 400	467, 469	--	0.55
P1 (DMF)	334, 403	492	25	0.56
P1 (Pyridine)	336, 405	494	27	0.68
P1 (CH$_3$COOH)	336, 449	605	138	-
P1 (Film)	336, 406	505	38	-

[a] Excited at the maximum absorption of acceptor emitter **PBBD** segments.

[b] Determined using quinine sulfate in 0.1 M H$_2$SO$_4$ as a standard (Φ_{PL} = 0.55).
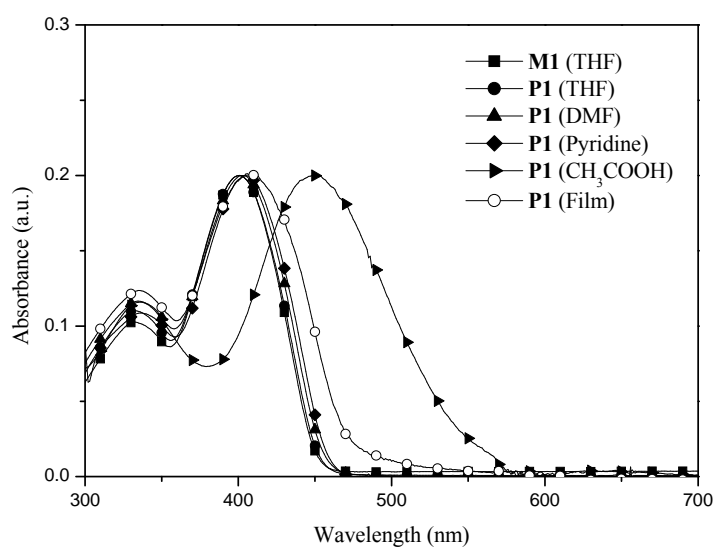
Figure 4.1 Absorption spectra of **M1** in THF solution and **P1** in various solvents

and solid film were normalized to the maximum absorption.
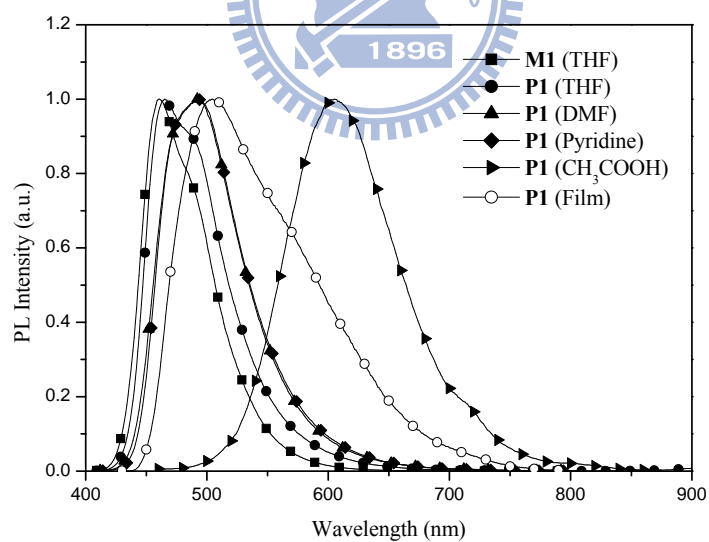
Figure 4.2 PL spectra of **M1** in THF solution and **P1** in various solvents and

solid film were normalized to the maximum PL intensity (excited at the maximum

absorption).

122

Furthermore, compared with polymers **P1** in various solvents as shown in Figure 4.2, with the increase of the solvent polarity in polymers **P1**, the PL peaks are red-shifted from 467 nm in THF solution to 605 nm in CH_3COOH. The red shifts observed in the PL spectra are also mirrored in the absorption spectra. Homopolymer **P1** in CH_3COOH solution exhibits the largest red-shift, i.e., 138 nm, in PL spectra. This phenomenon indicated that the PL spectral change observed in CH_3COOH solution due to the protonation of nitrogen atoms of pyridine rings (as H-acceptor) lead to form intrachain or intramolecular excimers.

4.4.4 UV-visible and photoluminescence titration

To explore the selectivity of this sensor, titration experiments were conducted with an addition of various metal ions, such as Fe^{2+}, Fe^{3+}, Mg^{2+}, Ni^{2+}, Zn^{2+}, Mn^{2+}, Co^{2+}, Cu^{2+}, Au^{3+}, Cr^{2+}, and Hg^{2+}, into the THF solutions of **P1** (with polymer concentrations of 5.0×10^{-6} M) . As an example, upon the addition of Ni^{2+} ion, absorption features of the polymer exhibit a red-shift of 11nm from 400 to 411 nm and the intensity of maximum absorption peak decreases with increasing Ni^{2+} concentration, as shown in Figure 4.2. Additionally, a new shoulder peak of low-energy absorption at ca. 425 nm concomitantly grows with increasing Ni^{2+} concentration, thus featuring an isosbestic point at ca. 405 nm in the spectra, and indicating that a neat interconversion between

the uncomplexed and complexed species occurs. This new absorption shoulder peak at longer wavelength may result from an internal charge transfer (ICT) process within the Ni^{2+}-**P1** complexes binding through the pyridyl unit of polymer to the metal ion. Figure 4.3 shows the PL spectra of the polymer **P1** in THF solution (5×10^{-6} M) in presence of the addition of Ni^{2+} ($[Ni^{2+}] = 0$–1.1×10^{-6} M), upon an excitation wavelength of 400 nm. A significant quenching of the PL spectra led by the addition of Ni^{2+} of polymer **P1** is observed, in which the fluorescence was almost thoroughly quenched up to a Ni^{2+} concentration of 1.1×10^{-6} M, suggesting that polymer **P1** could be an efficient Ni^{2+} fluorometric chemosensor. This PL-quenching effect is probably ascribed to energy/electron transfer within the Ni^{2+}-**P1** complexes, or the metal ion induced aggregation of the polymer chains.
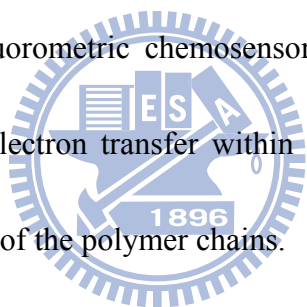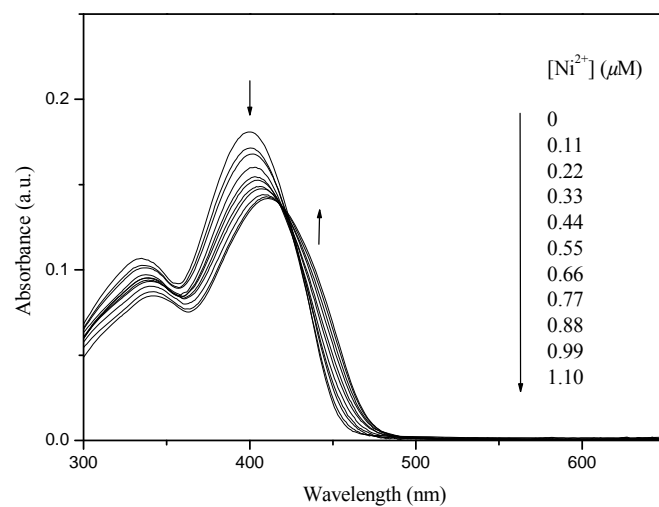
Figure 4.2 Changes in the absorption titration of **P1** (5×10^{-6} M) in THF at various concentrations of Ni^{2+} ion. The arrows indicate changes upon increased Ni^{2+} ion.
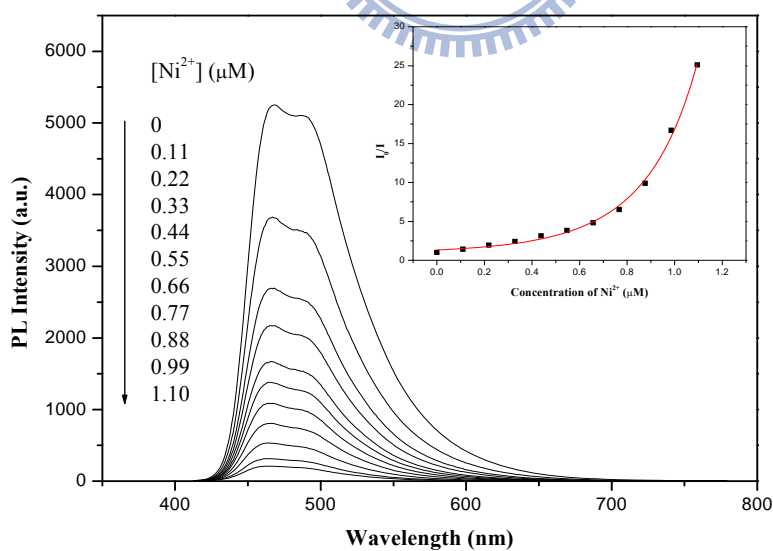
Figure 4.3 PL titration spectra of polymer **P1** (5×10^{-6} M) in THF before and after adding Ni^{2+} with versus Ni^{2+}. Excitation wavelength is at 400 nm.

The PL-quenching efficiency can be evaluated by static Stern–Volmer quenching constant, K_{SV}, through monitoring the corresponding decreases of PL intensity with increasing metal ion concentration in the linear region. According to the well-known static Stern–Volmer equation:

$$I_0/I = 1 + K_{SV} [Q]$$

where I_0 is the PL intensity in the absence of the quencher, I is the PL intensity in the presence of the quencher, and $[Q]$ is the quencher concentration.

As shown in Figure 4.3, the PL intensity changes linearly in the concentration range of $0\sim0.55 \times 10^{-6}$ M. The static Stern–Volmer equation was applied to determine K_{SV} value by linear regression of a plot of I_0/I against $[Q]$ in this linear region. The static Stern–Volmer quenching constants of Ni^{2+} and other metal ions were calculated, as shown in Table 4.2, ranges from 3.18×10^5 to 5.65×10^6 M^{-1}. It is worth noting that a metal ion induced aggregation of the polymer chains constitutes a nonlinear behavior in the static Stern–Volmer plot.

Table 4.2 K_{SV} **Value of P1 for Different Metal Ions**

metal ion	K_{SV} (M^{-1})
Cu^{2+}	2.82×10^6
Co^{2+}	2.75×10^6
Fe^{3+}	1.27×10^6
Fe^{2+}	9.23×10^5
Ni^{2+}	5.65×10^6
Zn^{2+}	3.62×10^6
Au^{3+}	7.51×10^5
Mn^{2+}	8.74×10^5
Mg^{2+}	6.63×10^5
Cr^{2+}	8.05×10^5
Hg^{2+}	3.18×10^5
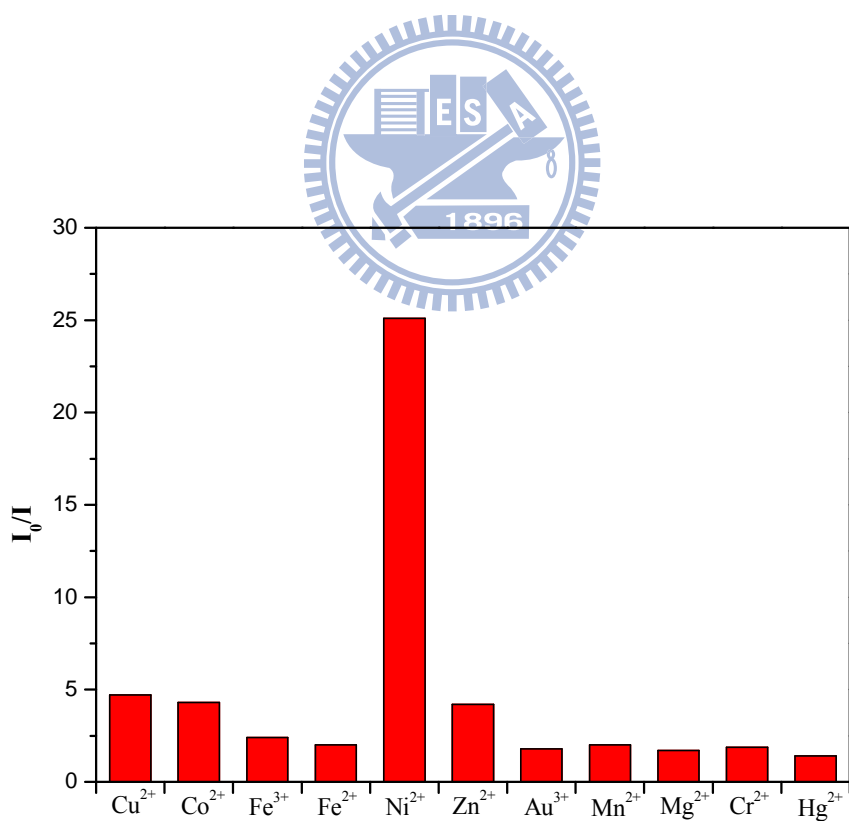
Figure 4.4 PL emission response profiles of polymer **P1** to various metal ions in THF solution.

To study the selectivity of the chemosensor, a variety of metal ions is investigated. The relative change in fluorescence intensity (I_0/I) of polymer **P1** solution in the presence of Fe^{2+}, Fe^{3+}, Mg^{2+}, Zn^{2+}, Mn^{2+}, Co^{2+}, Cu^{2+}, Au^{3+}, Cr^{2+}, and Hg^{2+} were shown in Figure 4.4. **P1** exhibited excellent selectivity for Ni^{2+} (the relative change in fluorescence intensity (I_0/I) of Ni^{2+} ranges from 5 folds higher than that of Cu^{2+} to 18 folds higher than that of Hg^{2+}). This result indicating that the binding of the Ni^{2+} ion to polymer **P1** is much stronger than the binding of the other metal ions.

To compare the sensitivity of polymer **P1** with its complementary monomer **M1**, PL-quenching characteristics toward Cu^{2+} ion were investigated. As shown in Figure 4.5 and 4.6, upon addition of Cu^{2+} of the same concentration (2.5×10^{-6} M), a relatively less intense PL-quenching and an incomplete PL-quenching feature of monomer **M1** compared to polymer **P1** are observed. On the other hand, a six-fold enhanced static Stem-Volmer constant of polymer **P1** relative to that of the small molecule indicates that the wired-in-series polymer chain within side-chain conjugated polymer **P1**, exhibits a enhanced quenching efficiency ($K_{SV} = 2.89 \times 10^6$ M^{-1}) relative to that of the small molecule ($K_{SV} = 4.77 \times 10^5$ M^{-1}). It is clearly evident that Cu^{2+} ion drastically affects the emission intensity of the polymer compared with its monomer. The quenching enhancement of the wired-in-series polymer chain system is believed owing to the synergistic summation for all pendant

receptor units in the side-chain conjugated polymer, while discrete receptors of the small molecules associate with the upcoming metal ions individually, and thus the PL intensity of the monomer is partly quenched. Therefore, this highly sensitive conjugated polymer exhibits a more manifest sensory signal response over its complementary monomer.
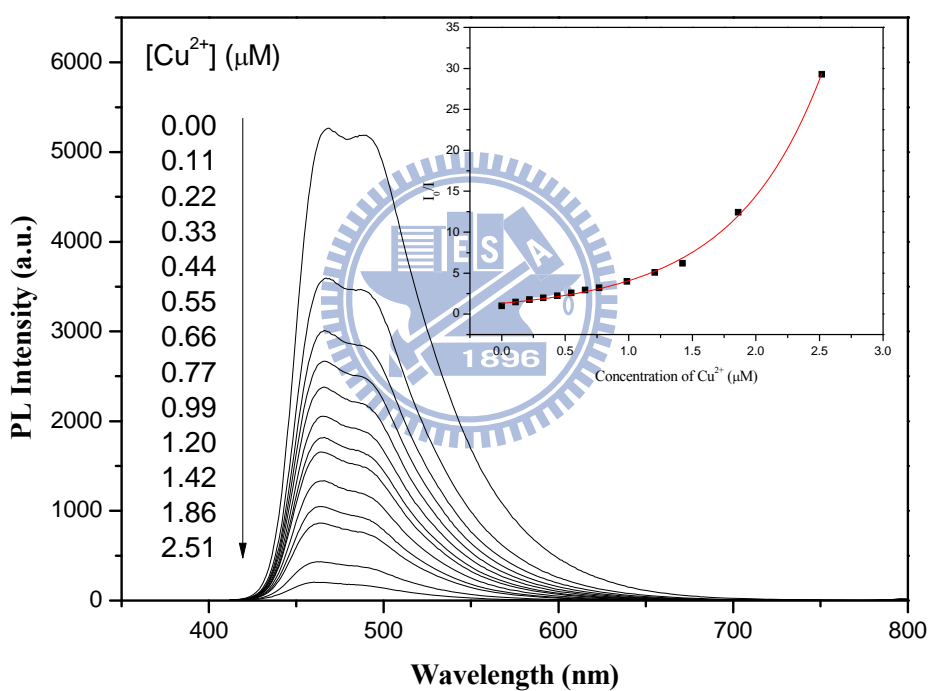
Figure 4.5   PL titration spectra of polymer **P1** (5×10^{-6} M) in THF before and after adding Cu^{2+} with versus Cu^{2+}. Excitation wavelength is at 400 nm.
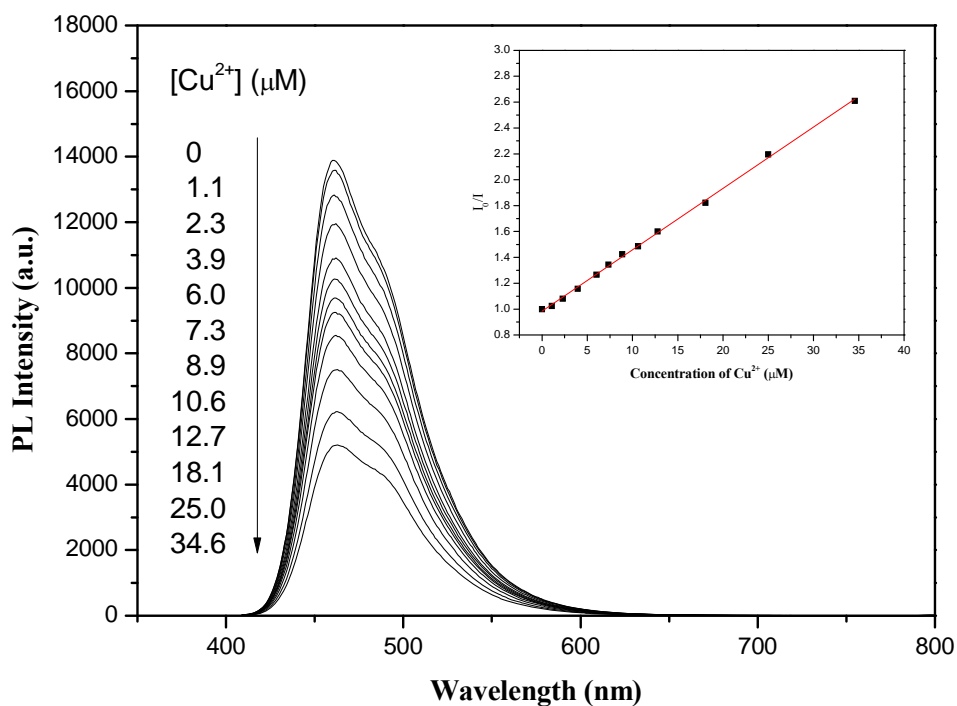
Figure 4.6 PL titration spectra of polymer **M1** (5×10^{-6} M) in THF before and

after adding Cu^{2+} with versus Cu^{2+}. Excitation wavelength is at 400 nm.

Furthermore, the **P1** based Cu^{2+} chemosensor is readily reusable. To investigate

this ability, the fluorescence of **P1** can be recovered upon the addition of 1, 1, 4, 7,

7-pentamethyldiethylenetriamine (**PMDTA)** to the **P1**-Cu^{2+} complexes solution. As

shown in Figure 4.7, the fluorescence of **P1** was quenched upon adding Cu^{2+}, and it

was recovered to 80% of its original PL intensity upon the second addition of

PMDTA to the solution. Because of the stronger binding ability between Cu^{2+} and

PMDTA, the Cu^{2+} in the **P1**-Cu^{2+} complexes were stripped and transferred to form

stable complexes with **PMDTA**, resulting in a recovered fluorescence of **P1** upon

adding **PMDTA**. The **PMDTA** acts as a competing ligand for metal ions and removes

the metal from the complexing site of the polymer. Noticeably, this

fluorescence-recovered solution can be quenched again by treatment Cu^{2+} and once

more can be reinstated upon the presence of **PMDTA**. The process is reversible,

suggesting that it could be also used as an ON-OFF-ON fluorescent switch material

(see Figure 4.8). In addition, the **P1** based chemosensor shows excellent stability

within at least seven successive cycles and almost without any observable fatigued

phenomenon, which is important for the practical use of chemosensor.
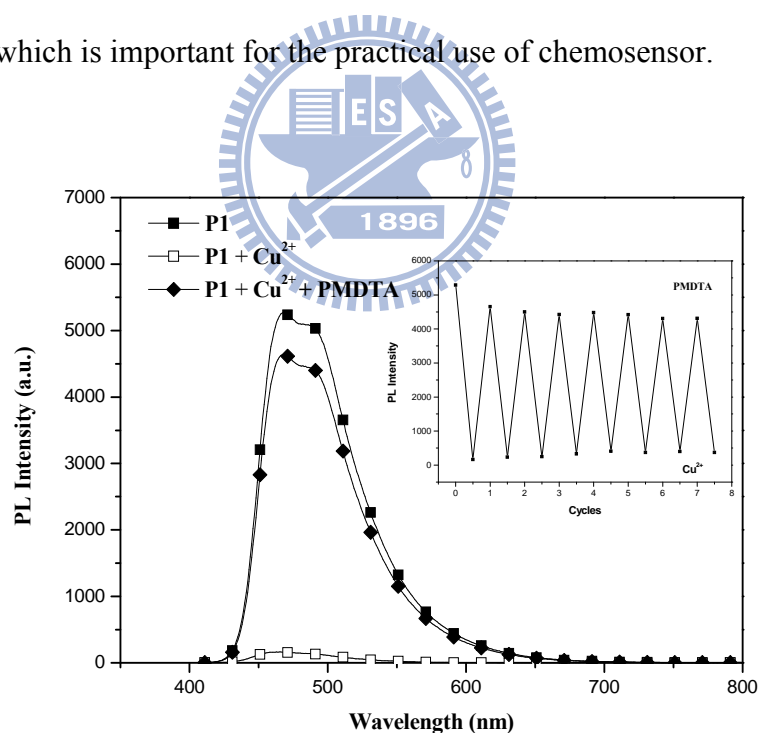
Figure 4.7   PL spectra of polymer **M1** (5×10^{-6} M) in THF before and after the

addition of Cu^{2+}, and recovered the addition of **PMDTA**. Excitation wavelength is at

400 nm.
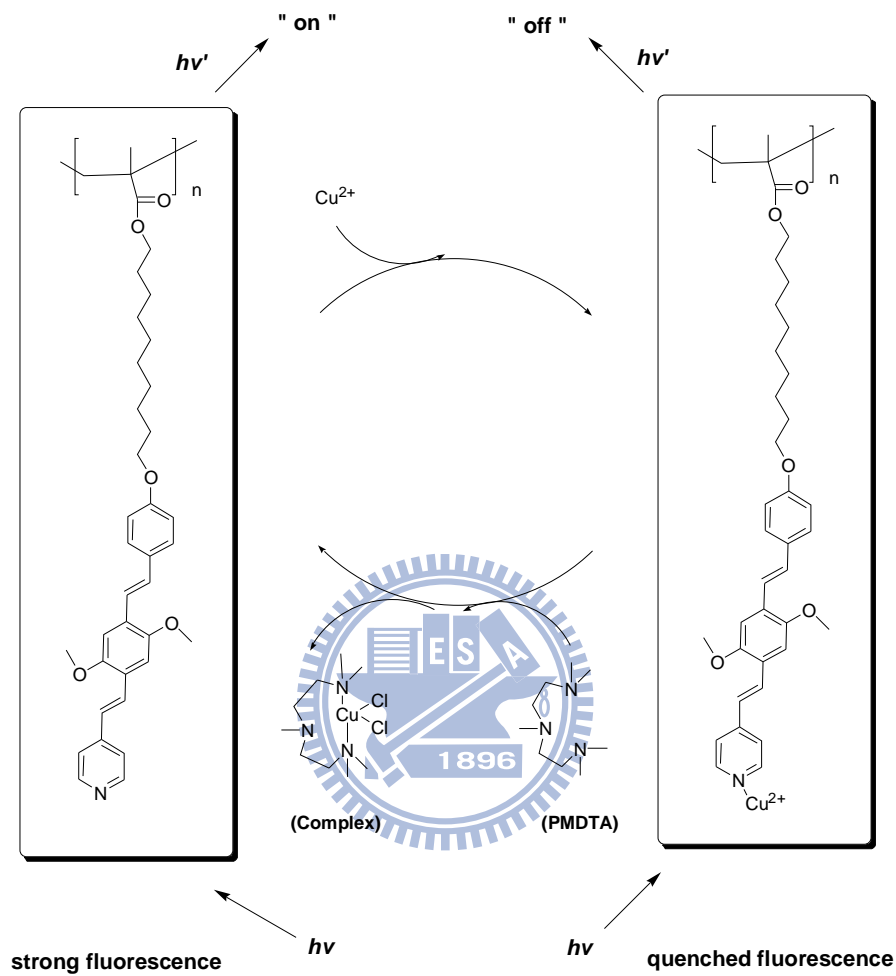
Figure 4.8 The speculated conversion cycle of **P1** in the presence of Cu^{2+} and

PMDTA.

4.5 Conclusions

In conclusion, a novel side chain conjugated polymer containing pyridyl group in

the Pendant was synthesized and its ability to sense metal ions was monitored by the

absorption and fluorescence emission spectra. The polymer can coordinate with many transition metals and the fluorescence was quenched or shifted by the addition of metal ions. The introduction of pyridyl groups into the conjugated polymer enhanced the efficiency of the energy or electron transfer reaction from the conjugated segments to the metal complex. Furthermore, the fluorescence of **P1** can be recovered upon the addition of **PMDTA** to the **P1**-Cu^{2+} complexes solution, which is important for the practical use of chemosensor.

Chapter 5

Conclusions

In conclusions, first, a series of novel H-bonded acceptor copolymers containing different molar ratios of hole-transporting carbazole (**CAZ**) units and light-emitting **PBB** moieties (bearing three conjugated aromatic rings and a terminal H-acceptor), were successfully synthesized. By the complementary surroundings via the complexation with different generations of **OXD** dendritic donors (**G1COOH−G3COOH**), the emission wavelengths of H-acceptor copolymers can be easily adjusted in their self-assembled structures of H-bonded side-chain dendritic complexes. As a result, all light-emitting, hole-transporting, and charge-transporting groups possessing novel photophysical and thermal properties are obtained in the supramolecular side-chain copolymers (i.e., H-bonded side-chain dendritic complexes). Moreover, the incorporation of carbazole units in the acceptor copolymers shows higher glass transition temperatures than the acceptor homopolymer itself and the emission wavelengths of H-acceptor polymers can be tuned (up to 61 nm of red-shift) by H-bonds. In addition, the larger dendritic size (i.e., the higher generation) of H-donors can afford stronger site-isolation and dendron-dilution effects, and thus better energy-transfer phenomena can be achieved. The PLED devices with the configuration of ITO/PEDOT:PSS/(**P4** or its H-bonded

dendritic complexes)/BCP/Alq₃/LiF/Al were fabricated, and the emission colors from

blue to green can be effectively tuned by incorporating various generations of **OXD**

dendritic donors in the supramolecular side-chain polymer structures.

Second, a series of well-defined H-bonded side chain mesogenic copolymer

networks containing proton acceptor emitter PBB with different molar ratios of proton

donor benzoic acid (**BA**) were successfully synthesized. The polymers **P1−P5** and full

H-bonded polymers networks **P1/P5** show enantiotropic mesomorphic behavior and

give rise to mesomorphic glasses at room temperature. Compared with acceptor

homopolymer **P1**, the H-bonded copolymer networks **P2−P4** exhibit red-shifted PL

emissions that due to H-boned effect. In addition, the higher benzoic acid contents in

H-bonded copolymer networks have higher dilution effect than lower benzoic acid

contents one, thereby the higher benzoic acid contents can be efficiently minimize

interchain interaction and lower the aggregation extent between emitter **PBB** cores.

So the benzoic acids play both roles as solid solvents and H-bonded donors at the

same time in H-bonded copolymer networks system. The four-layer PLED devices

with the configuration of ITO/PEDOT:PSS/(**P1** or its H-bonded

networks)/BCP/Alq₃/LiF/Al were fabricated, and effectively tuned the emission color

from greenish-blue to green by the incorporation **BA** moieties donors in the H-bonded

networks containing acceptor emitter **PBB** through a H-bonded self-assembly process.

In addition, a multilayered PLED device containing fully H-bonded cross-linking copolymer **P2** showed EL emission of 537 nm under a turn-on voltage of 8.5 V, with a maximum luminance of 268 cd/m^2 at 22 V and a luminance efficiency of 0.152 cd/A at 100 mA/cm^2.

Finally, a novel side chain conjugated polymer containing pyridyl group in the Pendant was synthesized and its ability to sense metal ions was monitored by the absorption and fluorescence emission spectra. The polymer can coordinate with many transition metals and the fluorescence was quenched or shifted by the addition of metal ions. The introduction of pyridyl groups into the conjugated polymer enhanced the efficiency of the energy or electron transfer reaction from the conjugated segments to the metal complex. Furthermore, the fluorescence of **P1** can be recovered upon the addition of **PMDTA** to the **P1**-Cu^{2+} complexes solution, which is important for the practical use of chemosensor.

References

(1) L. Pauling, "The Nature of the Chemical Bond and the Structure of Molecules and Crystals", Oxford University Press, **1939**.

(2) J.-M. Lehn, Supramolecular Chemistry, Wiley-VCH, **1995**.

(3) L. Brunsveld, B. J. B. Folmer, E. W. Meijer and R. P. Sijbesma, *Chem. Rev.*, **2001**, *101*, 4071.

(4) D. Phillip and J. F. Stoddart, *Angew. Chem.*, *Int. Ed. Engl.*, **1996**, *35*, 1154.

(5) T. Kato and J. M. J. Fre´chet, *Macromolecules*, **1989**, *22*, 3818.

(6) S. Ujiie and K. Iimura, *Macromolecules*, **1992**, *25*, 3174.

(7) T. Kato, *Science*, **2002**, *295*, 2414.

(8) U. Kumar, T. Kato and J. M. J. Fre´chet, *J. Am. Chem. Soc.*, 1992, *114*, 6630.

(9) G. A. van Ekenstein, E. Polushkin, H. Nijland, O. Ikkala and G. ten Brinke, *Macromolecules*, **2003**, *36*, 3684.

(10) Dimitrakopolous, C. D.; Malenfant, P. R. L. *Adv. Mater.* **2002**, *14*, 99.

(11) Braun, D. *Mater. Today* **2002**, *5*, 32.

(12) Eckert, J.-F.; Maciejczuk, U.; Guillon, D.; Nierengarten, J.-F. *Chem. Commun.* **2001**, 1278.

(13) Ajayaghosh, A.; George, S. J. *J. Am. Chem. Soc.* **2001**, *123*, 5148.

(14) El-Ghayoury, A.; Schenning, A. P. H. J.; Van Hal, P. A.; Van Duren, J. K. J.;

Janssen, R. A. J.; Meijer, E. W. *Angew. Chem., Int. Ed.* **2001**, *40*, 3660.

(15) El-ghayoury, A.; Peeters, E.; Schenning, A. P. H. J.; Meijer, E. W. *Chem. Commun.* **2000**, 1969.

(16) J.-M. Lehn, Angebt,. Chem., In&. Ed. Engl., **1990**, *29*, 1304.

(17) L-J. Fan, W. E. J. Jr. *J. Am. Chem. Soc.* **2006**, *128*, 6784.

(18) S. Bonacchi, E. Rampazzo, M. Montalti, L. Prodi, N. Zaccheroni, F. Mancin, P. Teolato. *Langmuir* **2008,** *24,* 8387.

(19) (a) Jenekhe, S. A.; Chen, X. L. *Science* **1999**, *283*, 372. (b) Whiteside, G. M.; Mathias, J. P.; Seto, C. T. *Science* **1991**, *254*, 1312.

(20) Kato, T.; Fréchet, J. M. J. *Macromolecules* **1989**, *22*, 3819.

(21) Kato, T.; Kihara, H.; Kumar, U.; Uryu, T.; Fréchet, J. M. J. *Angew. Chem., Int. Ed. Engl.* **1994**, *33*, 1644.

(22) Malik, S.; Dhal, P. K.; Mashelkar, R. A. *Macromolecules* **1995**, *28*, 2159.

(23) Kato, T.; Kihara. H.; Ujiie, S.; Uryu, T.; Fréchet, J. M. J. *Macromolecules* **1996**, *29*, 8734.

(24) (a) Schenning, A. P. H. J.; Jonkheijm, P.; Peeters, E.; Meijer, E. W. *J. Am. Chem. Soc.* **2001**, *123*, 409. (b) Ligthart, G. B. W. L.; Ohkawa, H.; Sijbesma, R. P.; Meijer, E. W. *J. Am. Chem. Soc.* **2005**, *127*, 810. (c) Roosma, J.; Mes, T.; Leclère, P.; Palmans, A. R. A.; Meijer, E. W. *J. Am. Chem. Soc.* **2008**, *130*, 1120.

(25) Medvedev, A. V.; Barmatov, E. B.; Medvedev, A. S.; Shibaev, V. P.; Ivanov, S. A.; Kozlovsky, M.; Stumpe, J. *Macromolecules* **2005**, *38*, 2223.

(26) (a) Cheng, Z.; Ren, B.; Shan, H.; Liu, X.; Tong, Z. *Macromolecules* **2008**, *41*, 2656.

(27) Canilho, N.; Kasëmi, E.; Schlüter, A. D.; Mezzenga, R. *Macromolecules* **2007**, *40*, 2822.

(28) Dinolfo, P. H.; Hupp, J. T. *Chem. Mater.* **2001**, *13*, 3113.

(29) McClenaghan, N.D.; Passalacqua, R.; Loiseau, F.; Campagna, S.; Verheyde, B.; Hameurlaine, A.; Dehaen, W. *J. Am. Chem. Soc.* **2003**, *125*, 5356.

(30) Chen, Y. Y.; Tao, Y. T.; Lin, H. C. *Macromolecules* **2006**, *39*, 8559.

(31) Kimura, M.; Sano, M.; Muto, T.; Hanabusa, K.; Shirai, H. *Macromolecules* **1999**, *32*, 7951.

(32) Frein, S.; Auzias, M.; Sondenecker, A.; Vieille-Petit, L.; Guintchin, B.; Maringa, N.; Süss-Fink, G.; Barberá, J.; Deschenaux, R. *Chem. Mater.* **2008**, *20*, 1340.

(33) Burroughes, J. H.; Bradley, D. D. C.; Brown, A. R.; Marks, R. N.; Mackay, K.; Friend, R. H.; Burn, P. L.; Holmes, A. B. *Nature (London)* **1990**, *347*, 539.

(34) Mitschke, U.; Bäuerle, P. *J. Mater. Chem.* **2001**, *10*, 1471.

(35) Kawamoto, M.; Mochizuki, H.; Ikeda, T.; Iino, H.; Hanna, J. I. *J. Phys. Chem. B* **2005**, *109*, 9226.

(36) Johansson, D. M.; Srdanov, G.; Yu, G.; Theander, M.; Inganas, O.; Anderson, M. R. *Macromolecules* **2000**, *33*, 2525.

(37) Zaumseil, J.; Sirringhaus, H. *Chem. Rev.* **2007**, *107*, 1296.

(38) (a) Greenham, N. C.; Moratti, S. C.; Bradley, D. D. C.; Friend, R. H.; Holmes, A. B. *Nature* **1993**, *365*, 628. (b) Burn, P. L.; Kraft, A.; Baigent, D. R.; Bradley, D. D. C.; Brown, A. R.; Friend, R. H.; Gymer, R. W.; Holmes, A. B.; Jackson, R. W. *J. Am. Chem. Soc.* **1993**, *115*, 10117.

(39) Marsitzky, D.; Vestberg, R.; Blainey, P.; Tang, B. T.; Hawker, C. J.; Carter, K. R. *J. Am. Chem. Soc.* **2001**, *123*, 6965.

(40) (a) Setayesh, S.; Grimsdale, A. C.; Weil, T.; Enkelmann, V.; Müllen, K.; Meghdadi, F.; List, E. J. W.; Leising, G. *J. Am. Chem. Soc.* **2001**, *123*, 946. (b) Pogantsch, A.; Wenzl, F. P.; List, E. J. W.; Leising, G.; Grimsdale, A. C.; Müllen, K. *Adv. Mater.* **2002**, *14*, 1061. (c) Oesterling, I.; Müllen, K. *J. Am. Chem. Soc.* **2007**, *129*, 4595.

(41) Kwok, C. C.; Wong, M. S. *Chem. Mater.* **2002**, *14*, 3158.

(42) Kimoto, A.; Masachika, K.; Cho, J. S.; Higuchi, M.; Yamamoto, K. *Chem. Mater.* **2004**, *16*, 5706.

(43) Pillow, J. N. G.; Halim, M.; Lupton, J. M.; Burn, P. L.; Samuel, I. D. W. *Macromolecules* **1999**, *32*, 5985.

(44) Kwon, T. W.; Alam, M. M.; Jenekhe, S. A. *Chem*. *Mater*. **2004**, *16*, 4657.

(45) (a) Kimura, M.; Sato, M.; Adachi, N.; Fukawa, T.; Kanbe, E.; Shirai, H. *Chem*. *Mater*. **2007**, *19*, 2809.

(46) Ma, C. -Q.; Mena-Osteritz, E.; Debaerdemaeker, T.; Wienk, M. M.; Janssen, R. A. J.; Bauerle, P. *Angew*. *Chem*. *Int*. *Ed*. **2007**, *46*, 1679.

(47) Taranekar, P.; Fulghum, T.; Patton, D.; Ponnapati, R.; Clyde, G.; Advincula, R. *J*. *Am*. *Chem*. *Soc*. **2007**, *129*, 12548.

(48) Burm, P. L.; Lo, S. C.; Samuel, I. D. W. *Adv*. *Mater*. **2007**, *19*, 1675.

(49) (a) Precup-Blaga, F. S.; Garcia-Martinez, J. C.; Schenning, A. P. H. J.; Meijer, E. W. *J*. *Am*. *Chem*. *Soc*. **2003**, *125*, 12953. (b) Schenning, A. P. H. J.; Peeters, E.; E. W. Meijer. *J*. *Am*. *Chem*. *Soc*. **2000**, *122*, 4489.

(50) Zhao, Z.; Xu, X.; Wang, H.; Lu, P.; Yu, G.; Liu, Y. *J*. *Org*. *Chem*. **2008**, *73*, 594.

(51) (a) Bo, Z.; Zhang, C.; Severin, N.; Rabe, J. P.; Schlüter, A. D. *Macromolecules* **2000**, *33*, 28, 2688. (b) Fu, Y.; Li, Y.; Li, J.; Yan, S.; Bo, Z. *Macromolecules* **2004**, *37*, 6395. (c) Zhu, B.; Han, Y.; Sun, M.; Bo, Z. *Macromolecules* **2007**, *40*, 4494.

(52) Lo, S. C.; Burn, P. L. *Chem*. *Rev*. **2007**, *107*, 1097.

(53) Köse, M. E.; Mitchell, W. J.; Kopidakis, N.; Chang, C. H.; Shaheen, S. E.; Kim, K.; Rumbles, G. *J*. *Am*. *Chem*. *Soc*. **2007**, *129*, 14257.

(54) Wu, C. W.; Lin, H. C. *Macromolecules* **2006**, *39*, 7985.

141

(55) Eaton, D. *Pure Appl. Chem.* **1998**, *60*, 1107.

(56) Lin, D. G.; Lin, G. Q. *Tetrahedron Lett.* **1999**, *40*, 337.

(57) (a) Okawara, R.; Wada, M. *J. Organomet. Chem.* **1963**, *1*, 81. (b) Wada, M.; Nishino, M.; Okawara, R. *J. Organomet. Chem.* **1965**, *3*, 70.

(58) Engels, C.; Steenwinckel, D. V.; Hendrickx, E.; Schaerlaekens, M.; Persoons, A.; Samyn, C. *J. Mater. Chem.* **2002**, *12*, 951.

(59) Hathaway, B. A.; Taylor, B. E.; Wittenborn, J. S. *Synth. Commun.* **1998**, *28*, 4629.

(60) (a) Arbuzov, B. A. *Pure Appl. Chem.* **1964**, *9*, 307. (b) Michaelis, A.; Kaehne, R. *Chem. Ber.* **1898**, *31*, 1048.

(61) (a) Horner, L. *Chem. Ber.* **1958**, *83*, 733. (b) Wadsworth, W. S.; Emmons, W. D. *J. Am. Chem. Soc.* **1961**, *83*, 1733.

(62) Sonogashira, K.; Tohda, Y.; Hagihara, N. *Tetrahedron Lett.* **1975**, 4467.

(63) Cui, L.; Lattermann, G. *Macromol. Chem. Phys.* **2002**, *203*, 2432.

(64) Lin, H. C.; Hendrianto, J. *Polymer* **2005**, *46*, 12146.

(65) (a) Kumar, U.; Kato, T.; Fréchet, J. M. J. *J. Am. Chem. Soc.* **1992**, *114*, 6630. (b) Kato, T.; Fréchet, J. M. J.; Wilson. P. G.; Saito, T.; Uryu, T.; Fujishima, A.; Jin, C.; Kaneuchi, F.; *Chem. Mater.* **1993**, *5*, 1094. (c) Kato, T.; Kihara, H.; Uryu, T.; Fujishima, A.; Fréchet, J. M. J. *Macromolecules* **1992**, *25*, 6836.

(66) (a) Kong, X.; Tang, B. Z. *Chem. Mater.* **1998**, *10*, 3352. (b) Lam, J. W. Y.; Dong, Y.; Law, C. C. W.; Dong, Y.; Cheuk, K. K. L.; Lai, L. M.; Li, Z.; Sun, J.; Chen, H.; Zheng, Q.; Kwok, H. S.; Wang, M.; Feng, X.; Shen, J.; Tang, B. Z. *Macromolecules* **2005**, *38*, 3290.

(67) (a) Wu, C. W.; Tsai, C. M.; Lin, H. C. *Macromolecules* **2006**, *39*, 4298. (b) Wu, C. W.; Sung, H. H.; Lin, H. C. *J. Polym. Sci., Part A: Polym. Chem.* **2006**, *44*, 6765.

(68) (a) Lin, H. C.; Sheu, H. Y.; Chang, C. L.; Tsai, C. *J. Mater. Chem.* **2001**, *11*, 2958.

(69) Leeuw, D. M.; Simenon, M. M. J.; Brown, A. R.; Einerhand, R. E. F. *Synth. Met.* **1997**, *87*, 53.

(70) Zhao, L.; Li, C.; Zhang, Y.; Zhu, X. H.; Peng, J.; Cao, Y. *Macromol. Rapid Commun.* **2006**, *27*, 914.

(71) Qu, J. Q.; Zhang, J. Y.; Grimsdale, A. C.; Müllen, K.; Jaiser, F.; Yang, X. H.; Neher, D. *Macromolecules* **2004**, *37*, 8297.

(72) Lehn, J.-M. *Chem. Soc. Rev.* **2007**, *36*, 151.

(73) Cordier, P.; Tournilhac, F.; Soulié-Ziakovic, C.; Leibler, L. *Nature* **2008**, *451*, 977.

(74) Greef, T. F. A.; Meijer, E. W. *Nature* **2008**, *453*, 171.

(75) (a) Zeng, F.; Zimmerman, S. C. *Chem. Rev.* **1997**, *97*, 1681. (b) Ong, H. C.;

Arambula, J. F.; Ramisetty, S. R.; Baranger, A. M.; Zimmerman, S. C. *Chem. Commun*. **2009**, 668.

(76) Prins, L. J.; Reinhoudt, D. N.; Timmerman, P. *Angew. Chem. Int. Ed*. **2001**, *40*, 2382.

(77) (a) Yagai, S.; Kinoshita, T.; Higashi, M.; Kishikawa, K.; Nakanishi, T.; Karatsu, T.; Kitamura, A. *J. Am. Chem. Soc*. **2007**, *129*, 13277. (b) Yagai, S.; Kitamura, A. *Chem. Soc. Rev*. **2008**, *37*, 1520.

(78) Santos, J.; Grimm, B.; Illescas, B. M.; Guldi, D. M.; Martín, N. *Chem. Commun*. **2008**, 5993.

(79) Yu, X.; Samanta, B.; Xu, H.; Arumugam, P.; Ofir, Y.; Jordan, B. J.; Rotello, V. M. *Small* **2009**, *5*, 86.

(80) Zubarev, E. R.; Sone, E. D.; Stupp, S. I. *Chem. Eur. J*. **2006**, *12*, 7313.

(81) Barik, S.; Valiyaveettil, S. *Macromolecules* **2008**, *41*, 6376.

(82) Houbenov, N.; Nykänen, A.; Iatrou, H.; Hadjichristidis, N.; Ruokolainen, J.; Faul, C. F. J.; Ikkala, O. *Adv. Funct. Mater*. **2008**, *18*, 2041.

(83) Chen, Z.; Stepanenko, V.; Dehm, V.; Prins, P.; Siebbeles, L. D. A.; Seibt, J.; Marquetand, P.; Engel, V.; Würthner, F. *Chem. Eur. J*. **2007**, *13*, 436.

(84) Leininger, S.; Olenyuk, B.; Stang, P. J. *Chem. Rev*. **2000**, *100*, 853.

(85) Wang, F.; Han, C. Y.; He, C. L.; Zhou, Q. Z.; Zhang, J. Q.; Wang, C.; Li, N.;

Huang, F. H. *J. Am. Chem. Soc.* **2008**, *130*, 11254.

(86) Eryazici, I.; Moorefield, C. N.; Newkome, G. R. *Chem. Rev.* **2008**, *108*, 1834.

(87) Chiper, M.; Winter, A.; Hoogenboom, R.; Egbe, D. A. M.; Wouters, D.; Hoeppener, S.; Fustin, C. A.; Gohy, J. F.; Schubert, U. S. *Macromolecules* **2008**, *41*, 8823.

(88) Kajitani, T.; Kohomoto, S.; Yamamoto, M.; Kishikawa, K. *J. Mater. Chem.* **2004**, *14*, 3449.

(89) McCubbin, J. A.; Tong, X.; Zhao, Y.; Snieckus, V.; Lemieux, R. P. *Chem. Mater.* **2005**, *17*, 2574.

(90) Yelamaggad, C. V.; Achalkumar, A. S.; Rao, D. S. S.; Prasad, S. K. *J. Org. Chem.* **2007**, *72*, 8308.

(91) Vera, F.; Serrano, J. L.; Sierra, T. *Chem. Soc. Rev.* **2009**, *38*, 781.

(92) (a) Gimeno, N.; Ros, M. B.; Serrano, J. L.; De la Fuente, M. R. *Angew. Chem. Int. Ed.* **2004**, *43*, 5235. (b) Barberá, J.; Gimeno, N.; Pintre, I.; Ros, M. B.; Serrano, J. L. *Chem. Commun.* **2006**, 1212. (c) Perez, A.; Gimeno, N.; Vera, F.; Ros, M. B.; Serrano, J. L.; De la Fuente, M. R. *Eur. J. Org. Chem.* **2008**, 826. (d) Gimeno, N.; Ros, M. B.; Serrano, J. L.; De la Fuente, M. R. *Chem. Mater.* **2008**, *20*, 1262.

(93) (a) Kato, T.; Fréchet, J. M. J. *J. Am. Chem. Soc.* **1989**, *111*, 8533. (b) Kato, T.; Fréchet, J. M. J. *Macromolecules* **1989**, *22*, 3818.

(94) (a) Kumar, U.; Kato, T.; Fréchet, J. M. J. *J. Am. Chem. Soc.* **1992**, *114*, 6630. (b) Kato, T.; Kihara, H.; Kumar, U.; Uryu, T.; Fréchet, J. M. J. *Angew. Chem.*, *Int. Ed. Engl.* **1994**, *33*, 1644. (c) Kihara, H.; Kato, T.; Uryu, T.; Fréchet, J. M. J. *Chem. Mater.* **1996**, *8*, 961. (d) Kato, T.; Yasuda, T.; Kamikawa, Y.; Yoshio, M. *Chem. Commun.* **2009**, 729.

(95) (a) Kohlmeier, A.; Janietz, D. *Chem. Mater.* **2006**, 18, 59. (b) Vlad-Bubulak., T.; Buchs, J.; Kohlmeier, A.; Bruma, M.; Janietz, D. *Chem. Mater.* **2007**, 19, 4460. (c) Kohlmeier, A.; Nordsieck, A.; Janietz, D. *Chem. Mater.* **2009**, 21, 491.

(96) (a) Huang, W.; Han, C. D. *Macromolecules* **2006**, *39*, 257. (b) Huang, W.; Han, C. D. *Macromolecules* **2006**, *39*, 4735.

(97) Kawatsuki, N.; Kawanishi, T.; Uchida, E. *Macromolecules* **2008**, *41*, 4642.

(98) Sallenave, X.; Bazuin, C. G. *Macromolecules* **2007**, *40*, 5326.

(99) (a) Xu, J.; He, C.; Toh, K. C.; Lu, X. *Macromolecules* **2002**, *35*, 8846. (b) Xu, J.; Toh, C. L.; Liu, X.; Wang, S. He, C.; Lu, X. *Macromolecules* **2005**, *38*, 1684.

(100) Cui, L.; Zhao, Y. *Chem. Mater.* **2004**, *16*, 2076.

(101) (a) Surez, M.; Lehn, J. M.; Zimmerman, S. C.; Skoulios, A.; Heinrich, B. *J. Am. Chem. Soc.* **1998**, *120*, 9526. (b) Jin, S.; Ma, Y. Zimmerman, S. C.; Cheng, S. Z. D. *Chem. Mater.* **2004**, *16*, 2975.

(102) Kishikawa, H.; Hirai, A.; Kohmoto, S. *Chem. Mater.* **2008**, *20*, 1931.

(103) De Wit, J.; van Ekenstein, G. O. R. A.; Polushkin, E.; Kvashnina, K.; Bras, W.;

Ikkala, O.; ten Brinke, G. *Macromolecules* **2008**, *41*, 4200.

(104) Hammond, M. R.; Mezzenga, R. *Soft Matter* **2008**, *4*, 952.

(105) Tanase, C.; Wildeman, J.; Blom, P. W. M. *Adv. Funct. Mater.* **2005**, *15*, 2011.

(106) Neher, D. *Macromol. Rapid Commum.* **2001**, *22*, 1365.

(107) Huang, F.; Zhang, Y.; Liu, M. S.; Cheng, Y. J.; Jen, A. K. Y. *Adv. Funct. Mater.*

2007, *17*, 3808.

(108) Günes, S.; Neugebauer, H.; Sariciftci, N. S. *Chem. Rev.* **2007**, *107*, 1324.

(109) Li, Y. F.; Zou, Y. P. *Adv. Mater.* **2008**, *20*, 2952.

(110) Mikroyannidis, J. A. *Chem. Mater.* **2003**, *15*, 1865.

(111) Spreitzer, H.; Becker, H.; Kluge, E.; Kreuder, W.; Schenk, H.; Demandt, R.;

Schoo, H. *Adv. Mater.* **1998**, *10*, 1340.

(112) Lim, S. F.; Friend, R. H.; Rees, I. D.; Li, J.; Ma, Y. G.; Robinson, K.; Holmes,

A. B.; Hennebicq, E.; Beljonne, D.; Cacialli, F. *Adv. Funct. Mater.* **2005**, *15*, 981.

(113) Mikroyannidis, J. A.; Gibbons, K. M.; Kulkarni, A. P.; Jenekhe, S. A.

Macromolecules **2008**, *41*, 663.

(114) Wang, E.; Li, C.; Zhuang, W.; Peng, J.; Cao, Y. *J. Mater. Chem.* **2008**, *18*, 797.

(115) Qu, J.; Zhang, J.; Grimsdale, A. C.; Müllen, K. *Macromolecules* **2004**, *37*,

8297.

(116) Dobrawa, R.; Lysetska, M.; Ballester, P.; Grüne, M.; Würthner, F. *Macromolecules* **2005**, *38*, 1315.

(117) Kim, H.-J. Jung, E.-Y. Jin, L. Y.; Lee, M. *Macromolecules* **2008**, *41*, 6066.

(118) Fang, H.; Wang, S.; Xiao, S.; Yang, J.; Li, Y.; Shi, Z.; Li, H.; Liu, H.; Xiao, S.; Zhu, D. *Chem. Mater.* **2003**, *15*, 1593.

(119) Sánchez, L.; Martín, N.; Guldi, D. M. *Angew. Chem. Int. Ed.* **2005**, *44*, 5374.

(120) Ajayaghosh, A.; Praveen, V. K. *Acc. Chem. Res.* **2007**, *40*, 644.

(121) Fang, F. C. Chu, C. C.; Huang, C. H.; Wong, K. T.; Bassani, D. M. *Chem. Commun.* **2008**, 6369.

(122) Hirai, Y.; Monobe, H.; Mizoshita, N.; Moriyama, M.; Hanabusa, K.; Shimizu, Y.; Kato, T. *Adv. Funct. Mater.* **2008**, *18*, 1668.

(123) (a) Hoeben, F. J. M.; Schenning, A. P. H. J. Meijer, E. W. *ChemPhysChem* **2005**, *6*, 2337. (b) Jonkheijm, P.; van Duren, J. K. J.; Kemerink, M.; Janssen, R. A. J.; Schenning, A. P. H. J.; Meijer, E. W. *Macromolecules* **2006**, *39*, 784. (c) Abbel, R.; Grenier, C.; Pouderoijen, M. J.; Stouwdam, J. W.; Leclère, P. E. L. G.; Sijbesma, R. P.; Meijer, E. W.; Schenning, A. P. H. J. *J. Am. Chem. Soc.* **2009**, *131*, 833.

(124) Thiagarajan, V.; Ramamurthy. P; Thirumalai, D.; Ramakrishnan, V. T. *Org. Lett.* **2005**, *7*, 657.

(125) Gawley, R. E.; Mahbubul Haque, H. M. M.; Thorne, J. B.; Pharr, J. S. *J. Org.*

Chem. **2007**, *72*, 2187.

(126) Gunnlaugsson, T.; Davis, A. P.; Obrien, J. E.; Glynn, M. *Org. Lett*. **2002**, *4*, 2449.

(127) Kumar, M.; Dhir, A.; Vandana, Bhalla, V. *Org. Lett*. **2009**, *11*, 2567.
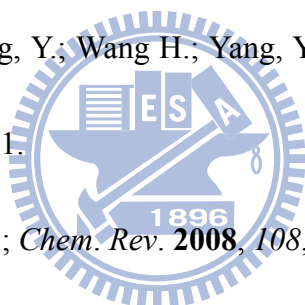
(128) Guo, X.; Qian, X.; Jia, L. *J. Am*. *Chem*. *Soc*. **2004**, *126*, 2272.

(129) Shiraishi, Y.; Kohno, Y.; Hirai, T.; *J. Phys*. *Chem*. *B* **2005**, 109, 19139.

(130) Liu, B.; Yu, W. L.; Pei, J.; Liu, S. Y.; Lai, Y. H.; Huang, W. *Macromolecules* **2001**, *34*, 7932.

(131) Long, Y.; Chen, H.; Yang, Y.; Wang H.; Yang, Y.; Li, N.; Li, K.; Pei, J.; Liu, F. *Macromolecules* **2009**, *42*, 6501.

(132) Zou, H.; Wu, S.; Shen, J.; *Chem*. *Rev*. **2008**, *108*, 3893.

Appendix

Powder X-ray diffraction (XRD) Installation. Synchrotron powder X-ray diffraction (XRD) measurements were performed in transmission mode with synchrotron radiation at beamline BL17A of the National Synchrotron Radiation Research Center (NSRRC), Taiwan, where the X-ray wavelength was 1.334431 Å. The XRD data were collected using imaging plates (IP, of an area $= 20 \times 40$ cm^2 and a pixel resolution of 100) curved with a radius equivalent to the sample-to-image plate distance of 280 mm, and the diffraction signals were accumulated for 10 min. The powder samples were packed into a capillary tube and heated by a heat gun, where the temperature controller is programmable by a PC with a PID feed back system. The scattering angle theta was calibrated by a mixture of silver behenate and silicon. Note: In the XRD experiments, the background scattering data were subtracted from the sample scans.
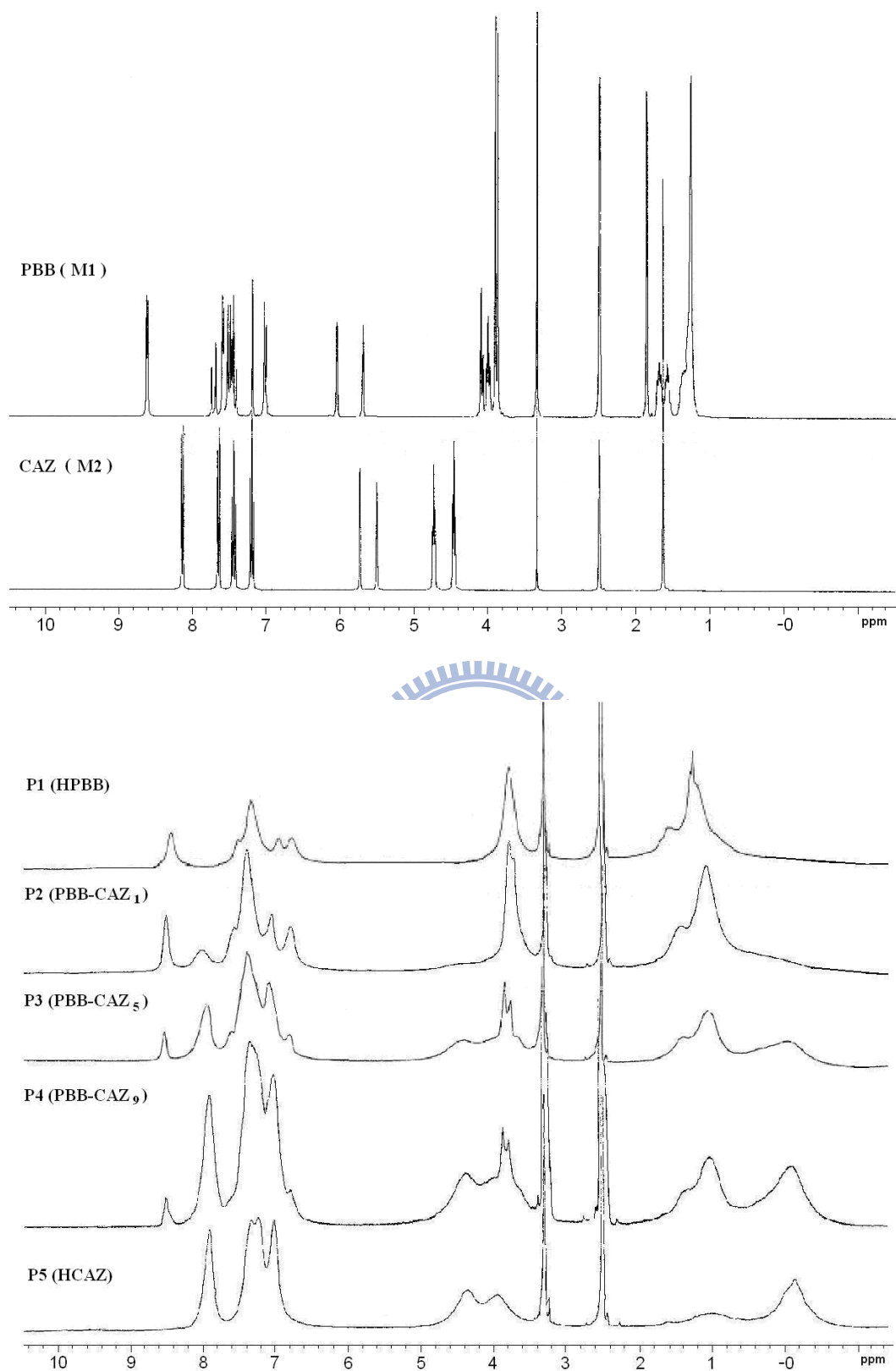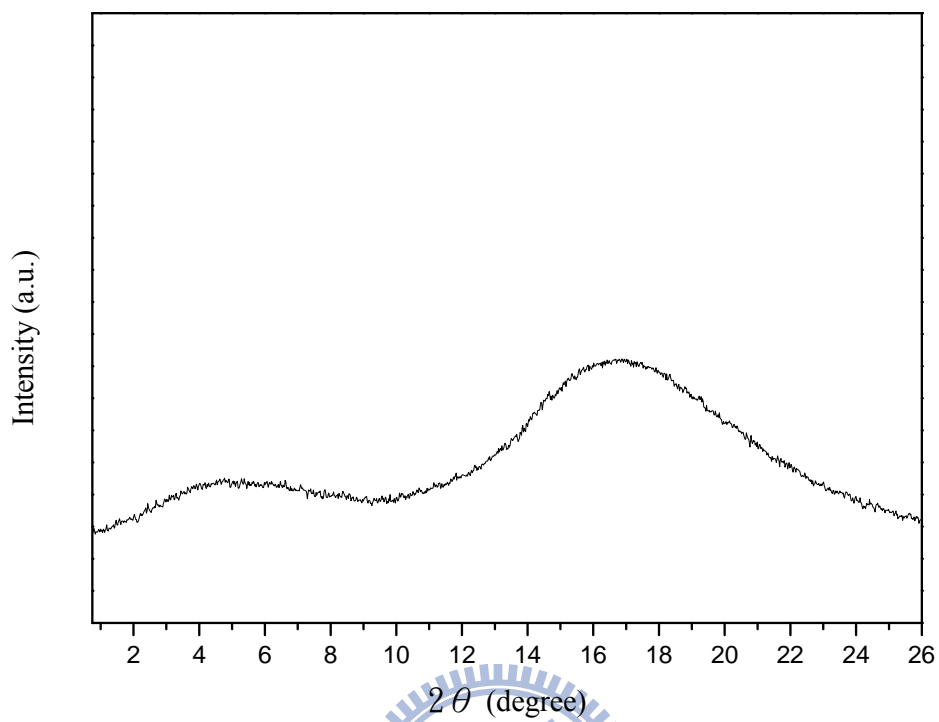
Figure A1 ^{1}H-NMR spectra of monomers **PBB (M1)** and **CAZ (M2)**, and
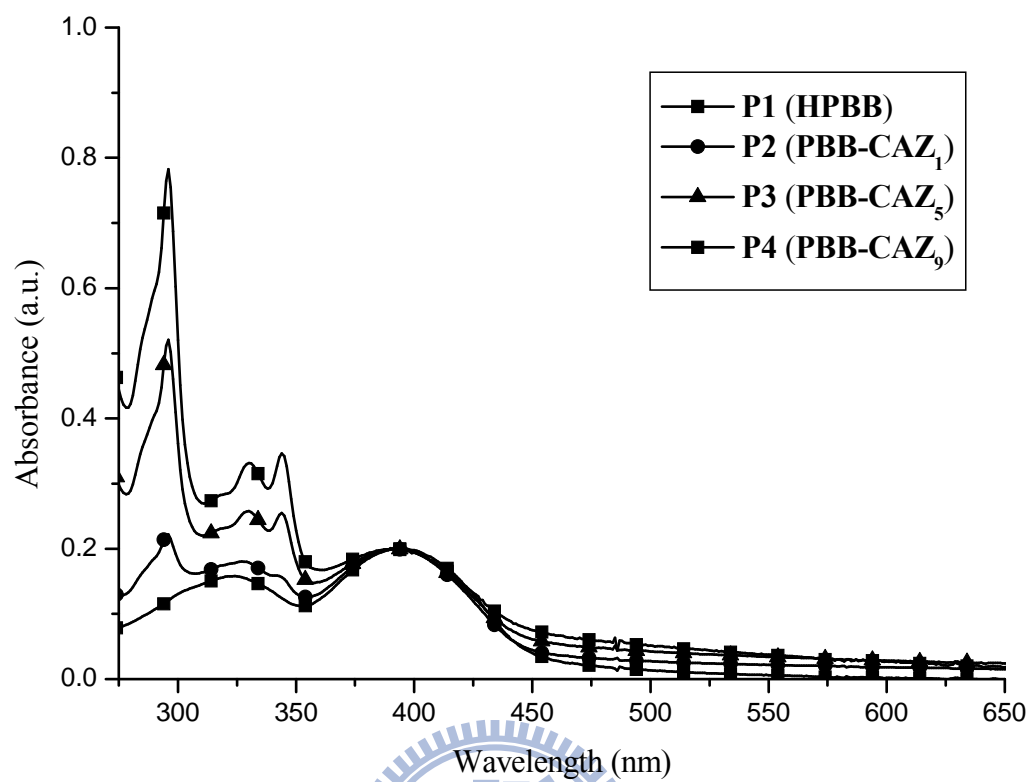
polymers **P1–P5** in DMSO-d_6.
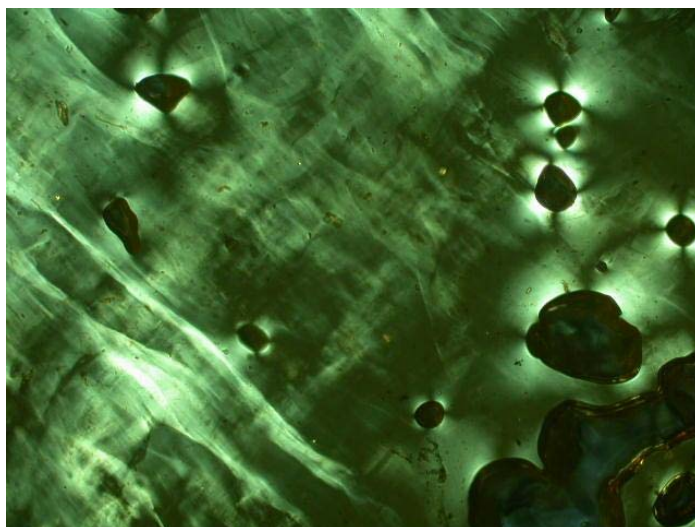
Figure A2 Polarized optical micrograph (POM) image of homopolymer **P1** exhibited a weak birefringent region in the nematic phase at 90 °C (heating).
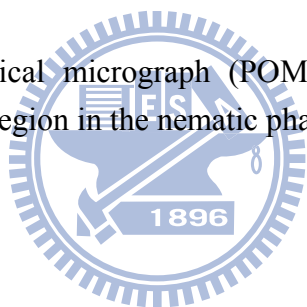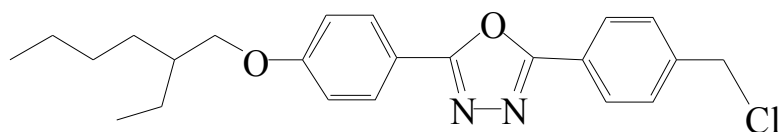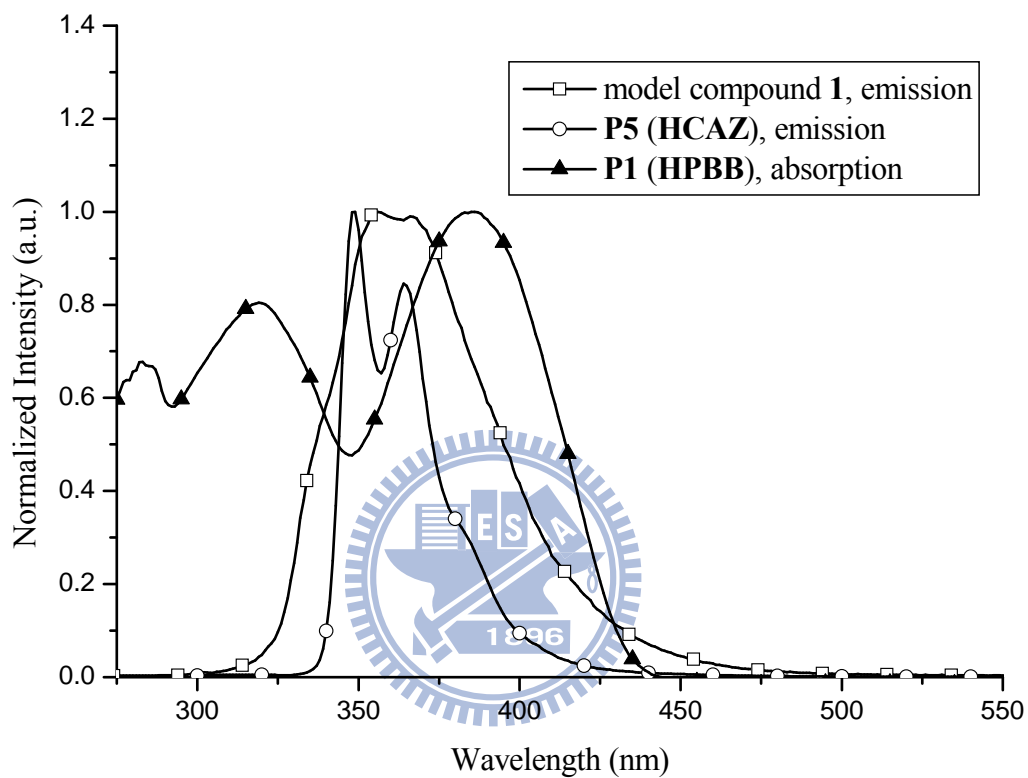
Figure A3   Powder X-ray diffraction (XRD) intensity against angle profiles obtained in the nematic phase of homopolymer **P1** at 90 °C (heating).

Figure A4 Absorption spectra of polymers **P1−P4** are normalized at the maximum absorption of light-emitting **PBB** segments in solid films.
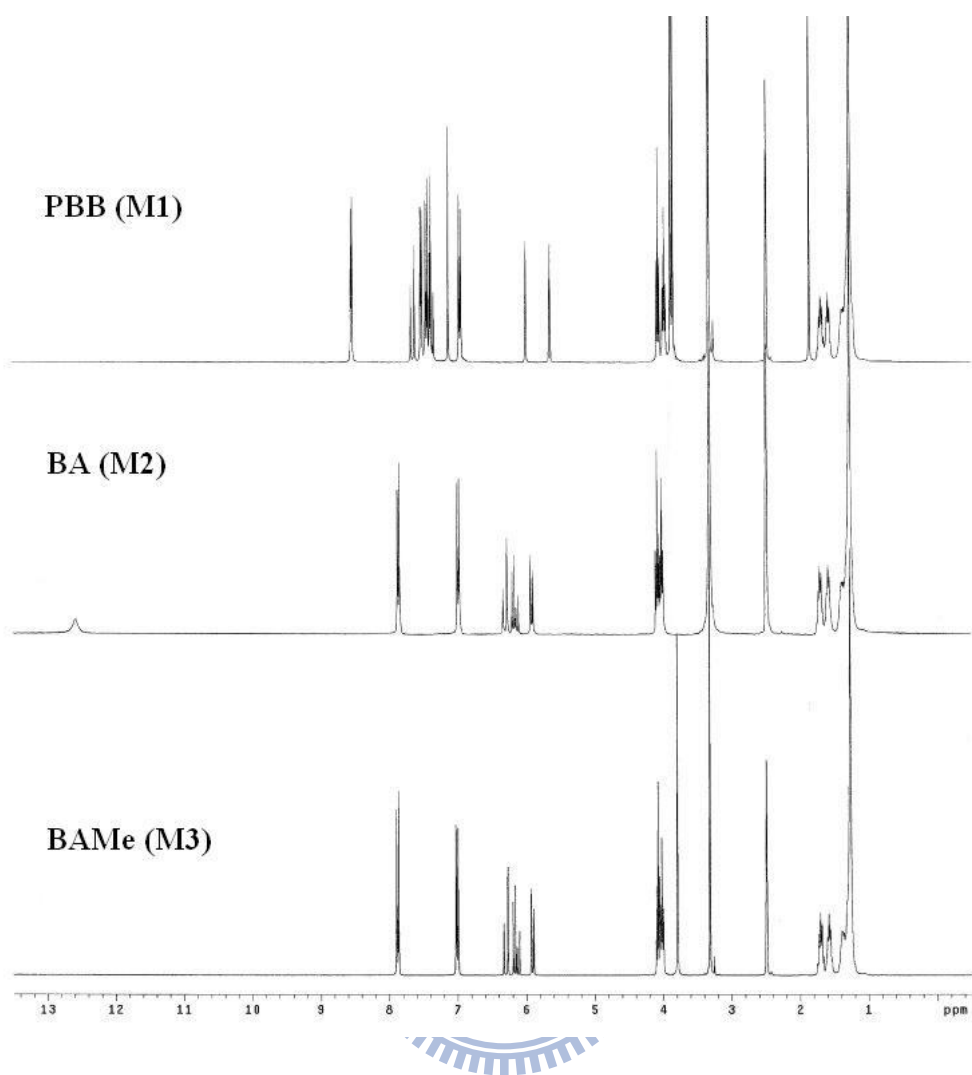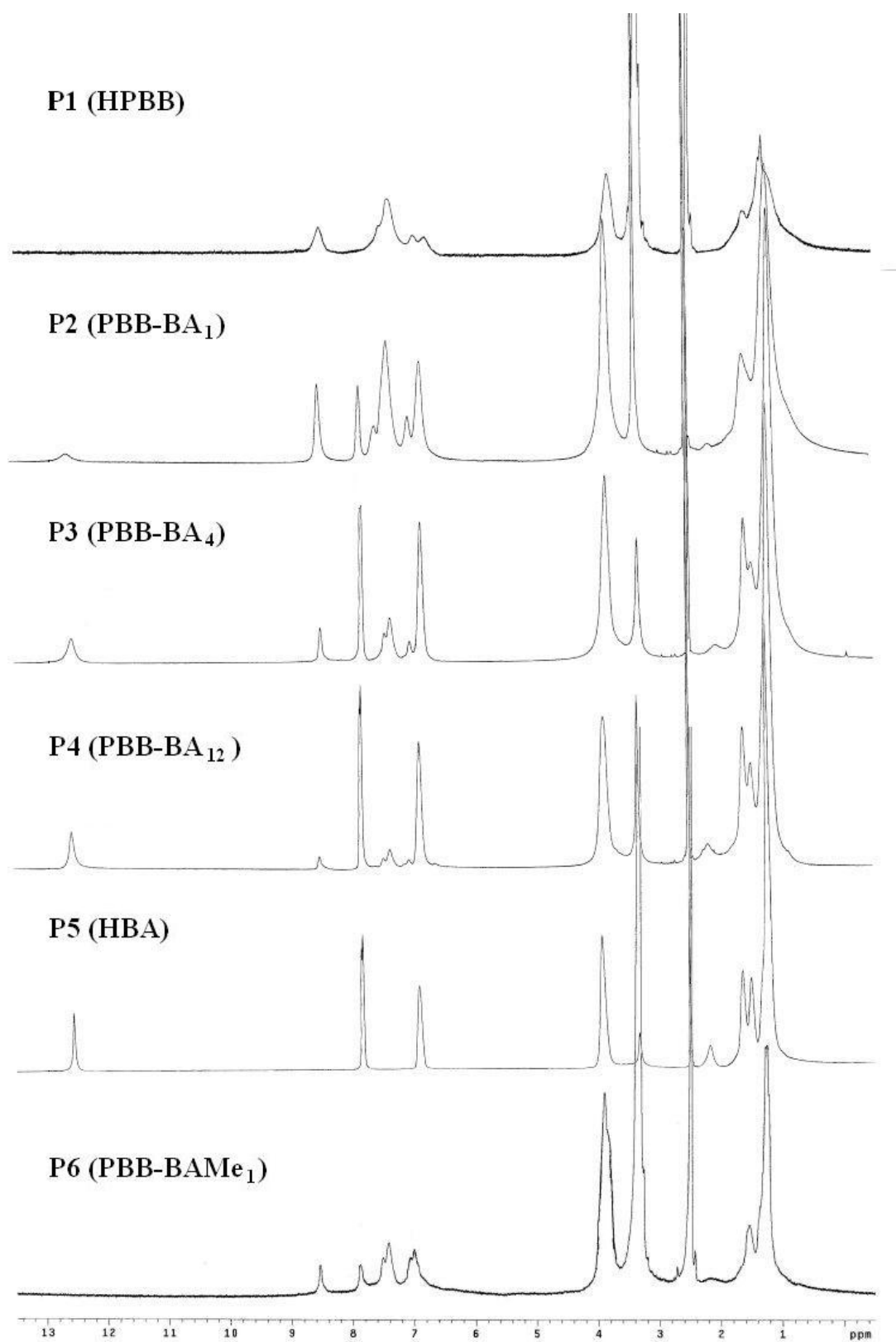
(a)

(b)

Figure A5 (a) Chemical structure of model compound **1** and (b) the spectral overlap in the emission of model compound **1** and homopolymer **P5** and the absorption of homopolymer **P1** in THF solutions. Note: excited at 305 nm for model compound **1** and homopolymer **P5**.

Figure A6 ^{1}H-NMR spectra of monomers PBB (**M1**) and BA (**M2**), and BAMe (**M3**) in DMSO-d_6.

Figure A7 ^{1}H-NMR spectra of polymers **P1**–**P6** in DMSO-d_6.

157

學經歷資料

- 姓名：楊博仁 (Po-Jen Yang)
- 性別：男
- 生日：1978 年 07 月 25 號
- 電子郵件信箱：wai.mse89g@nctu.edu.tw
- 聯絡電話：(家) 04-26398655　(手機)
- 聯絡地址：台中縣梧棲鎮中央路一段 447 號

學歷

博士：國立交通大學材料科學與工程學系	2003.9 ~ 2009.11
碩士：國立交通大學材料科學與工程學系	2000.9 ~ 2003.6
學士：國立台灣科技大學纖維工程系	1996.9 ~ 2000.6

專長

- **有機材料合成與材料分析**
1. 有機反應合成
2. 奈米材料開發
3. 液晶材料設計、合成與物性鍵定
4. 共軛高分子材料設計、合成與物性鍵定

論文發表

期刊論文(博)

1. Po-Jen Yang and Hong-Cheu Lin*, "Synthesis and characterization of achiral banana-shaped liquid crystalline molecules containing bisnaphthyl moieties", *Liquid Crystals*, **2006**, *33*, 587-603.

2. Po-Jen Yang, Chung-Wen Wu, Duryodhan Sahu, and Hong-Cheu Lin* "Study of Supramolecular Side-Chain Copolymers ContainingLight-Emitting H-Acceptors and Electron-Transporting Dendritic H-Donors", *Macromolecules*, **2009**, *41*, 9692.

3. Po-Jen Yang, Ling-Yung Wang, Chieh-Yin Tang, and Hong-Cheu Lin*, "Polymeric Dopant Effects of Bent-Core Covalent- and Hydrogen-Bonded Structures on Banana-Shaped Liquid Crystalline Complexes" *Journal of Polymer Science: Part A: Polymer Chemistry*, 2009, Accepted.

List of Publications

1. Po-Jen Yang and Hong-Cheu Lin*, "Synthesis and characterization of achiral banana-shaped liquid crystalline molecules containing bisnaphthyl moieties", *Liquid Crystals*, **2006**, *33*, 587-603.

2. Po-Jen Yang, Chung-Wen Wu, Duryodhan Sahu, and Hong-Cheu Lin* "Study of Supramolecular Side-Chain Copolymers ContainingLight-Emitting H-Acceptors and Electron-Transporting Dendritic H-Donors", *Macromolecules*, **2009**, *41*, 9692.

3. Po-Jen Yang, Ling-Yung Wang, Chieh-Yin Tang, and Hong-Cheu Lin*, "Polymeric Dopant Effects of Bent-Core Covalent- and Hydrogen-Bonded Structures on Banana-Shaped Liquid Crystalline Complexes" *Journal of Polymer Science: Part A: Polymer Chemistry*, 2009, Accepted.